Stony Brook University

Targeting Cancer Cell Invasion at the Molecular and Cellular Levels: Unraveling the role of KIAA1199 in Cancer Cell Migration and Development of a Novel 3D Invasion Assay for Anti-cancer Drug Discovery

A Dissertation Presented

by

Nikki Ann Evensen

to

The Graduate School

in Partial Fulfillment of the

Requirements

for the Degree of

Doctor of Philosophy

in

Molecular and Cellular Biology

Stony Brook University

August 2013

Stony Brook University

The Graduate School

Nikki Ann Evensen

We, the dissertation committee for the above candidate for the

Doctor of Philosophy degree, hereby recommend

acceptance of this dissertation.

Jian Cao, MD – Dissertation Advisor
Associate Professor, Department of Medicine

Suzanne Scarlata, Ph.D. - Chairperson of Defense
Professor, Department of Physiology and Biophysics

Robert S. Haltiwanger, Ph.D.
Professor and Chairman, Department of Biochemistry and Cell Biology

Deborah A. Brown, Ph.D.
Professor, Department of Biochemistry and Cell Biology

Stanley Zucker, MD
Professor, Department of Medicine

This dissertation is accepted by the Graduate School

Charles Taber
Interim Dean of the Graduate School

Abstract of the Dissertation

Targeting Cancer Cell Invasion at the Molecular and Cellular Levels: Unraveling the role of KIAA1199 in Cancer Cell Migration and Development of a Novel 3D Invasion Assay for Anti-cancer Drug Discovery

By

Nikki Ann Evensen

Doctor of Philosophy

in

Molecular and Cellular Biology

Stony Brook University

2013

Cell migration is an early and essential step required for cancer cell invasion and metastasis, which remains a major hurdle in the war against cancer. Therefore, it is imperative that we find novel strategies and targets aimed at preventing this cellular process. The goal of my thesis was two-fold: 1) to characterize the role of KIAA1199 in cancer cell migration and 2) to develop and optimize a novel 3-dimensional (3D) invasion assay. KIAA1199 is highly upregulated in various forms of cancers but its function was hitherto unknown. By employing both loss-of- and gain-of-function studies the role of KIAA1199 in cancer cell migration was determined. Silencing of KIAA1199 in aggressive cancer cells lead to a mesenchymal-to-epithelial-transition (MET), while overexpression in epithelial cells resulted in loss of epithelial-like traits. KIAA1199 was found localized within the endoplasmic reticulum (ER) via interaction with the chaperone protein binding immunoglobulin protein (BiP). Mechanistically, expression of KIAA1199 resulted in a leak of calcium from the ER and a subsequent increase in cytosolic calcium. These alterations in calcium were found to be required for KIAA1199-mediated migration via translocation and activation of protein kinase c alpha (PKCα). Upregulation of KIAA1199 was linked to hypoxia-induced activation of the KIAA1199 promoter via hypoxia-inducible-factor-2alpha (HIF-2α). Cell migration downstream of HIF-2α was impaired upon silencing of KIAA1199, suggesting a role for KIAA1199 in

response to hypoxia. Together, these data support the critical role of KIA1199 in cancer cell migration and maintaining cancer mesenchymal status.

Although the data presented herein support KIAA1199 as a potential target for inhibiting cancer dissemination, the use of a phenotypic screen targeting cancer cell invasion may expedite drug discovery programs. Therefore, considerable effort has been made in developing and optimizing a novel 3D invasion assay that involves surrounding cell-collagen hemispheres/dots within collagen to create a 3D environment for invasion. For standardization, a pitted plate was designed that controls location and shape of the dots, while dialdehyde dextran was added to the cell-collagen dots to maintain size by inhibiting collagen contraction. A protocol for dual staining was established to allow for automated counting and simultaneous detection of cytotoxicity. As proof of principle, the National Cancer Institute's Diversity Compound Library was screened, resulting in the positive identification of a compound known to inhibit cell motility. Together, these data validate the use of our assay in anti-cancer drug discovery programs aimed at converting life-threatening cancer into a chronic disease.

Dedication Page

I would like to dedicate my dissertation to my family who has provided me with a tremendous amount of support through all the triumphs and tribulations of graduate school. To my husband, Kenny, who has always supported me and put up with my long hours at lab. To my sisters, Kristie and Caitlyn, who would actually listen to my practice talks. To my parents, Laura and John, who have always been there for me to guide and support me. My mother, specifically, has done more for me during these past 5 years than I thought humanly possible. I would not have made it without all of them.

Table of Contents

List of Figures/Tables/Illustrations

List of Tables

List of Abbreviations

ATF - Activating Transcription Factor
BiP - binding immunoglobulin protein
Ca^{2+} - calcium
ChIP- chromatin immunoprecipitation
CHX – cycloheximide
CNS - central nervous system
Con A - Concanavalin A
DAG – diacylglycerol
DCIS - ductal carcinoma in situ
DTT – dithiothreitol
ECM - extracellular matrix
eIF2α - eukaryotic initiation factor 2 alpha
EMT - epithelial-to-mesenchymal transition
ER - endoplasmic reticulum
ERAD - ER-associated degradation
ERSE - ER stress response elements
FFPE - formalin-fixed, paraffin-embedded
FRET – fluorescence resonance energy transfer
GRP78 - Glucose-Regulated Protein 78
HIF - hypoxia-inducible factor
HRE - hypoxia response elements
HTS - high-throughput screen
IHC – immunohistochemical
IP3 - inositol 1,4,5-trisphosphate
IP3R - 1,4,5-inositol trisphosphate receptor
IRE1 - Inositol-requiring enzyme 1
LCM - laser capture microdissection
MMPs - matrix matelloproteinase
MET - mesenchymal-to-epithelial transition
PDI - protein disulfide-isomerase
PERK - PKR-like ER kinase
PI - Propidium iodide
PKC – Protein Kinase C
PS – phosphatidylserine
RYR - ryanodine receptor
SSH - suppression subtractive hybridization
STS – staurosporine
TG – thapsigargin
TN – tunicamycin
UPR - Unfolded Protein Response
XBP-1 - X-box-binding protein 1

Acknowledgments

I would like to thank my mentor Dr Jian Cao for being a great mentor. I have learned much more than techniques working alongside Jian. I consider myself lucky to have had a mentor that truly wants his students to learn as much as possible and to be successful in their future careers.

I would like to thank Dr. Cem Kuscu, Dr. Hoang-Lan Nguyen, Kevin Zarrabi, Dr. Antoine Dufour, Dr. Jian Li, Ashleigh Pulkoski-Gross, and Deborah Kim for all of their contributions and helpful advice throughout my graduate work.

I would like to thank my committee members, Drs. Suzanne Scarlata, Robert Haltiwanger, Deborah A. Brown, and Stanley Zucker, for their thoughtful insight and help with experiments for my thesis projects.

Prologue: Introduction

Despite remarkable progress over the past few decades, cancer still remains as one of the leading causes of death in the United States. The complexity of cancer stems from the fact that cancer cells are able to grow and survive by essentially hijacking normal cellular processes and using them in unregulated, inappropriate ways, outlined in Hanahan and Weinberg's Hallmarks of Cancer [1, 2]. Cancer cells arise and become unregulated by acquiring genetic mutations that cause aberrant expression or regulation of genes involved in those cellular processes that allow for tumor growth and progression. By gaining a better understanding of these processes and the genes involved in cancer progression we can potentially identify novel ways to inhibit and control cancer as a disease.

One of the hallmarks of cancer is the capacity for cancer metastasis or cancer cell dissemination. Metastasis, the spreading of cancer cells from a primary tumor to a secondary site, consists of multiple steps that each requires different phenotypic properties. The steps for metastasis include degradation and invasion through the extracellular matrix (ECM) surrounding the primary tumor, intravasation into the blood or lymphatic systems, circulation and survival throughout the body, extravasation from circulation into a new site followed by survival and growth at the secondary location [3, 4] (Fig. 1). Due to the complexity of this overall process, little progress in targeting cancer dissemination has been made, even though it is the leading cause of treatment failure in patients with cancer.

The initial step of metastasis is cancer cell invasion. Cancer cell invasion encompasses both proteolytic activity and migratory ability. Cancer cells within a tumor are surrounded by a basement membrane and various components that make up the ECM, such as collagen. Proteolytic activity involves the digestion and breakdown of cell adhesion components, the basement membrane, and the ECM by proteases that are located on the cell surface or secreted by a variety of cells within the tumor microenvironment [5]. In particular, the matrix matelloproteinase (MMPs) family of proteases has been widely implicated in cancer progression [6, 7]. These proteases are able to clear a path through the ECM, which can facilitate cancer cell dissemination,

however the cancer cells must be able to actively move or migrate through to eventually intravasate into the vasculature. The ability to move requires morphological changes via activation of various signal transduction cascades that ultimately lead to a reorganization of the cytoskeleton [8, 9]. There have been numerous studies demonstrating the molecular pathways involved in cell migration since cell motility is a necessity in many physiological processes, such as development, wound healing, immune response, etc. Despite the advancement of knowledge of aberrant regulation of signaling pathways in cancer cells [10-12], much remains to be understood about the overall regulation and maintenance of an invasive, aggressive phenotype of cancer cells.

In recent years there have been various reports regarding how and when cancer cells acquire the phenotypic properties required for cells to become invasive and metastatic, including increased motility. The cellular properties that are necessary to establish a primary tumor, such as proliferation, angiogenesis, survival, etc., are not the same traits that cells utilize for spreading throughout the body. It is hypothesized that not all tumor cells are capable of metastasizing but instead there is a subpopulation that has or possibly acquires the characteristics necessary for a more aggressive phenotype that leads to dissemination. Additionally, the importance of the effects of the various stressors or stimuli produced by the microenvironment surrounding the tumor cells, such as hypoxia (low oxygen), on the behavior of individual cancer cells has become increasingly evident. Many studies have been focused on determining gene signatures or profiles that could provide insight into the transition of stationary cancer cells to invasive, aggressive cells at the molecular level. One of the leading hypotheses for how cells acquire an invasive phenotype is a transcriptional reprogramming of the cancer cells referred to as an epithelial-to-mesenchymal transition (EMT), which ultimately leads to repression of specific cell adhesion related genes and induction of genes involved in the invasion process, such as proteases (EMT related reviews: [13, 14]).

Due to the fact that metastasis accounts for 90% of treatment failure, it is imperative that we begin to target this process in the hopes of making cancer a more manageable and treatable disease. Because the initial invasion of cancer cells away from the primary tumor is a critical determinant of metastasis, it is an important and viable

target for novel treatments. Whether the strategy relies on the identification and characterization of novel targets involved in different aspects of cell invasion or the discovery of new compounds that inhibit this aggressive behavior, it has become increasingly clear that it is necessary to stop cancer dissemination if the war on cancer is to be won. Therefore, the overall focus of my thesis project is on gaining insight into possible ways of inhibiting cancer cell invasion. Two different approaches have been undertaken to reach this goal: 1) characterization of the molecular mechanisms of KIAA1199's increased expression in cancer and its function in migration of cancer cells, and 2) development and optimization of a phenotypic assay to test potential drug candidates for their ability to inhibit cancer cell invasion.

Figure 1

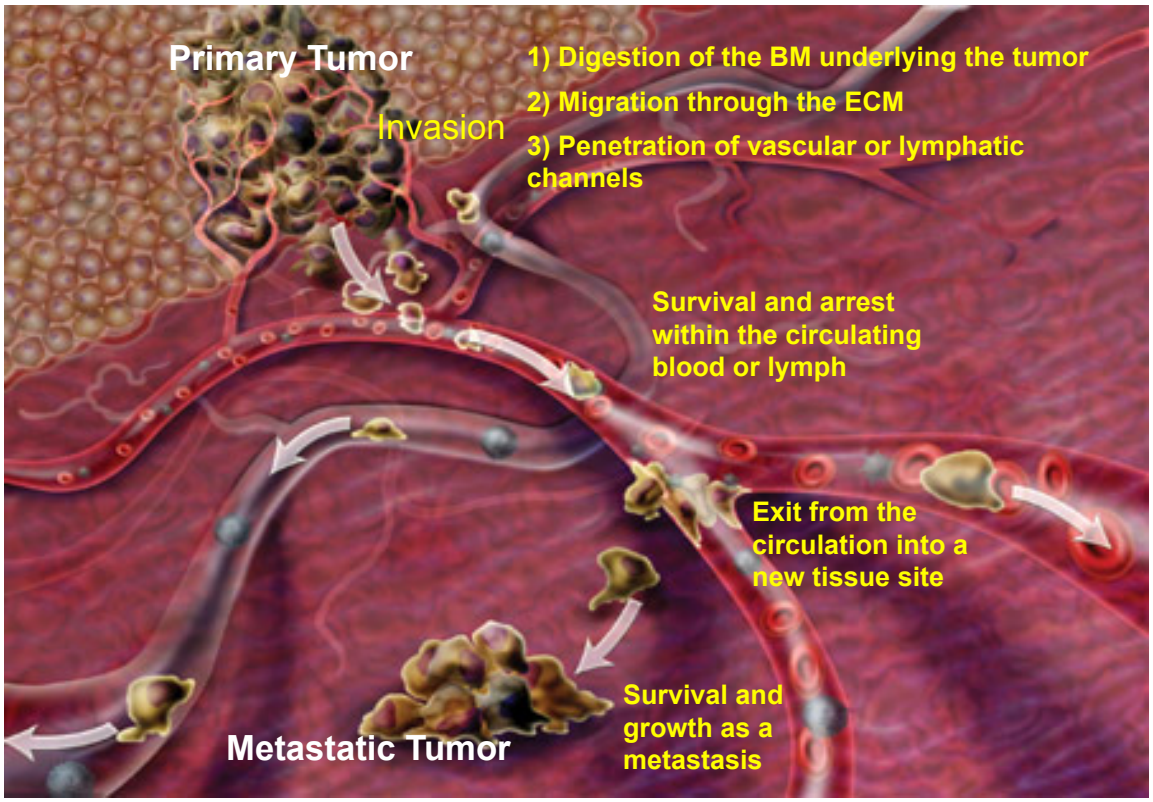

Figure 1 Illustration of Cancer Metastasis: Metastasis is a multistage process beginning with cancer cell invasion. Invasion requires the three steps outlined above. Following invasion and intravasation into the blood or lymphatic vasculature, cancer cells will circulate throughout the body until eventually halting and extravasating at a particular location. Cells that leave the circulation and are able to travel to and grow at a new site

will form a metastatic, or secondary tumor. Image modified from an article written by Charlie Schmidt [15].

Chapter 1: Unraveling the Role of KIAA1199, A Novel Endoplasmic Reticulum Protein, in Cancer Cell Migration

(Work from this chapter will be published in the *Journal of the National Cancer Institute* in the Sept. 18th 2013 issue.)

1.1 Summary

Since cell migration is a critical determinant of cancer invasion and metastasis, a better understanding of genes involved in controlling cancer cell migration will potentially lead to the identification of novel therapeutic targets aimed at preventing cancer dissemination. Our observations herein have expanded our understanding of cancer progression by characterizing the role of and dissecting the mechanism of a functionally unknown gene, KIAA1199, in cancer progression. KIAA1199 has been reported as upregulated in various forms of cancer. We discovered that KIAA1199 is a novel endoplasmic reticulum (ER) resident protein that plays a critical role in both maintaining a mesenchymal phenotype and inducing cancer cell migration and invasion. Further, KIAA1199 enhances cell migration through its interaction with ER glucose-regulated protein (GRP)-78/binding immunoglobulin protein (BiP), leading to ER calcium release. Increased cytosolic calcium results in the translocation and activation of Protein Kinase C alpha (PKCα), ultimately leading to enhanced cell migration. We also demonstrate that upregulation of KIAA1199 in cancer cells is in response to hypoxia via hypoxia-inducible factor-2alpha (HIF-2α) and KIAA1199 plays a role in cell migration in response to hypoxic stress.

1.2 Background

1.2A KIAA1199

Although many molecular players involved in cell motility are known, there still remains a lack of complete understanding of the signaling pathways involved in cancer cell migration. Characterizing new genes that could be potential targets for anti-cancer drug discovery platforms will lead to novel treatment strategies. With this in mind, our lab set out to identify novel genes involved in the process of cancer cell invasion. One of many approaches is to examine differential gene expression in response to stimuli known to induce an aggressive phenotype in cells. Concanavalin A (Con A), a lectin or carbohydrate binding protein, has been shown to induce the expression of proto-oncogenes [16] as well as increase cell surface expression of MMP-14, [17, 18] an MMP known to play a vital role in cancer cell migration and invasion. Based on these reports, our lab used Con A treatment as a stimulus for induction of invasion related genes. Examination of global gene expression in HT-1080 human fibrosarcoma cells untreated or treated with Con A was accomplished via a PCR-based cDNA suppression subtractive hybridization (SSH) technique, which has been demonstrated to be effective in isolating, normalizing, and enriching differentially expressed genes over 1,000-fold in a single round of hybridization [19]. The SSH method revealed approximately 90 clones that were differentially expressed upon stimulation with Con A.

One of the cDNA clones (Clone 43, 724 bp in length) that was differentially expressed (Figure 2A) exhibited a 5.5-fold increase in ConA-treated HT-1080 cells (Figure 2B). Sequence analysis of this clone revealed a high degree of similarity (99%) to a functionally unknown cDNA clone, DKFZp58600118 (Genbank accession #AL049389). By screening a cDNA library from human spinal cord that was found to highly express the identified gene under physiological conditions, a final 6.7 kb cDNA was obtained. This complete cDNA sequence contains a 4083-bp open reading frame (ORF) encoding 1361 amino acids with a predicted molecular mass of 163 kDa. Transfection of COS-1 cells with the full-length cDNA fused with a C-terminal Myc tag revealed a protein of approximately 160 kDa (Figure 2C). BLAST analysis using this cDNA's ORF indicated that this gene is identical to a previously obscure gene,

KIAA1199, which is reported in the Human Unidentified Gene-Encoded Large Proteins (HUGE) database.

Figure 2:

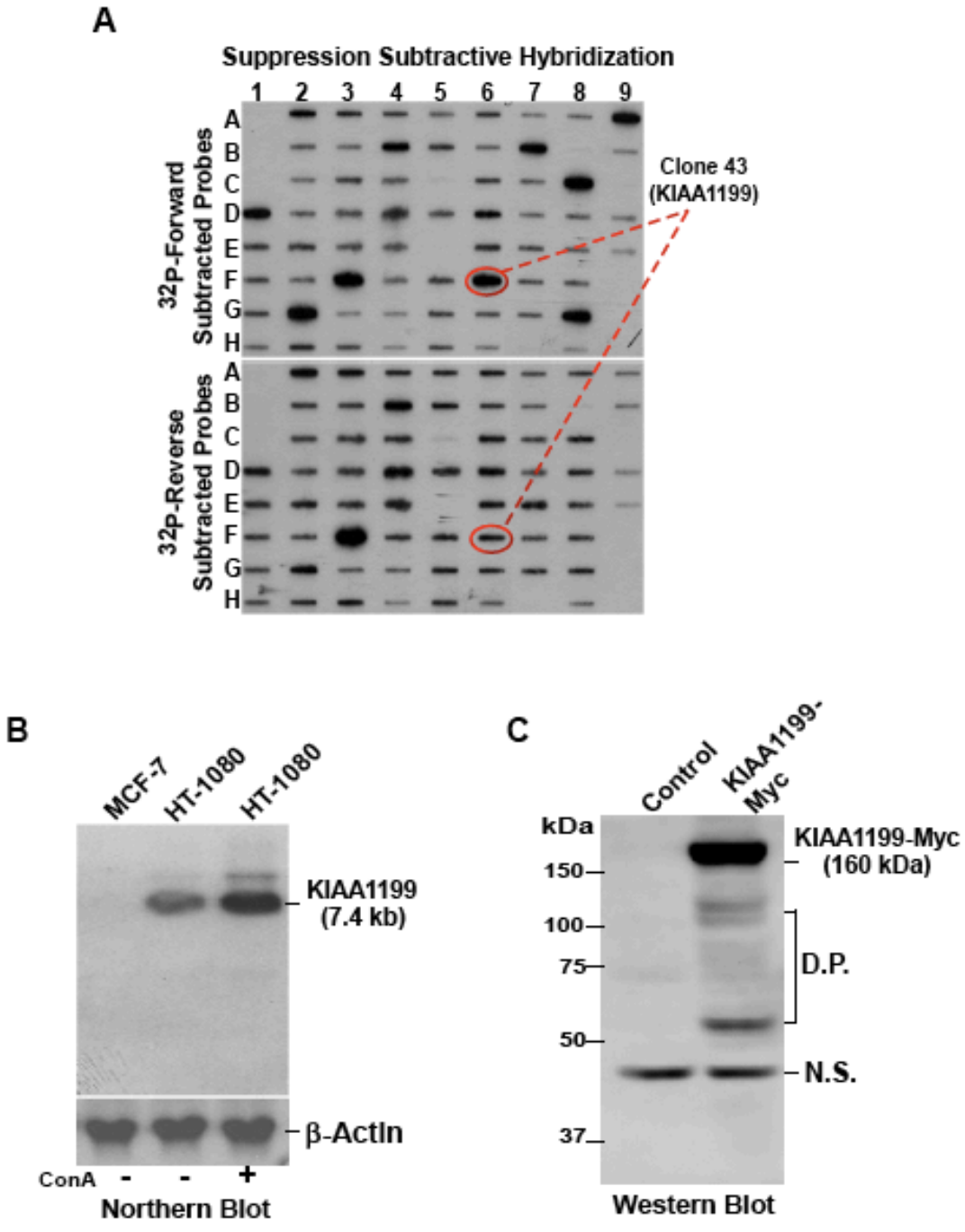

Figure 2 Identification of KIAA1199: (A) PCR-based suppression subtractive hybridization was performed using HT-1080 cells treated with ConA (as tester) and

without ConA treatment (as driver) to generate forward subtraction probes. Reverse subtraction was performed to generate reverse subtraction probes. Both forward and reverse probes were labeled with ^{32}P and hybridized with forward-subtracted cDNA clones. (B) Northern blot analysis of total RNA extracted from MCF-7, HT-1080, and ConA (30 μg/ml)-treated HT-1080 cells probed by a ^{32}P-labeled KIAA1199 probe (724 bp). (C) Western blotting analysis of total cell lysate from transfected COS-1 cells using anti-Myc Ab. D.P.: degradation products; N.S.: non-specific band. *The experiments presented in this figure were performed by Dr. Jian Cao.

Both the DNA and protein sequences are highly conserved among mammals and vertebrates down to zebrafish. Genetically, KIAA1199 was shown to have a G8 domain containing eight conserved glycine residues and five β-strand pairs, as well as two GG domains composed of seven β-strand pairs and two α-helices [20, 21], although no characteristic function is associated with these motifs. Under normal physiological conditions, KIAA1199 is mainly expressed in the central nervous system (CNS) [22].

Currently there is very little information regarding the function of KIAA1199. One of the first reports on KIAA1199 was on the correlation of specific point mutations within KIAA1199 with nonsyndromic hearing loss, which suggests that KIAA1199 could potentially be involved in auditory functioning [23]. Following this article, a number of reports have highlighted the potential importance of KIAA1199 in cancer, although none have focused on the specific role of KIAA1199 in cancer progression. KIAA1199 transcript and protein levels were found to be highly elevated in colon cancer tissue as compared to normal colon tissue and its expression was correlated with the Wnt signaling cascade [24, 25]. High expression of KIAA1199 was also found in gastric cancer and was found to correlate with poor prognosis and metastasis [26]. Furthermore, a recent paper published from our lab revealed increased expression of KIAA1199 in numerous cancers via data-mining and further verified expression of KIAA1199 in aggressive, human prostate and breast cancer cell lines [27]. Together, these studies indicate a potential role for KIAA1199 in cancer progression and warrant further studies to elucidate the function of this gene.

1.2B Cell Migration and Epithelial-To-Mesenchymal-Transition

Cell migration requires many physical and signaling alterations within a cell. Collectively these changes allow a cell to extend itself outwards and attach to a new location, reorganize and reshape structural components to extend and contract, and finally to detach from its current location and complete the forward motion [5]. It is known that there are many different signaling cascades that can alter a cell's capacity to migrate. For instance, the mitogen activated protein kinase (MAPK) pathway has been implicated in cancer cell migration due to activation via amplifications or mutations of the genes involved [28]. Activation of upstream regulators, such as cell surface receptors, and/or loss of inhibitory mechanisms, such as downregulation of phosphatases, involved in the MAPK pathways has been associated with a migratory phenotype [28-32]. Studies have also shown activation of other downstream molecules, including PKCs and Src, leads to cancer cell migration in response to unregulated receptor tyrosine kinases [33]. These cascades culminate in the reorganization of actin filaments and adhesion contacts that ultimately lead to enhanced motility. Although much literature has been dedicated to elucidating molecular mechanisms that increase cancer cell migration, many questions still remain about potential novel players involved in this process.

In addition to undergoing signal transduction changes, it is believed that cancer cells must undergo the transcriptional reprogramming of EMT, which ultimately results in phenotypic and morphological changes that allow for more aggressive behavior. EMT occurs during normal cellular processes, such as development and wound healing, that require increased invasiveness and cell motility [13]. However, it is believed that cancer cells undergo this transition to allow for dissemination. There is controversy surrounding the idea of EMT in cancer due to the fact that there is little evidence that this occurs *in vivo*. One of the major observations from tumor cells *in vivo* is that cancer cells from the metastatic site often share epithelial-like characteristics with the primary tumor rather than expressing more mesenchymal markers. While this may seem counterintuitive, the reason for this is thought to be that once the tumor cells have metastasized to a secondary site, they must revert to an epithelial phenotype that is better suited for growth in the new

environment [34]. This reversion is referred to as the mesenchymal-to-epithelial transition (MET).

In order to better understand this phenotypic switch of cancer cells, it is vital to know the general characteristics associated with the different cell types. Epithelial cells have a cobblestone morphology and are organized into sheets of cells that have tight cell-to-cell and cell-basement membrane adhesion junctions mainly due to expression of E-cadherins. The individual cells are polarized such that their apical surfaces express different properties than the basal surface that is in contact with the underlying basement membrane. The cell junctions and polarization of the cells are orchestrated by the arrangement of the actin cytoskeleton and cytokeratin type filaments. Epithelial cells have limited movement capabilities due to the tight adhesive properties of these cells. Mesenchymal cells, on the other hand, have a spindle-like morphology and do not form cell layers as they do not form tight cell-cell junctions. Instead, they form more site-specific, pointed adhesion junctions with the ECM and have no cellular polarity. Typically, mesenchymal cells also express different filamentous proteins and cadherins as compared to epithelial cells, such as vimentin instead of cytokeratins and N-cadherin instead of E-cadherin, respectively. Due to these variations in mesenchymal cells, they tend to have an increased migratory capacity. Furthermore, mesenchymal-like cells often show increased expression of ECM remodeling proteins, such as members of the MMP family. These defining characteristics are summarized by Thompson and Newgreen and by Jean Paul Theiry and Jonathan P. Sleeman [35, 36], and depicted in figure 3.

Figure 3

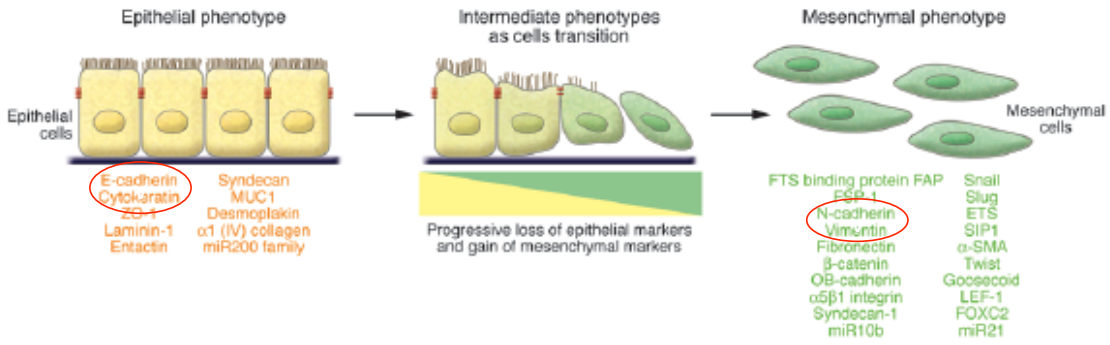

Figure 3 EMT: Depiction of the gradual transition from an epithelial-like cell to a mesenchymal-like cell, which involves the loss of cell-cell adhesions, cellular polarity, and cuboidal morphology. Mesenchymal cells are characterized by a spindle-shaped morphology, no polarity, and no tight cell-cell contacts. These changes are orchestrated by a variety of proteins listed below each cell type. Those circled in red are most often used as common EMT markers. Image modified from [13].

These morphological and behavioral changes are initiated at the transcriptional level via repression of genes involved in maintaining a normal epithelial-like phenotype and activation of genes responsible for maintaining the mesenchymal-like phenotype. Various transcription factors have been implicated in the orchestration of EMT in cancer cells, such as Twist, Snail, and Slug, all of which have also been shown to play roles in EMT during normal physiological processes. Twist is a known master regulator involved in development and its expression in human cancer cells correlates with invasiveness. Additionally, knocking down expression of Twist in an aggressive breast cancer cell line significantly abrogated lung metastasis [37], while overexpression in various less-aggressive cell lines has been shown to cause both the morphological change and gene expression changes associated with EMT [38]. Snail and Slug have also been shown to lead to EMT via repression of E-cadherin expression [39].

Targets of the transcription factors involved in EMT include genes involved in signal transduction, cell-adhesion, and cell structure. The differential expression of these proteins is what ultimately orchestrates the phenotypic changes associated with EMT/MET. It is these changes in gene expression that are commonly used as markers for EMT/MET. Furthermore, these characteristic EMT markers have been shown to be predictive of invasiveness in various human breast cancer cell lines [40]. Of particular interest is the family of adhesion proteins known as cadherins. As mentioned above, both E-cadherin and N-cadherin have been shown to play pivotal roles in the loss or acquisition of an invasive phenotype in cancer cells, respectively, by altering cell-cell adhesions and intracellular signaling pathways [41]. For example, simply silencing E-cadherin in human mammary epithelial cells was shown to lead to a change from an epithelial to fibroblastic morphology, which coincided with an increase in N-cadherin and vimentin expression. Furthermore, this loss of E-cadherin resulted in an increase in lung

metastasis [42]. Although E-cadherin has been recognized as a standard marker for EMT, N-cadherin has been shown to play a pivotal role in invasion and metastasis as well [41, 43]. In a prostate cancer model, cells overexpressing N-cadherin had increased vimentin expression and invasive ability, while knocking down N-cadherin resulted in decreased invasion. Furthermore, by targeting N-cadherin with an antibody, local invasion as well as distant metastasis was abrogated in an *in vivo* model [44]. Other common markers are intermediate filamentous proteins that are involved in maintaining cell architecture. Vimentin expression alone has also been shown to cause morphological changes in epithelial cells resulting in increased migration [45, 46]. Together, these studies highlight the impact of a single transcription factor or gene on the transition of cancer cells from a more stationary, epithelial-like state to an aggressive, metastatic form.

1.2C Cellular Localization – Endoplasmic Reticulum (ER)

Due to the complexity of EMT and the many signaling pathways that lead to enhanced cancer cell migration, one of the initial steps in elucidating a mechanism of action for novel proteins found to have the ability to enhance cell migratory ability is determining the cellular localization of the protein. The localization of a protein can help in beginning to unravel the downstream signaling cascade.

The ER is a major site for protein synthesis, folding, and post-translational modifications within a cell. Proteins that are destined for various organelles, the plasma membrane, or for secretion to the extracellular environment are transported into the ER as they are being translated and then further modified as necessary. The ability to fold and process proteins depends on maintaining the expression levels of chaperone proteins and enzymes involved in modifications such as N-linked glycosylation, an oxidation-reduction (Redox) state conducive to formation of disulfide bonds, and calcium and ATP levels required for proper activity of chaperone proteins. It is these duties of the ER that make it a vital organelle in maintaining homeostasis and adapting to changes in protein expression and assembly within a cell. Therefore, any perturbations of protein processing that leads to an accumulation of misfolded proteins within the ER will lead to ER stress,

which ultimately affects many cellular processes and signaling cascades. A complete overview of the ER was written by Daniel N. Hebert and Maurizio Molinari [47].

Various stressors, including nutrient or oxygen deprivation and resultant changes in redox potential, as well as numerous pathological conditions, including neurological diseases and cancer, are known to cause ER stress [48]. When a cell experiences these stimuli, protein folding becomes compromised; nascent polypeptides and misfolded proteins accumulate within the ER, lowering the output of functional proteins. In order for a cell to compensate for this increased protein burden, a series of cellular responses are initiated that are collectively referred to as the Unfolded Protein Response (UPR). The UPR is the cell's protective mechanism to alleviate the stress quickly and restore homeostasis by implementing three major steps: shutting down general protein translation, inducing the expression of ER chaperone proteins, and activating ER-associated degradation (ERAD) to eliminate excess proteins. If the stress is prolonged and becomes too much for the cell to cope with, apoptosis, or programmed cell death, will be initiated. These three aspects are often assessed experimentally to determine the induction of the UPR in response to stress inducers. Among the most common ER stress inducers used experimentally are dithiothreitol (DTT), a reducing agent that disrupts the Redox environment of the ER preventing disulfide bond formation, tunicamycin (TN), an N-linked glycosylation inhibitor, and thapsigargin (TG), an inhibitor of an ER calcium (Ca^{2+}) pump that leads to ER Ca^{2+} depletion [49].

In order for the cell to activate the UPR, the ER must have a way to sense and respond to these changes. There are three ER resident proteins that are responsible for coordinating the transcriptional and translational changes that occur upon sensing ER stress: PKR-like ER kinase (PERK), Inositol-requiring enzyme 1 (IRE1), and Activating Transcription Factor 6 (ATF6). One of the initial steps of the UPR is performed by PERK and involves the phosphorylation of eukaryotic initiation factor 2 alpha (eIF2α). This in turn leads to inhibition of protein translation, which decreases the amount of new proteins being synthesized to allow the ER to deal with the current protein load. Additionally, eIF2α phosphorylation permits the translation of specific proteins that contain upstream open reading frames (uORFs), including ATF4 [50], which can then induce the

transcription of genes that help alleviate the stress. Further transcriptional changes are also a consequence of the endoribonulease activity of IRE1 activated in response to ER stress. This activity of IRE1 is responsible for the splicing of the mRNA of the transcription factor X-box-binding protein 1 (XBP-1), which then allows for XBP-1 translation. Proteins involved in chaperone functions and ERAD have been shown to be dependent on XBP-1 transcription factor activity [51]. ATF6 is a transcription factor that is post-translationally cleaved upon stress allowing for its nuclear translocation. ATF6 is known to bind to ER stress response elements (ERSE) within promoters of the ER chaperone proteins involved in increasing the ER's folding capacity [52], and within the XBP-1 promoter [53]. Together these changes provide the ER with the necessary components to recover from insult. The pathways initiated by these three proteins outlined above (depicted in figure 4), as well as other cascades involved in the cellular response to ER stress, are summarized in more detail in numerous reviews [54, 55].

Figure 4

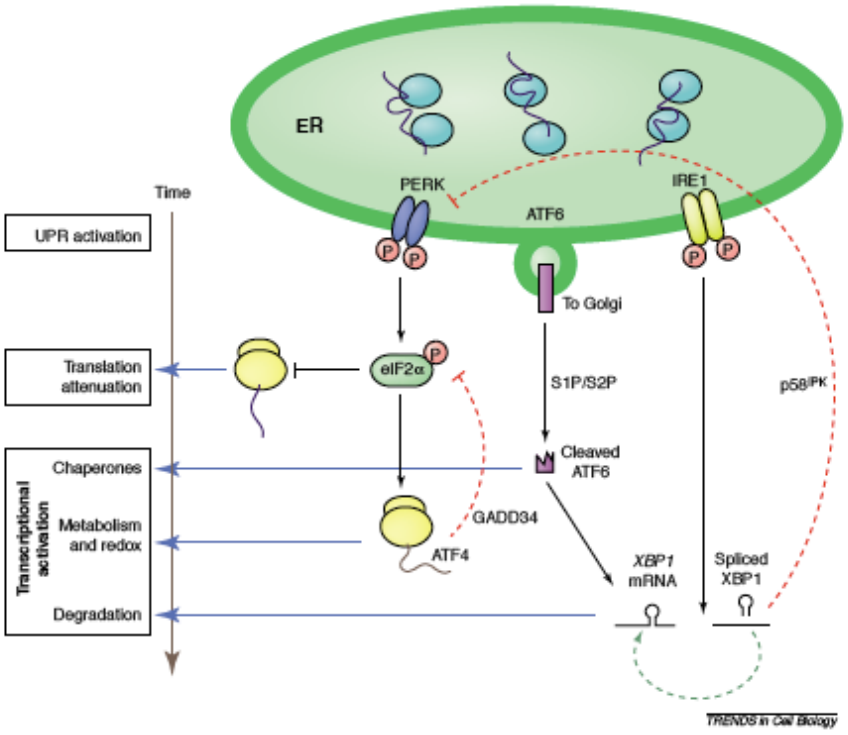

Figure 4 Molecular pathways involved in ER stress response: PERK, IRE1, and ATF6 each play major roles in the cellular response to stress by initiating various signaling cascades that ultimately aim to alleviate the stress. Image from [54].

1.2D GRP-78/BiP

The molecular players described above occur upon a shift in the environment within the ER that does not allow for efficient processing, but it is also vital to understand how the ER senses this shift. The major sensory protein is one of the most abundant and important ER resident proteins, GRP78 or BiP. BiP is a member of the 70 kilodalton heat shock family of proteins characterized as molecular chaperones involved in protecting cells from stress. BiP is specifically induced upon ER stress. Chaperone proteins, including BiP, transiently interact with incompletely folded proteins to stabilize and assist in folding as well as inhibiting aggregation of protein intermediates. This binding to polypeptides is considered non-specific and is usually due to the presence of exposed hydrophobic regions of the substrates that are only available prior to folding. Additionally, the transient binding and release of nascent proteins is dependent on the ATPase activity of BiP, with ATP hydrolysis playing a role in substrate release [56, 57]. Under normal physiological unstressed conditions, BiP has been shown to directly interact with the UPR activating proteins PERK, IRE1, and ATF6 keeping these molecules in inactive states. Upon stress, BiP must release these proteins in order to fulfill its role as a chaperone in dealing with the increased presence of proteins. As a result, PERK and IRE1 are free to dimerize and become phosphorylated and ATF6 can be further processed and translocated to the nucleus [58-61]. Additionally, BiP has been shown to play a role in ERAD in response to misfolded proteins, which results in the degradation of proteins, thus lowering the burden of the ER [62, 63]. These functions of BiP are illustrated in figure 5.

ER stress and BiP specifically have been shown to play roles in cancer progression. Tumor cells often experience harsh conditions that alter the balance of a cell, including hypoxia, acidic pH, glucose deprivation, etc. Cancer cells must constantly adapt to these toxic perturbations to avoid cell death and the UPR is one pathway by which cancer cells do this. Thus, much research has been done to determine the role of various UPR related molecular players in cancer progression and how they can potentially be targeted to treat cancer [64, 65]. Of particular interest is the increased expression level of BiP observed in cancer and the correlation with increased

aggressiveness and poor prognosis in human cancer [66, 67]. Numerous studies have also identified a role for BiP in cancer progression as an anti-apoptotic protein due to its role in maintaining balance within the cell under stress. BiP protects human breast cancer cells from nutrient deprivation-induced apoptosis and tumors heterozygous for BiP show increased apoptosis and reduced proliferation [68, 69]. Even more problematic for treating cancer, BiP has also been shown to increase resistance to chemotherapeutic drugs [70, 71]. In relation to a more aggressive phenotype, reports have demonstrated increased migratory and invasive ability upon increased BiP expression. In a hepatocellular model, overexpression of BiP resulted in increased cell spreading and invasion via a pathway involving focal adhesion kinase [72]. Similarly, silencing of BiP reduced migratory and invasive abilities of head and neck cancer cell lines and diminished metastasis *in vivo* [73]. Together, these findings support BiP as a crucial player in cancer progression.

Figure 5

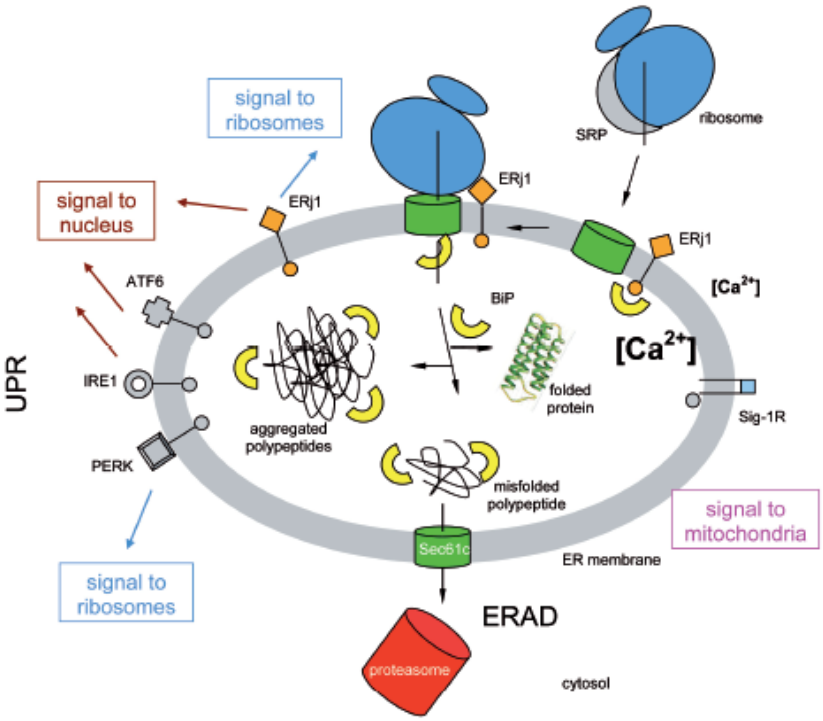

Figure 5 Functions of GRP78/BiP: BiP plays a vital role in the processing of proteins within the ER, the sensing of ER stress, activation of the UPR, and the maintenance of calcium balance within the cell. Image from [74].

1.2E Calcium

The details outlined above support the vital role of the ER and its resident proteins in maintaining balance within the cell. However, the ER also contributes to signal

transduction cascades. Calcium (Ca^{2+}) is an important and complicated second messenger involved in numerous cellular processes including development, apoptosis, and cell motility [75-77], as well as in disease-associated processes including cancer progression [78-80]. For this reason it is important that intracellular Ca^{2+} concentrations are strictly regulated to avoid inappropriate activation of various processes.

The way cells ultimately regulate Ca^{2+} is by compartmentalization with the major storage site being the ER. The ER thus plays an essential role in coordinating cellular responses mediated by Ca^{2+} signaling [81, 82]. In order to maintain high levels of Ca^{2+} within the ER and low resting Ca^{2+} levels within the cytosol, the cell utilizes ATPase pumps. The sarcoendoplasmic reticular Ca^{2+} ATPases (SERCA pumps) actively pump Ca^{2+} into the ER against its concentration gradient, while the plasma membrane Ca^{2+} ATPases (PMCA pumps) are responsible for removing Ca^{2+} from the cytosolic compartment to the extracellular medium. Also present on the plasma membrane are ion exchangers that function in Ca^{2+} extrusion. In relation to Ca^{2+} signaling events, there are two major ER membrane, non-selective ion channels, the 1,4,5-inositol trisphosphate receptor (IP_3R) and the ryanodine receptor (RYR), that respond to various upstream signals, such as activation of G-protein coupled receptors, to allow release of Ca^{2+} from the ER [77]. In recent years, evidence has developed to support the idea that a basal calcium leak from the ER also plays a role in dynamic Ca^{2+} changes and in maintaining specific concentrations of calcium, but the mechanism is still unclear [81]. Present within the ER lumen are also numerous Ca^{2+} binding proteins that serve to buffer ER Ca^{2+}, including BiP [83]. Several studies provide evidence to support BiP's role in Ca^{2+} homeostasis by securing the translocon involved in protein synthesis into the ER lumen in order to inhibit leakage of ions (including Ca^{2+}) from the ER [84, 85].

The cell has evolved different mechanisms to be able to control the levels of Ca^{2+} within the cellular compartments due to the important signaling pathways that are activated in response to Ca^{2+}. Changes in intracellular Ca^{2+} levels have been directly linked to cell migration through activation of downstream signaling events, such as focal adhesion kinase activation, as well as changes in cytoskeletal arrangements [80, 86, 87]. Elevated resting levels of cytosolic Ca^{2+}, induced by genetic or metabolic stress, have

been correlated with increased invasiveness in myoblasts and human lung carcinoma cell lines and have been found to be dependent on PKC activation [88]. In addition, increased expression of invasion related proteins, such as TGF-β and cathepsin L, a protease, have also been observed [89]. Studies have also linked Ca^{2+} release via the IP_3R to activation of the PI3K-AKT pathway required for cell motility [90]. Together these reports are indicative of the signal transduction mechanisms downstream of calcium fluctuations that support the necessity for tight regulation of cellular calcium concentrations.

1.2F Protein Kinase C (PKC)

One group of key molecules that require calcium for activation and subsequent downstream signaling is the conventional Protein Kinase C (cPKC) family members. PKC comprises a family of enzymes that phosphorylate serine and threonine residues within their target proteins. This family of proteins all have multiple domains that have well defined functions, including a pseudosubstrate domain for autoinhibition, regulatory domains (C1 and C2) that have specific cofactor requirements, a kinase catalytic site, and a carboxyl-terminal tail that contains key phosphorylation sites involved in maturation of the proteins (Fig. 6 left panel) [91]. The maturation of the proteins is achieved after completion of three ordered phosphorylation reactions. The first is considered a priming reaction that occurs within the kinase domain of the protein and is necessary for the other two to sites to be modified [92]. The next two sites are within the carboxyl-terminal tail motif and phosphorylation at these sites stabilizes the PKC proteins and allows for proper localization and function. The inactive, unphosphorylated protein is found in the detergent-insoluble fraction of cells, whereas the modified, mature protein, in the absence of second messengers, is localized within the cytosolic (soluble) compartment. Once the necessary second messengers are available for interaction with the primed PKCs, the protein can be relocalized to the membrane (detergent-soluble) where they interact with phosphatidylserine (PS) and become functionally active [93].

The ten isozymes of the PKC family that have been identified to date are grouped into categories based on the cofactor, or second messenger, requirements of the regulatory domains for translocation to the plasma membrane. Conventional PKCs

require calcium and diacylglycerol (DAG), novel PKCs require only DAG, and atypical PKCs require protein-protein interactions for their translocation and activation [94, 95]. Of particular interest are the conventional isoforms which include PKCα, PKCβI and II, and PKCγ. For cPKCs, it is the binding of the C2 domain to Ca^{2+} released from the ER that specifically increases the affinity of cPKCs for anionic phospholipids present within the plasma membrane specifically. Following the calcium-induced translocation, the C1 domain can bind its ligand DAG which changes the hydrophobicity of the surface of the protein to allow for engagement of PS (Fig. 6 right panel) [93]. The conventional signaling cascade that leads to cPKC activation involves the hydrolysis of phosphatidylinositol 4,5-bisphosphate (PIP_2) to inositol 1,4,5-trisphosphate (IP_3) and DAG by phosphoinositide-specific phospholipase C (PLC). The IP_3 functions as an agonist for the IP_3R in the ER membrane to cause Ca^{2+} release and the DAG serves as one of the ligands at the membrane. Studies have shown that Ca^{2+} release triggered by stimulation with an ER Ca^{2+} ATPase pump inhibitor can result in translocation of cPKC without affecting IP_3 or DAG levels [96], suggesting that the translocation and activation of cPKC is highly dependent on calcium. Furthermore, this group provides evidence to suggest a positive feedback loop between Ca^{2+} oscillations and the PLC pathway [96]. Once activated by the presence of these second messengers, the cPKCs can phosphorylate their downstream targets leading to changes in cellular processes including proliferation, apoptosis, migration, etc.

Figure 6

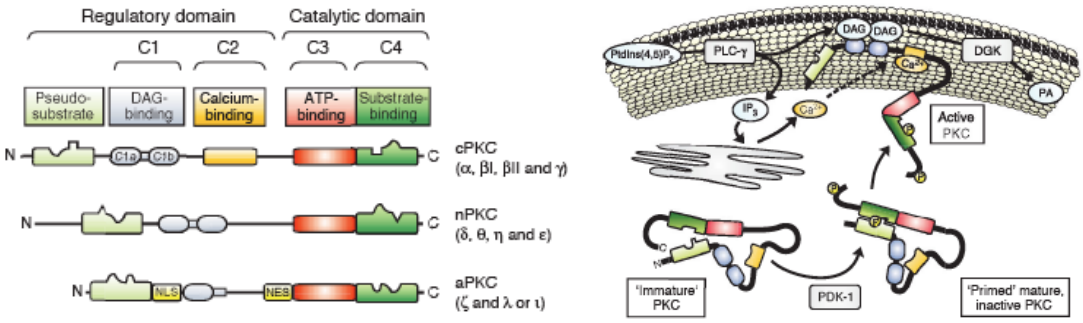

Figure 6 PKC regulation Left panel: The PKC family of enzymes is categorized into 3 groups based on the regulatory domains. The C1 domain binds DAG and the C2 domain binds calcium ions. All the enzymes have the pseudosubstrate domain for autoregulation and the catalytic domain, which acts as a kinase and phosphorylates downstream target proteins. Right panel: PKCs are normally in a mature, phosphorylated state within the cytosol. For cPKCs, upon release of Ca^{2+} from the ER, the cPKCs can translocate to the plasma membrane and interact with DAG freeing the active site within the catalytic domain for enzymatic activity. Both images from [97].

The PKC family has been implicated in cancer progression since the realization that the tumor-promoting ability of phorbol esters was linked to PKC activation. Since that discovery, many studies have been undertaken to determine the role of the isozymes in cancer, including cancer cell migration and invasion. The cPKCs have been shown to mediate cell migratory pathways [98-100]. More specifically, PKCα expression has been reported in breast and ovarian cancer [101] and *in vivo* and *in vitro* findings support the use of PKCα as a marker for breast cancer aggressiveness since silencing of this protein reduces proliferation and migration of breast cancer cell lines [102]. Mechanistically, PKCα can regulate a variety of downstream signaling cascades. PKCα has been demonstrated to activate ERK in a calcium dependent manner, leading to migration of Chinese hamster ovarian cells [99], as well as actin binding proteins that affect migration via cytoskeletal changes [103].

1.2G Hypoxia

It has become increasingly clear that the tumor microenvironment plays a vital role in tumor cell behavior and progression, including influencing invasiveness and migratory ability [2]. One of the most common stressors encountered by tumor cells within the microenvironment is low oxygen tension or hypoxia [104], which occurs in solid tumors due to rapid tumor growth and insufficient angiogenesis. This stress drives malignant progression by imposing a powerful selective pressure, resulting in a more aggressive population of cancer cells that can resist death and escape the environment [105, 106]. The cellular responses to hypoxic stress are mediated by the hypoxia-inducible factor (HIF) that consists of two subunits, HIF-α and HIF-1β [107, 108]. The HIF-1β is constitutively expressed, independent of oxygen levels within the cell, whereas

the HIF-α subunit, encoded by three genes (HIF-1α, -2α and -3α), serves as the oxygen sensing subunit [109]. Under normoxia, proline residues within HIF-α are hydroxylated, targeting it for proteasomal degradation [109]. Under low oxygen conditions HIF-α can accumulate and dimerize with HIF-1β in order to bind to hypoxia response elements (HRE) within gene promoters, ultimately leading to activation of target genes necessary for cellular adaptation to hypoxia (Fig. 7) [110, 111].

Figure 7

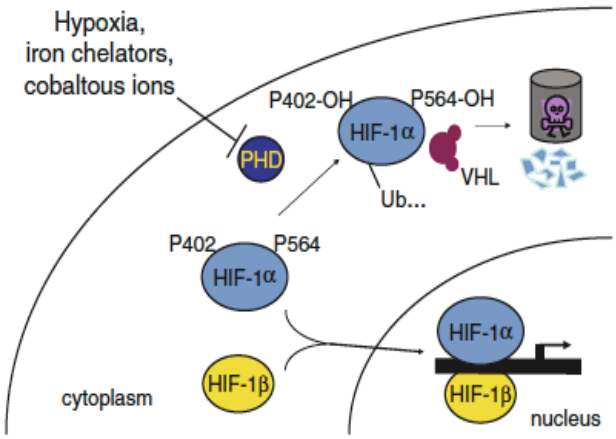

Figure 7 Regulation of HIFs: The cellular response to hypoxic stress is orchestrated by the HIF heterodimer consisting of HIF-α and HIF-1β. The alpha subunits are hydroxylated by PHDs under normoxic conditions targeting them for degradation. Under hypoxic conditions, the alpha subunit is not degraded and can therefore dimerize with HIF-1β and bind to HREs within promoters of various genes to activate transcription [112].

Hypoxic stress is known to be a crucial mechanism underlying the transition of tumor cells to a more aggressive phenotype and increased metastasis [112, 113]. This hypoxia-induced aggressiveness is dependent on the activation of genes involved in EMT, including the transcription factors Twist and NF-κB [114], and signal transduction pathways leading to cell migration and invasion [29, 115]. Previous reports using breast and head and neck cancer models have revealed that metastasis is mediated by hypoxia-induced *Twist* activation and that HIF-1α directly activates transcription of *Twist* by binding to the HRE within the *Twist* promoter [116]. NF-κB, a transcription factor whose nuclear translocation is induced by hypoxia [117, 118], has been demonstrated to play a role in the induction and maintenance of EMT in various cancer cell models [119, 120]. The discoveries of molecules such as PKC, which potentiate hypoxia-mediated selection for aggressiveness, have expanded our understanding of the many mechanisms of cancer cell migration and invasion. However, further elucidation of novel proteins and

transduction pathways will ultimately lead to novel diagnostic and therapeutic strategies aimed at targeting cancer metastasis.

Based on our finding of increased KIAA1199 in response to ConA and information from the literature outlined above, we hypothesize that KIAA1199 mediates cancer progression by potentially effecting cancer cell mobility and that a possible mechanism of upregulation in cancer cells could be attributed to hypoxic stress. Unraveling the mechanism(s) of KIAA1199 upregulation in cancer cells and KIAA1199's involvement in cancer progression will have a great impact on our understanding of the transition to a more aggressive phenotype that cancer cells undergo while under stressful conditions within a tumor. The studies present herein can provide insight into new molecular pathways and new potential drug targets for prevention of cancer progression.

1.3 Results

KIAA1199 is Upregulated in Human Cancers and Correlates with Poor Prognosis

In an effort to determine the clinical relevance of KIAA1199 expression in human cancer progression, human breast cancer cells and benign epithelial cells in formalin-fixed, paraffin-embedded (FFPE) specimens isolated using laser capture microdissection (LCM) [121] were examined by our lab. KIAA1199 mRNA was significantly upregulated in both ductal carcinoma in situ (DCIS) and invasive breast cancer cells compared to benign epithelial cells ($p=0.0024$) (Fig. 8A). Using immunohistochemical (IHC) analyses with an anti-KIAA1199 polyclonal antibody (Fig. 8B), high levels of KIAA1199 were detected in the cytoplasm of breast carcinoma cells, whereas minimal to no expression of KIAA1199 was found in adjacent normal epithelial, stromal cells or benign breast tissues (Fig. 8C). Furthermore, IHC analyses using human breast cancer tissue microarrays (US Biomax), which contained a total of 135 samples, revealed a significant difference in KIAA1199 staining in invasive cancer tissue as compared to benign breast tissue samples ($p<0.0001$) (Fig. 8D). However, there was no significant difference between grades of invasive tissue.

To elucidate the clinical significance of KIAA1199 on the survival probability of breast cancer patients, three publicly available DNA microarray datasets [122-124] were analyzed. When these samples were grouped based on KIAA1199 mRNA expression dichotomized at the mean, high KIAA1199 expression inversely correlated with patient survival in all datasets (Fig. 9). Together, these results suggest an important role of KIAA1199 in cancer progression.

Figure 8

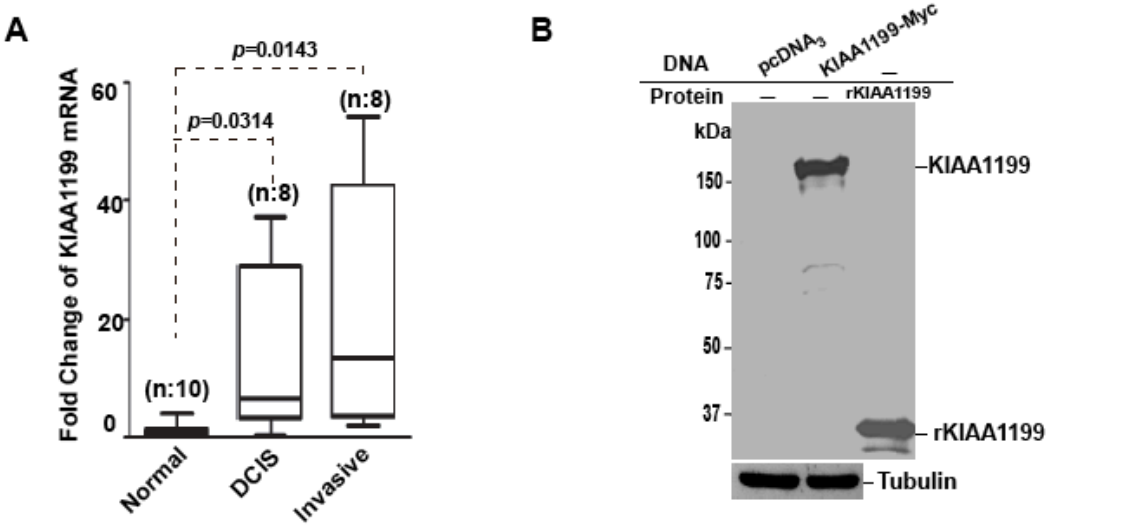

C

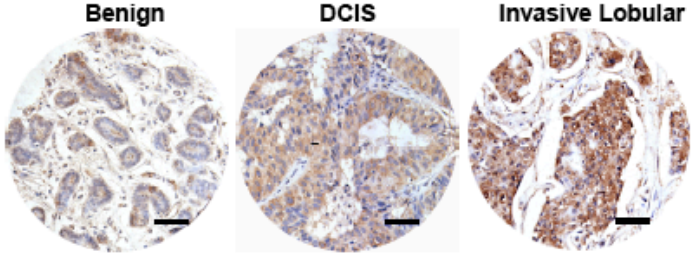

KIAA1199 IHC (p=0.0024)

Intensity / Tissues	+	++	+++
Benign	8	2	-
DCIS	3	4	3
Invasive	-	4	6

D

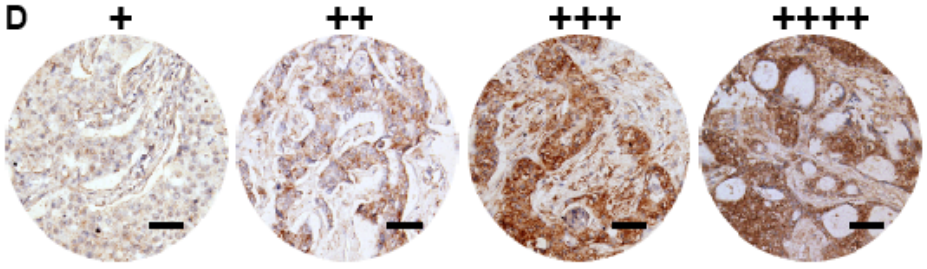

KIAA1199 IHC (p<0.0001)

Intensity / Tissue	+	++	+++	++++
Grade I	-	5	5	6
Grade II	7	27	16	13
Grade III	3	6	5	1
Benign	37	4	-	-

Figure 8 Clinical relevance of KIAA1199 in human breast cancer: (A) KIAA1199 mRNA expression analysis using real-time RT-PCR of RNA isolated from FFPE tissue sections of human DCIS, invasive breast cancer, and benign breast epithelium control by a LCM approach. n=case number. Error bar represents the mean ±SD. Student's two-sided *t*-test was used to assess differences. (B) A polyclonal Ab was generated using recombinant KIAA1199 (rKIAA1199 from Gly^{1108} to Thr^{1340}, 30 kDa) expressed in an *E. coli* system. KIAA1199 in transfected COS-1 cells was detected as a 160 kDa protein. Tubulin was used as a loading control. rKIAA1199 refers to recombinant KIAA1199. (C & D) Tissue distribution of KIAA1199 in breast cancer tissues: Samples from benign breast, DCIS, and invasive ductal and lobular breast cancers tissues (C) and from human breast cancer tissue microarrays containing invasive breast cancers and benign breast tissues (US Biomax Inc.) (D) were examined by IHC with anti-KIAA1199 Ab. Representative images of tissue types (C) and staining intensities of invasive breast cancer tissue array samples (D) are shown. Bar = 50 μm. Overall results summarized in KIAA1199 IHC charts where + indicates intensity level of KIAA1199 staining and the number equals the number of cases with indicated intensity level for each tissue type. *The experiments presented in this figure were performed by Drs. Cem Kuscu and Hoang-Lan Nguyen.

Figure 9

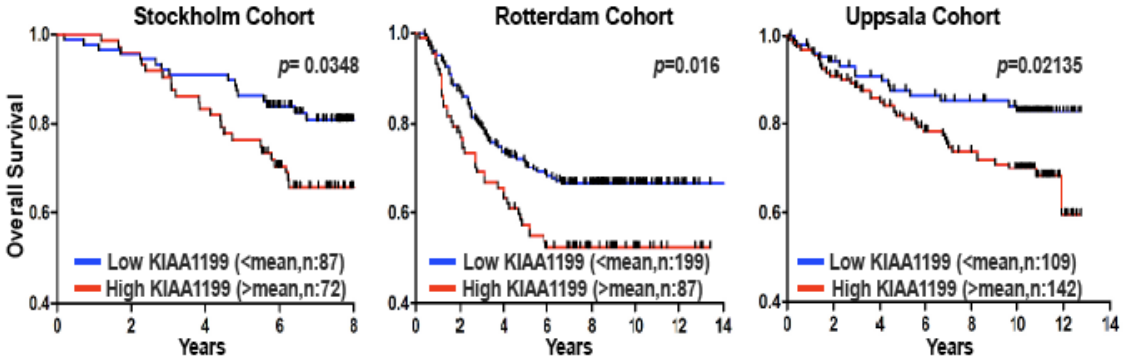

Figure 9 Correlation of patient survival probability: Kaplan-Meier analysis of KIAA1199 expression (DNA microarray data mining) from three cohorts of patients with breast cancer. Log Rank (Mantel Cox) was used to determine statistical significance. *The experiments presented in this figure were performed by Dr. Cem Kuscu.

KIAA1199 is a Novel Cell Migration-Promoting Gene

To unravel the function of KIAA1199 in cancer, we first surveyed KIAA1199 expression in cell lines derived from different cancers. Notably, KIAA1199 is highly expressed in invasive cell lines compared to corresponding minimally invasive lines in all lines tested, which included prostate, breast, and colon cancer lines (Fig. 10A). A targeted gene silencing technique was then employed to silence KIAA1199 in metastatic human

MDA-MB-435 cancer cells [125] (Fig. 10B, C& D), since they were found to express high levels of endogenous KIAA1199 in Fig. 10A. Surprisingly, the KIAA1199-silenced cells gradually changed their morphology from a typical mesenchymal-like shape to a polarized epithelial-like shape (Fig. 10E), which was accompanied by a reorganization of F-actin from stress fibers to a cortical ring-like staining pattern. Further analysis revealed a state of MET as indicated by a decrease in mesenchymal markers (vimentin, N-cadherin, and Twist-1) and an increase in epithelial markers (cytokeratin-8/-18) (Fig. 10F).

Since MET phenotypic changes often result in decreased cell migration, we hypothesized that KIAA1199 may be associated with cancer cell migration. Indeed, silencing of endogenous KIAA1199 resulted in a significant decrease in migratory ability as examined by a Transwell chamber migration assay (Fig. 11A). The migratory ability was rescued by overexpression of KIAA1199 cDNA in the silenced cells (Fig. 11B). Similar morphological and migratory changes were observed in invasive MDA-MB-231 cells expressing KIAA1199 shRNAs (Fig. 11C & D). Additionally, overexpression of KIAA1199 cDNA in minimally invasive MCF-7 cells (Fig. 12A), significantly induced cell migration comparable to that of highly migratory matrix metalloproteinase 14 (MMP-14), a membrane anchored-matrix metalloproteinase, transfected cells (Fig. 12B). This increased migratory ability of MCF-7 cells is correlated with phenotypic changes associated with an EMT as demonstrated by increased mesenchymal markers (Twist-1) and decreased epithelial markers (E-cadherin and cytokeratin-8/-18) in cells stably expressing KIAA1199-GFP (Fig. 12C).

Since cell migration is a critical determinant of invasion, we examined the function of KIAA1199 in cancer invasion using a 3D invasion assay [126]. Silencing of KIAA1199 in MDA-MB-435 cancer cells abrogated invasion into surrounding matrices (Fig. 12D) without notably affecting cell proliferation (Fig. 12E). Collectively, these results from both loss- and gain-of-function studies further support the role of KIAA1199 as a key molecule involved in maintaining an aggressive, mesenchymal phenotype of cancer cells.

Figure 10

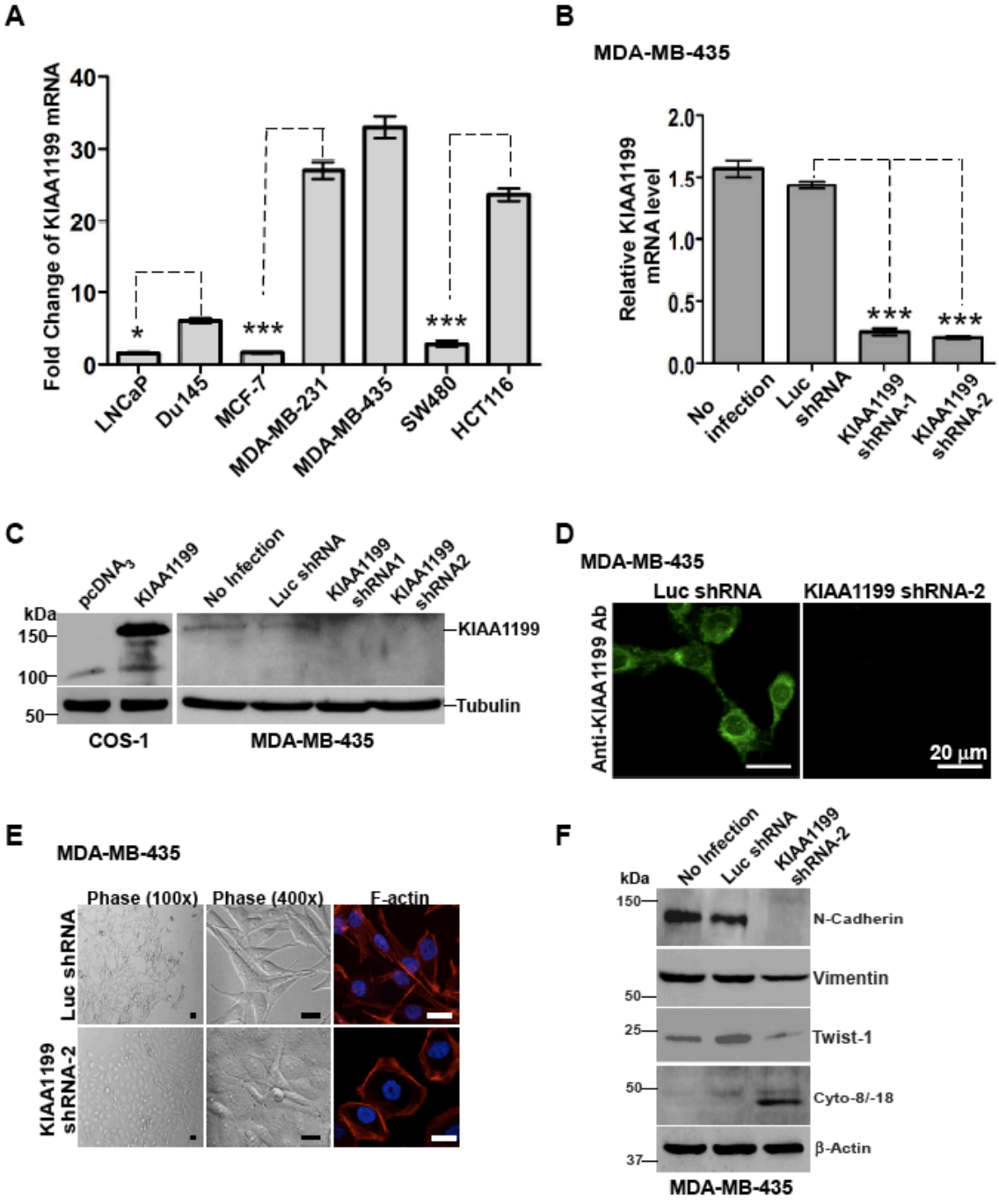

Figure 10 KIAA1199 is involved in maintaining a mesenchymal phenotype: (A) Real-time RT-PCR was used to examine the expression level of KIAA1199 in the following cell lines: minimally invasive LNCaP and invasive DU145 prostate cancer; minimally invasive MCF-7 and invasive MDA-MB-231 breast cancer; invasive MDA-MB-435

cancer; and minimally metastatic SW480 and metastatic HCT116 colon cancer. The relative fold change was normalized to HPRT-1. Error bar represents the mean ±SD. (B) Total RNA was analyzed by real-time RT-PCR using KIAA1199-specific primers. The expression of KIAA1199 was normalized using housekeeping genes HPRT-1. Error bar represents the mean ± SD. (C) Western blotting analysis of luciferase- and KIAA1199-silenced MDA-MB-435 cells confirms knockdown of KIAA1199 endogenous expression. COS-1 cells transfected with vector and KIAA1199 cDNAs were used as controls. Tubulin was used as a loading control. (D) Microscopic examination of immunofluorescent staining of endogenous KIAA1199 in MDA-MB-435 cells expressing Luc shRNA or KIAA1199 shRNA-2 using Abs against KIAA1199. No staining was observed in KIAA199 silenced cells. (E) Morphological examination of MDA-MB-435 cancer cells expressing Luc shRNA control and KIAA1199 shRNA (Phase contrast images). The distribution of filamentous actin in KIAA1199-silenced and control MDA-MB-435 cells was examined by TRITC-Phalloidin staining (F-actin). Scale bars represent 20 μm. (F) Western blotting analysis of total cell lysate from MDA-MB-435 cells (control) or MDA-MB-435 cells expressing Luc or KIAA1199 shRNAs using Abs against EMT markers. β-actin was used as a loading control. *The experiments presented in panels A-D were performed by Drs. Cem Kuscu and Hoang-Lan Nguyen.

Figure 11

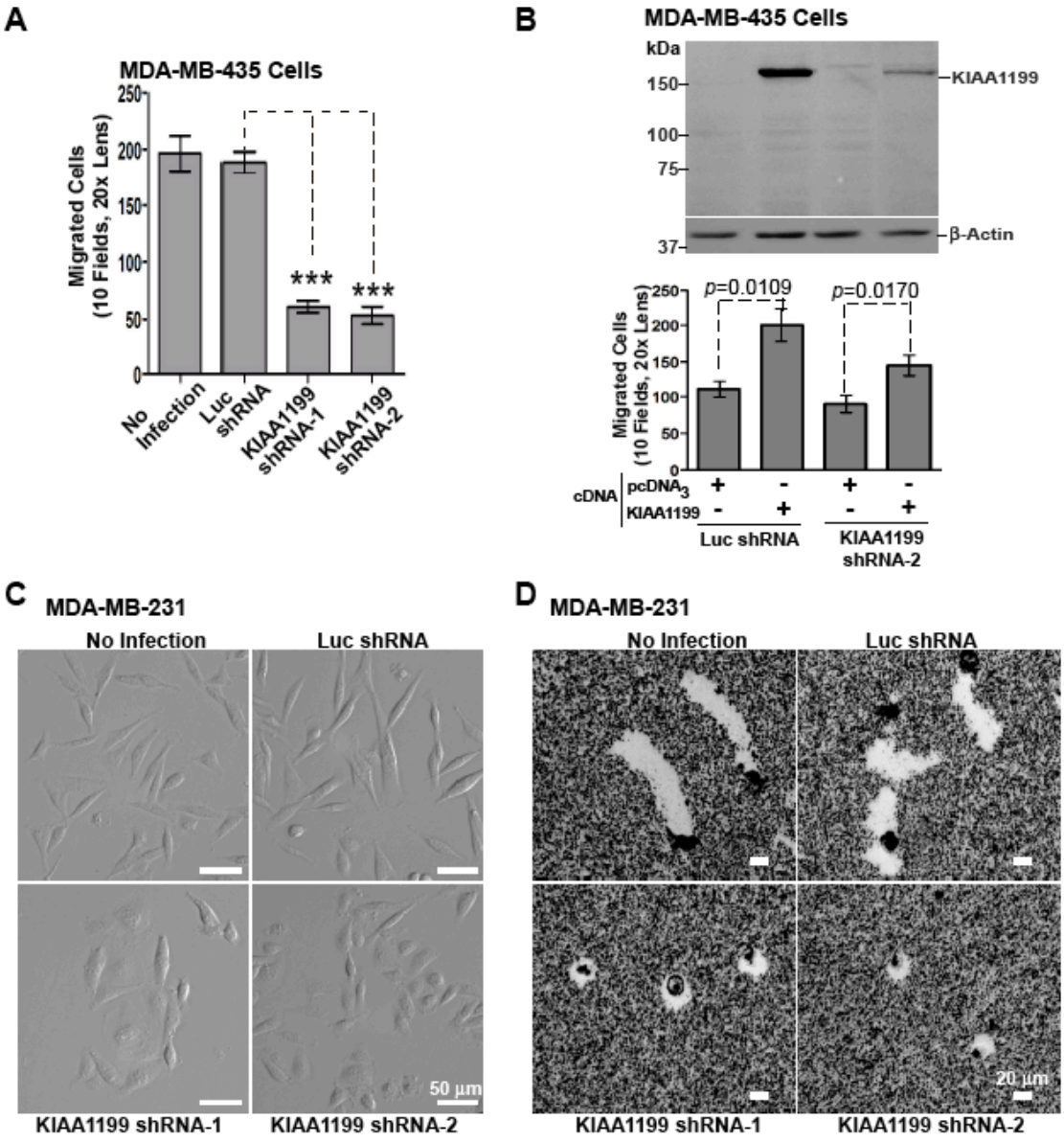

Figure 11 KIAA1199 is a novel cell migration-promoting gene – Loss-of-function: (A) Transwell chamber migration assay performed using MDA-MB-435 cells expressing shRNAs as indicated. Error bar represents the mean ±SEM. (B) Western blotting analysis of Luc- and KIAA1199-silenced cells transiently transfected with KIAA1199 cDNA (Top panel). β-actin was used as a loading control. Cell migratory ability was assessed using Transwell chamber migration assay (Bottom panel). Error bar represents the mean ±SEM. (C) Morphological examination of MDA-MB-231 cancer cells expressing Luc shRNA control and KIAA1199 shRNA (Phase contrast images). (D) A phagokinetic assay performed using Luc- and KIAA1199-silenced cells. *The experiment presented in panel A this figure was performed by Dr. Antoine Dufour.

Figure 12

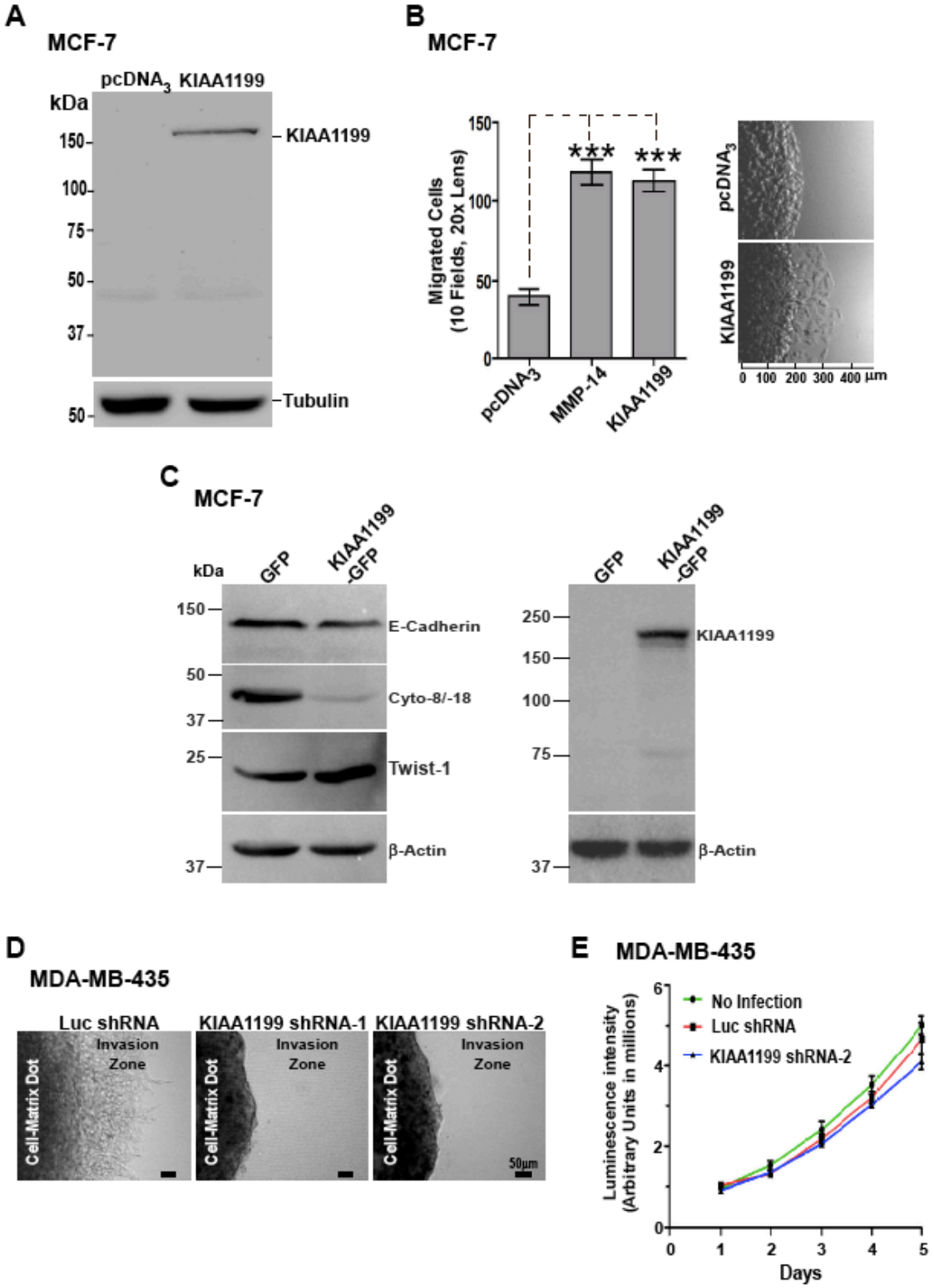

Figure 12 KIAA1199 is a novel cell migration-promoting gene: (A) Expression level of

KIAA1199 in MCF-7 transfected cells shown via western blotting using anti-Myc Ab. Tubulin was used as a loading control. (B) Transwell chamber migration assay performed using MCF-7 cells transfected with cDNAs as indicated (Left panel). Error bar represents the mean ±SEM. The cell migratory ability was also assessed using a dot-based cell migration assay by monitoring cell movement away from the initial dot (Right panel). (C) Western blotting analysis of cell lysates from MCF-7 cells stably expressing either GFP (control) or KIAA1199-GFP cDNAs using Abs against EMT markers and KIAA1199. β-actin was used as a loading control. (D) 3D invasion assay performed in MDA-MB-435 cells expressing shRNAs as indicated. Invaded cells were microscopically determined by monitoring cells movement away from the initial 3D cell-matrix dot. Images represent day 8 under phase contrast microscopy. (E) Cell proliferation assay was performed using MDA-MB-435 cells stably expressing Luc shRNA or KIAA1199 shRNA-2 using CellTiter-Glo over 5 days. Parental cells (No infection) were used as a control. *The experiment presented in panel E was performed by Dr. Cem Kuscu.

KIAA1199 is a Novel ER Resident Protein

To unravel the mechanism underlying KIAA1199-mediated cell migration, we first determined the subcellular localization of KIAA1199 by employing immunostaining and fluorescent tagging approaches. KIAA1199 fused with a green fluorescent protein (GFP) at the C-terminus exhibits a polygonal network of interconnected tube-like structures with lengths ranging from 1 to 2.5 mm when transfected into COS-1 cells, an immortalized monkey kidney epithelial cell line, and co-localizes with calreticulin-OFP, an ER marker fused with orange fluorescent protein (Invitrogen) (Fig. 13A). To rule out the possibility that KIAA1199 ER localization is due to temporal ER retention of the overexpressed proteins, MMP-14-GFP chimera (with signal peptide; plasma membrane localization) and GFP (lacks signal peptide; diffuse throughout cells) were used as controls. The KIAA1199 distribution pattern is distinguishable from GFP and MMP-14 (Fig. 13A). Immunostaining of endogenous KIAA1199 in MDA-MB-435 cells revealed 78.8% co-localization with protein disulfide-isomerase (PDI), another well characterized ER marker (Fig. 13B). No staining was observed in KIAA1199-silenced MDA-MB-435 cells demonstrating specificity of the anti-KIAA1199 antibody as shown in Fig. 10D. Detection of KIAA1199 in the membrane fraction but absence of KIAA1199 in cytosolic, nuclear, and cytoskeletal fractions of MCF-7 cells stably expressing KIAA1199-Myc further strengthens the ER localization data (Fig. 13C). This characteristic ER staining

pattern, along with the absence of nuclear staining, is also observed in transfected COS-1 and MCF-7 examined by immunostaining (Fig. 13D).

Figure 13

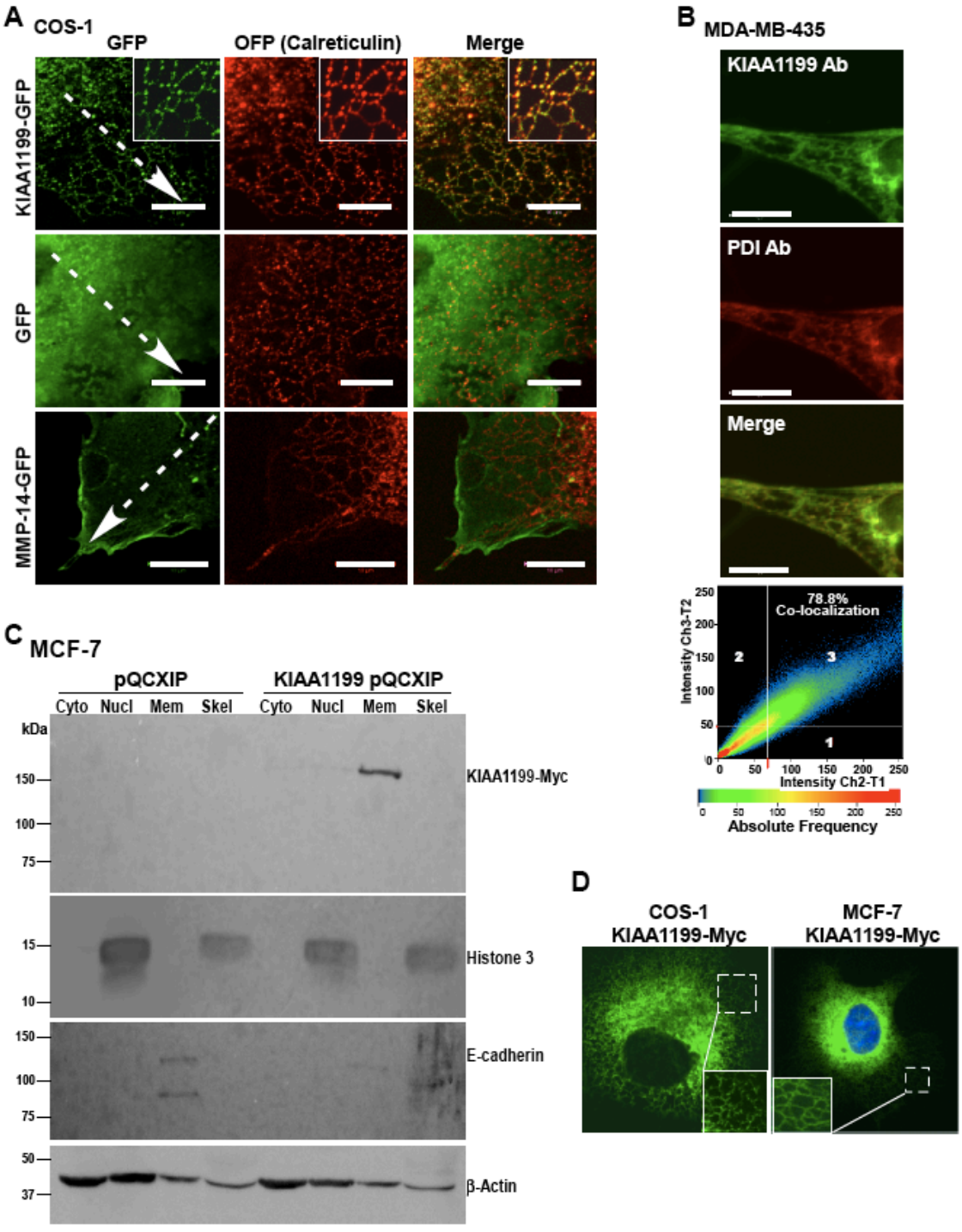

Figure 13 Cellular localization of KIAA1199: (A) Microscopic determination of KIAA1199 cellular localization using Calreticulin-OFP expressing-COS-1 cells transfected with GFP, MMP-14-GFP, and KIAA1199-GFP chimeric cDNAs. Dashed arrow lines represent orientation from nucleus to plasma membrane. Inserts represent enlarged areas showing polygonal meshwork. Bar: 10 μm. (B) Confocal microscopic examination of immunofluorescent staining of endogenous KIAA1199 in MDA-MB-435 cancer cells using Abs against KIAA1199 and PDI (Top panel). 78.8% colocalization was found between KIAA1199 and PDI staining using Zeiss LSM 3.2 software (Bottom panel). Images represent part of the cell to display ER polygonal meshwork. Bar: 10 μm. (C) Western blotting analysis of fractionated cell lysates from MCF-7 stable cells using anti-Myc Ab. Anti-histone 3 Ab used as a control for nuclear fraction and E-cadherin Ab used as control for membrane fraction. β-actin was used as a loading control. Cyto-cytosolic, Nucl-nuclear, Mem-membrane, Skel-skeletal. (D) Immunofluorescent staining of COS-1 and MCF-7 cells transfected with KIAA1199 using anti-Myc Ab. The nucleus in MCF-7 cells was stained with DAPI. Images represent the whole cell and inserts were used to display ER polygonal meshwork. Bar: 10 μm.

KIAA1199 is Retained in ER Compartment by Interacting with GRP78/BiP

Since KIAA1199 lacks an ER retention signal (KDEL), we investigated the requirement for a specific region of KIAA1199 for ER retention. A series of KIAA1199 deletion mutants with a C-terminal Myc tag, which allows for detection of mutants regardless of loss of epitope, was generated (Fig. 14A). ER retention was assessed based on the release of recombinant protein to the extracellular medium. As shown in Figure 14B, deletion from amino acid 296 (KIAA1199$^{\Delta B}$), resulted in secretion of the mutant. However, mutant KIAA1199$^{\Delta D}$, which is deleted from amino acid 591, is retained within the cell, indicating that the motif spanning Ala295 to Thr591 (termed the B domain) is required for KIAA1199 ER retention. Deletion from the C-terminal half of the B-domain (KIAA1199$^{\Delta C}$-Myc) resulted in partial secretion of the protein.

The requirement of the B-domain in ER retention of KIAA1199 was further evaluated by fusing the B-domain to the C-terminus of an unrelated secretory protein, soluble MMP-14 (SolMMP14), an MMP-14 mutant that lacks the transmembrane and cytoplasmic domains (SolMMP14-B) [127]. Secretion of SolMMP14 was disrupted by addition of the B-domain as shown in COS-1 cells transfected with SolMMP14-B cDNA (Fig. 14C). Furthermore, SolMMP14-B chimera exhibits a meshwork-staining pattern that is distinguishable from wild-type and SolMMP-14 cellular distributions (Fig. 14D).

However, retention of SolMMP14 in the ER was unable to induce cell migration comparable to wild-type MMP-14 (Fig. 14E). Taken together, our data suggest that although the B domain is necessary for KIAA1199 ER retention, it alone is insufficient for increased cell migration.

Figure 14

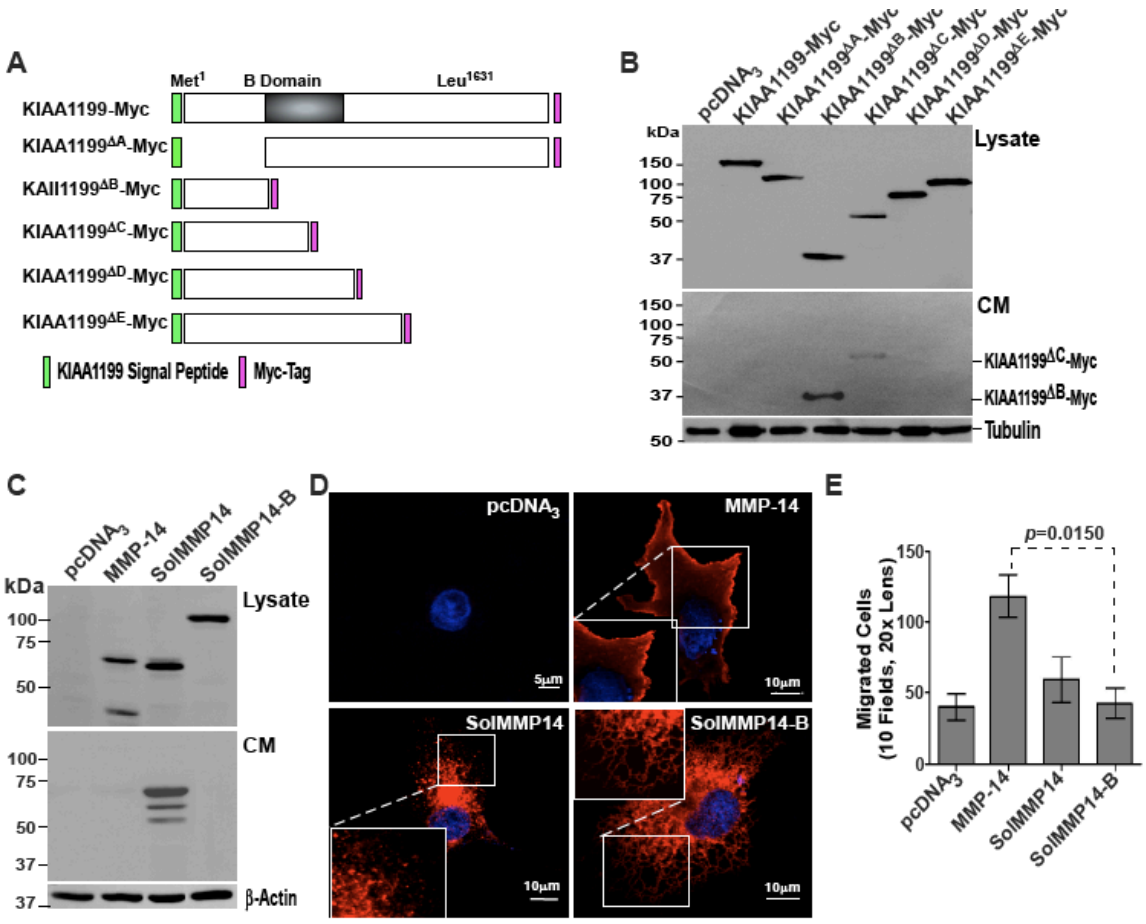

Figure 14 ER retention of KIAA1199 via B-domain: (A) A schematic diagram of deletion mutants of KIAA1199. KIAA1199 signal peptide (green box) and a Myc tag (pink box). (B) Western blotting analysis of TCA-precipitated conditioned media (CM) and cell lysates from COS-1 cells transfected with the series of KIAA1199 deletion mutants using anti-Myc Ab. Tubulin was used as a loading control. (C) Western blotting analysis of TCA-precipitated CM and cell lysate in COS-1 cells transfected with cDNA as indicated using anti-MMP-14 Ab. β-actin was used as a loading control. (D) Immunostaining of COS-1 cells transfected with cDNA as indicated using anti-MMP-14 Ab. Inserts represent an enlarged area for detailed structures. (E) Transwell chamber migration assay of COS-1 cells transfected with cDNAs as indicated. Error bar represents the mean ±SEM. *The experiments presented in panel A-B this were performed with help from Kevin Zarrabi.

To investigate the mechanism of KIAA1199 ER retention, a SNAP-tag pull-down assay followed by proteomic analysis was performed. The ER chaperone protein, GRP78/BiP, was specifically pulled down by KIAA1199 (Table 1).

Table 1: SNAP-tag Pull Down

Protein	Peptides	Sequence Coverage	Total of Spectra	SNAP	KIAA1199-SNAP
KIAA1199 Isoform 1 of protein KIAA1199	116	65.40%	707	0	164
P11021 HSPA5 HSPA5 protein*	29	57.40%	161	0	49

*HSPA5 = GRP78/BiP

The authenticity of this interaction was verified by co-immunoprecipitation showing that wild-type, but not KIAA1199$^{\Delta B}$, co-precipitated with BiP in transfected COS-1 cells (Fig. 15A). To rule out the possibilities that the KIAA1199-BiP interaction is a consequence of BiP's chaperone function or role in degradation of misfolded proteins in response to ER stress, a series of experiments was performed. First, to ensure expression of KIAA1199 and interaction with BiP does not induce a global shut down of protein synthesis in response to ER stress, total protein synthesis was measured using serum-starved, ^{35}S-methionine/cysteine labeled COS-1 cells 48 hrs post-transfection with KIAA1199 or vector control cDNA. Thapsigargin (TG), an ER stress-inducing agent, decreased global protein synthesis, while no difference in total protein level was observed between vector control and KIAA1199 expressing cells (Fig. 15B). The induction of XBP-1 protein expression, an ER stress marker, was then analyzed via Western blotting. XBP-1 was detected in cells treated with TG, but not in KIAA1199-expressing cells (Fig. 15C). Since BiP transiently binds to nascent or misfolded proteins for periods of time until completion of folding or degradation of the protein, the stability of the interaction was also assessed. BiP was specifically pulled down in KIAA1199-SNAP expressing COS-1 cells following 16 hrs of treatment with cycloheximide (CHX), a protein synthesis inhibitor, indicating a stable rather than transient interaction between KIAA1199 and BiP (Fig. 15D). To ascertain the stability of KIAA1199 a CHX half-life experiment was performed. KIAA1199-SNAP was not detected in the conditioned media (CM),

indicating retention of KIAA1199 within the cell, compared to increased solMMP14 in the CM following CHX treatment. No significant decrease in KIAA1199 protein level was observed within the 24hrs, suggesting that KIAA1199 is not degraded as a misfolded (Fig. 15E). Collectively, these data suggest that the KIAA1199-BiP interaction is not due to BiP's role as a chaperone protein.

Figure 15

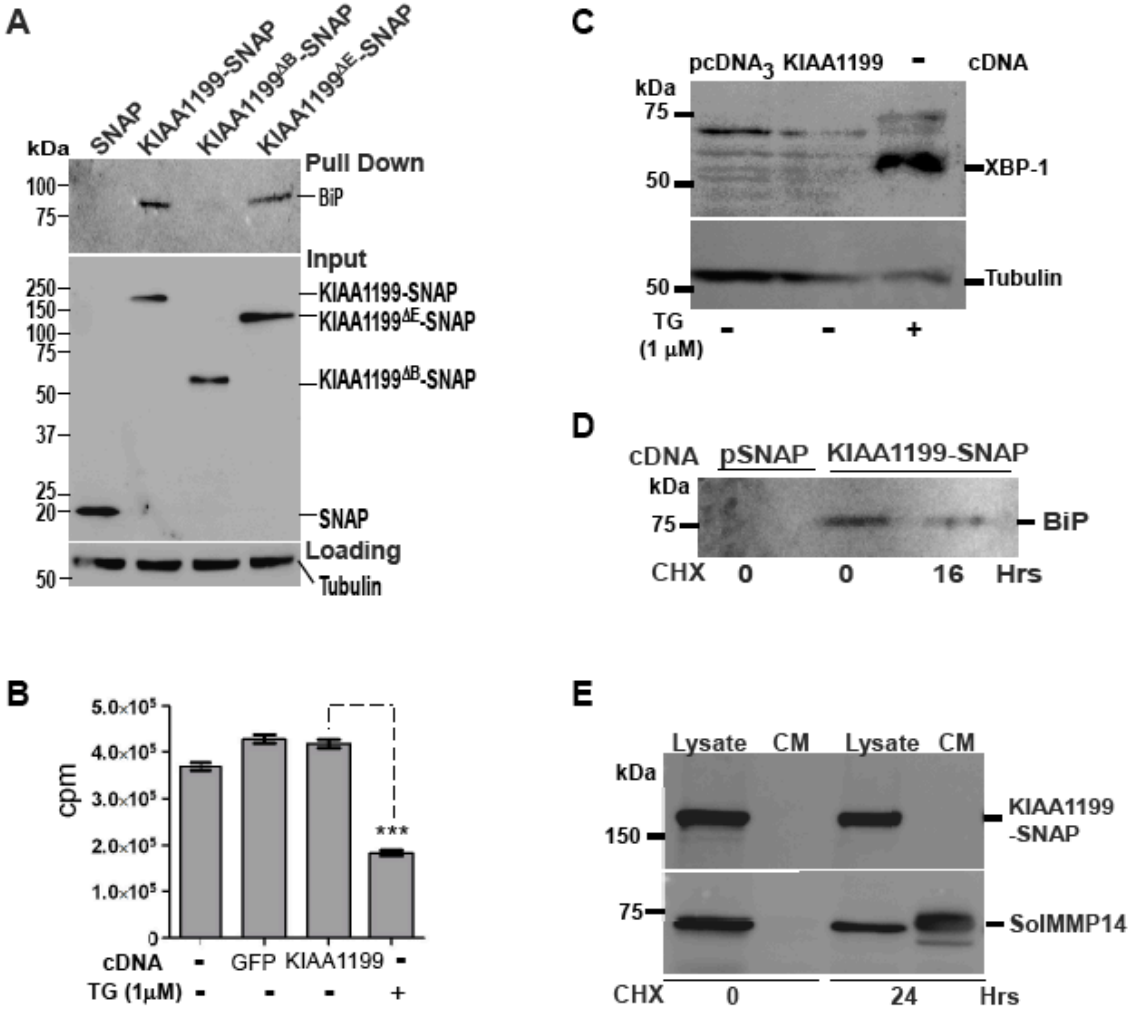

Figure 15 KIAA1199 interaction with BiP does not result in ER stress: (A) SNAP pull-down assay using COS-1 cells transfected with cDNA as indicated followed by Western blotting analysis (Top panel). Input (SNAP Ab, Middle panel) and loading controls (tubulin Ab, Bottom panel) were examined by Western blotting. (B) Total protein synthesis was measured using serum-starved, ^{35}S-methionine/cysteine labeled COS-1 cells 48 hrs post-transfection with KIAA1199 or vector control cDNA. COS-1 cells treated with TG were used as a positive control. (C) Western blotting analysis of XBP-1

expression in MCF-7 cells transiently transfected with KIAA1199 or vector control cDNA, or treated with 1 μm TG for 6 hrs. (D) SNAP pull down assay followed by Western blotting analysis with lysates from KIAA1199-SNAP expressing COS-1 cells treated with 10 mg/mL of CHX. COS-1 cells expressing pSNAP vector were used as a control. (E) Western blotting analysis of lysate and TCA precipitated CM from COS-1 cells transfected with KIAA1199-SNAP or solMMP14 cDNA treated with 10 mg/mL CHX for 24 hrs.

Since BiP has been shown to enhance cell migration and metastasis [67, 128], the role of the KIAA1199-BiP interaction in cell migration was examined by transiently silencing BiP using a shRNA approach (Fig. 16A). KIAA1199-mediated cell migration was abrogated in BiP-silenced COS-1 cells expressing KIAA1199 cDNA (Fig. 16B). No effect on $pcDNA_3$ vector control cell migration was observed upon knockdown of BiP indicating that the effect observed was specific to KIAA1199-enhanced migration. In support of this, COS-1 cells overexpressing $KIAA1199^{\Delta B}$, which failed to interact with BiP, resulted in no enhancement of cell migration (Fig. 16C). Taken together, these data indicate that KIAA1199 forms a stable complex with BiP, leading to ER retention and cell migration.

Figure 16

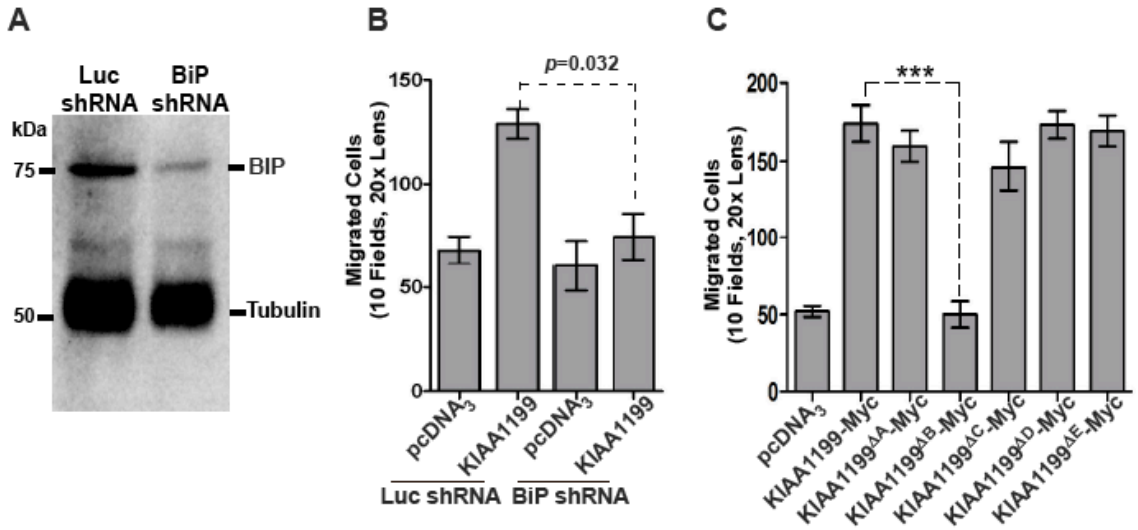

Figure 16 ER retention of KIAA1199 via BiP interaction is required for migration: (A) Western blotting analysis of whole cell lysates from COS-1 cells infected with retrovirus encoding luciferase (Luc) shRNA control or BiP shRNA. Tubulin was used as a loading control. (B) Transwell chamber migration assay using COS-1 cells transiently expressing BiP or Luciferase (Luc) shRNA along with vector $pcDNA_3$ and KIAA1199 cDNAs.

Error bar represents the mean ±SEM. (C) Transwell chamber migration assay using COS-1 cells transfected with mutant KIAA1199 cDNAs as indicated. Error bar represents the mean ±SEM. *The experiment presented in C was performed with help from Dr. Antoine Dufour and Kevin Zarrabi.

KIAA1199-Induced Cell Migration Involves a Cascade of KIAA1199-BiP-ER Calcium Release-PCKα

Based on the role of BiP in calcium homeostasis and the regulation of cell migration by calcium signaling [83, 86, 129], we analyzed cytosolic calcium (Ca^{2+}) levels in KIAA1199-expressing cells. Using flow cytometry to analyze cells loaded with the Ca^{2+}-sensitive dye Calcium Green-1AM, we observed an increase in the percentage of cells exhibiting an elevated level of cytosolic Ca^{2+} in COS-1 cells transfected with KIAA1199 cDNA compared to control cells expressing vector, MMP-14, or an engineered ER-resident protein (a chimera of SolMMP14 and the KDEL motif), (Fig. 17A & B). Increased cytosolic Ca^{2+} was further confirmed using Fura-2AM and spectrofluorometry in both COS-1 and MCF-7 cells stably expressing KIAA1199 (Fig. 17C).

Since KIAA1199 is localized in the ER and interacts with BiP, we hypothesized that the increased cytosolic Ca^{2+} is due to Ca^{2+} leakage from ER stores. To test this hypothesis, we performed fluorescence resonance energy transfer (FRET) using the ER-targeted Ca^{2+} sensor, D1ER, a cameleon that consists of fusions of CFP and YFP separated by Ca^{2+}-responsive elements[130]. A significantly diminished level of ER Ca^{2+}, as evidenced by a lower YFP/CFP ratio, was found in both COS-1 and MCF-7 cells stably expressing KIAA1199 as compared to pQCXIP vector control cells (Fig. 18A).

To link KIAA1199-induced cytosolic Ca^{2+} increase with enhanced cell migration, the intracellular Ca^{2+} chelator BAPTA-AM was used in a cell migration assay. Treatment of COS-1 stable cells with BAPTA-AM significantly reduced KIAA1199-mediated cell migration but had little effect on control cell migration (Fig. 18B). Similar results were obtained using MCF-7 stable cells (Fig. 18C). These results suggest that the KIAA1199-induced ER Ca^{2+} leakage, leading to elevated cytosolic Ca^{2+}, is required for the enhanced cell migration.

Figure 17

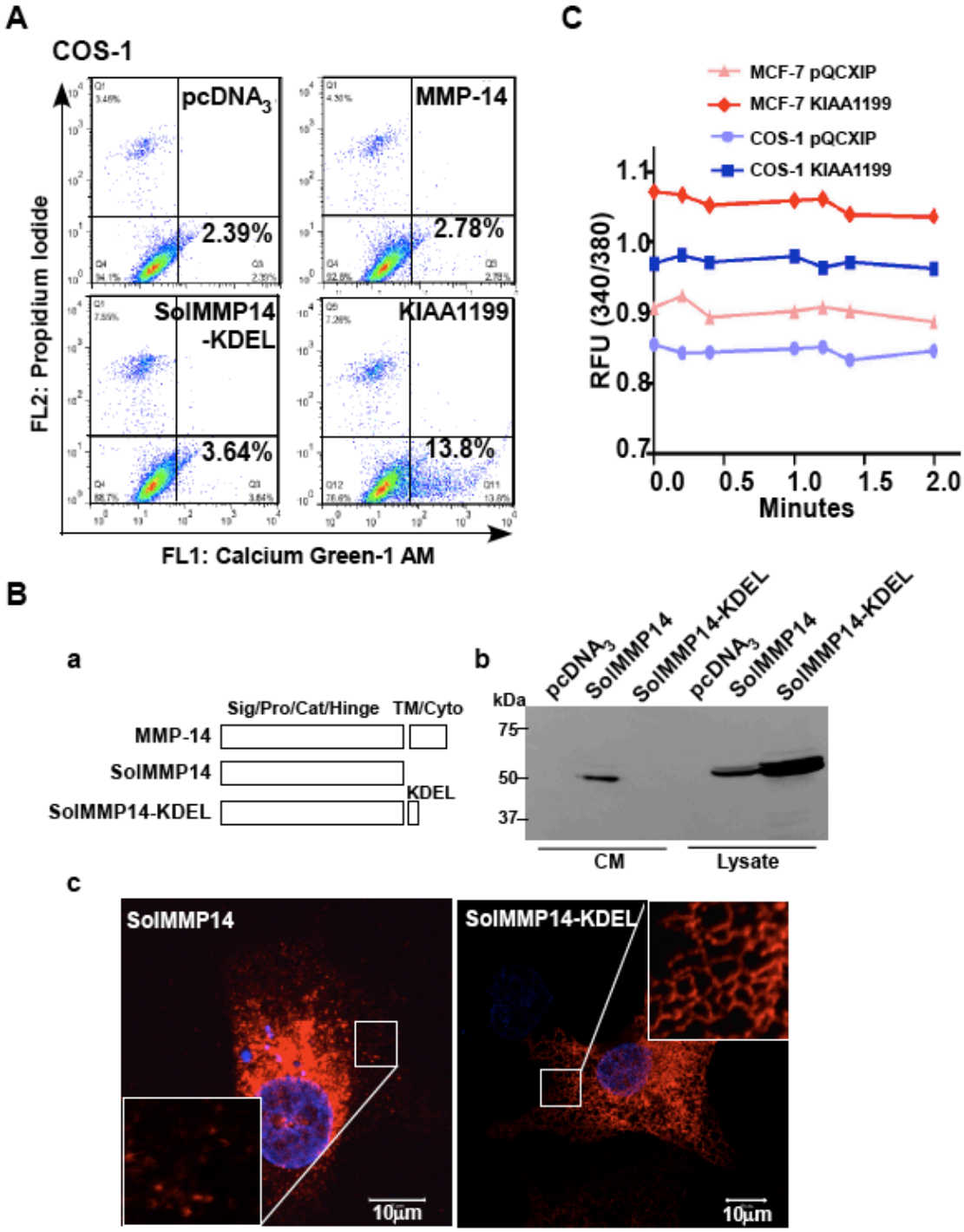

Figure 17 KIAA1199 expression in the ER results in increased cytosolic Ca^{2+}: (A) Flow cytometry of cytosolic Ca^{2+} in COS-1 transfected cells loaded with Calcium Green1-AM and propidium iodide (PI). Vector, plasma membrane anchored MMP-14, and ER-

retained soluble MMP-14 were used as controls. (B) a. A schematic diagram of MMP-14, soluble MMP-14 (SolMMP14) and KDEL linked SolMMP14. The ER retention signal (KDEL) was fused to the C-terminus of SolMMP14 cDNA that lacks the transmembrane and cytoplasmic domains to generate SolMMP14-KDEL chimeric cDNA. b. CM and whole cell lysates from COS-1 cells transfected with indicated cDNAs were analyzed by Western blotting using anti-MMP-14 Ab. c. Immunofluorescent staining of transfected COS-1 cells using anti-MMP-14 hinge Ab. Inserts are enlarged images. (C) Spectrofluorometry of cytosolic Ca^{2+} in FURA-2AM-loaded COS-1 and MCF-7 cells stably expressing KIAA1199 or pQCXIP vector control cDNA. The ratios of the fluorescence intensities (emission at 340/380 nm; Ca^{2+} bound/unbound) were plotted against time. RFU: relative fluorescence units.

To elucidate the signaling cascade of KIAA1199-induced cell migration, an antibody array was performed (Kinex Microarray). The array revealed a significant increase in the Thr^{674} phosphorylated form of the protein kinase Cγ isoform (PKCγ) in MCF-7 cells stably expressing KIAA1199 cDNA as compared to vector control (data not shown) using an antibody that cross-reacts with the phosphorylated PKCα, βI, and γ isoforms (Invitrogen). Validation of the array was demonstrated by increased phosphorylation of PKC in whole cell lysates of KIAA1199-expressing MCF-7 stable cells using the cross-reactive Ab (Fig. 19A). Immunostaining revealed a redistribution of PKC from the cytosolic compartment in control cells to the plasma membrane in KIAA1199-expressing cells (Fig. 19B).

Since this translocation of PKC to the plasma membrane is required for activation and function of PKCs [131], crude membrane fractions were analyzed using pan-specific antibodies to determine which cross-reacting PKC isoform(s) is specifically translocated in KIAA1199-expressing cells. PKCα showed increased membrane localization in KIAA1199-expressing MCF-7 stable cells as compared to control cells (Fig. 19C, top panel). Furthermore, decreased membrane localization of PKCα was observed upon silencing of KIAA1199 in MDA-MB 231 cells (Fig. 19C, bottom panel), which is consistent with the decreased migratory capacity of these cells (Fig. 11D). Neither the βI nor γ isoforms were detected (Fig. 20); these results agree with reports showing no βI or γ expression in MCF-7 cells [132].

Figure 18

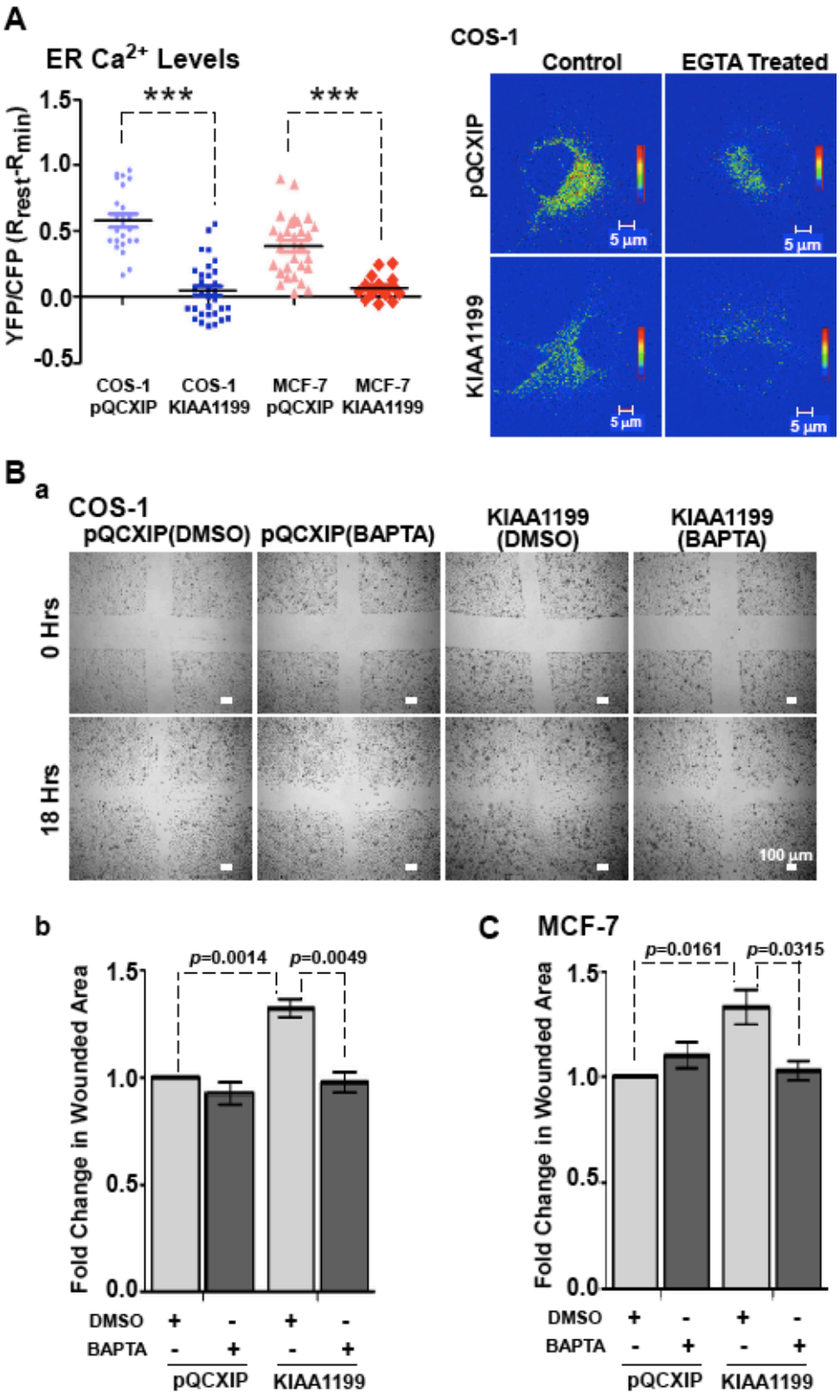
A
ER Ca2+ Levels
YFP/CFP (Rrest-Rmin)
1.5
1.0
0.5
0.0
-0.5
***
***
COS-1 pQCXIP
COS-1 KIAA1199
MCF-7 pQCXIP
MCF-7 KIAA1199
COS-1
Control
EGTA Treated
pQCXIP
KIAA1199
5 µm
B
a
COS-1
pQCXIP(DMSO)
pQCXIP(BAPTA)
KIAA1199 (DMSO)
KIAA1199 (BAPTA)
0 Hrs
18 Hrs
100 µm
b
Fold Change in Wounded Area
p=0.0014
p=0.0049
DMSO
BAPTA
pQCXIP
KIAA1199
C
MCF-7
p=0.0161
p=0.0315

Figure 18 KIAA1199 expression in the ER results in ER Ca^{2+} release and increased cytosolic Ca^{2+} leading to enhanced cell migration: (A) FRET analysis for determination of ER Ca^{2+} level in pQCXIP vector and KIAA1199 stably expressing COS-1 and MCF-7 cells transfected with D1ER cDNA. Ratio of YFP/CFP was determined by measuring individual cells. pQCXIP: COS-1 n=23 and MCF-7 n=29; KIAA1199: COS-1 n=32 and MCF-7 n=16 (Left panel). R_{min} was determined by treating cells with 3 mM EGTA + 2 mM ionomycin. The images show representative cells taken by a two-photon confocal microscope (Right panel). (B & C) a. Scratch wound healing assay for assessing the effect of BAPTA-AM on KIAA1199-mediated COS-1 and MCF-7 stable cell migration. Representative images of COS-1 cells are shown in Bb. Quantification of fold change in wounded area was analyzed using NIS Elements software (Nikon) (Bb-COS-1, C-MCF-7). Error bar represents the mean ±SEM.

Figure 19

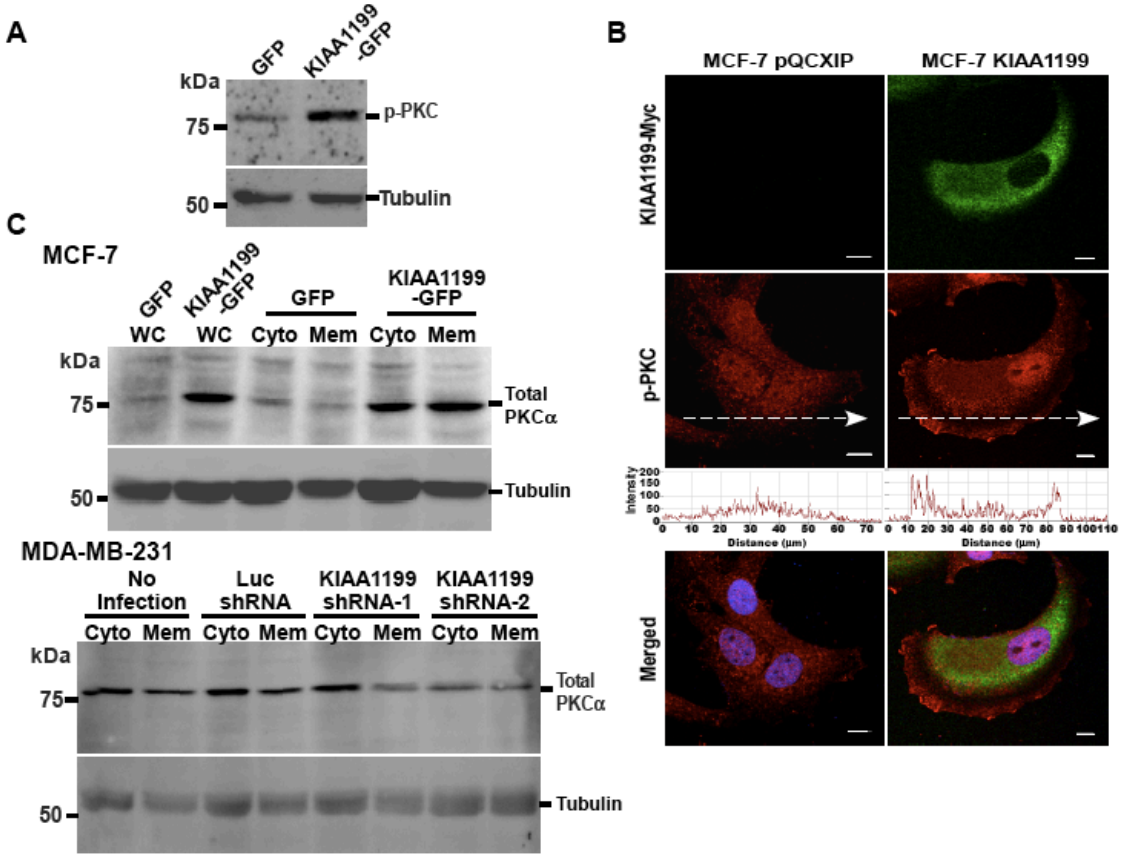

Figure 19 KIAA1199 expression leads to PKCα translocation/activation: (A) Western blotting analysis of MCF-7 cells stably expressing vector control or KIAA1199 cDNAs using non-selective phospho-PKCγ Ab. (B) Immunofluorescence staining of MCF-7 cells stably expressing vector control or KIAA1199 using anti-phospho-PKCγ Ab. The signal strength of fluorescence was scanned along the white arrow lines. Graphs were plotted using Metamorph software. Bar: 10 μm. (C) Western blotting analysis of whole cell (WC) and fractionated cell lysates (C-cytosolic; M-membrane) of MCF-7 stable cells

(Top panel) and fractionated cell lysates from MDA-MB 231 wild-type (WT), Luc shRNA, and KIAA1199 shRNA-1 and -2 cells (Bottom panel) using anti-pan PKCα Ab. Tubulin was used as a loading control.

Figure 20

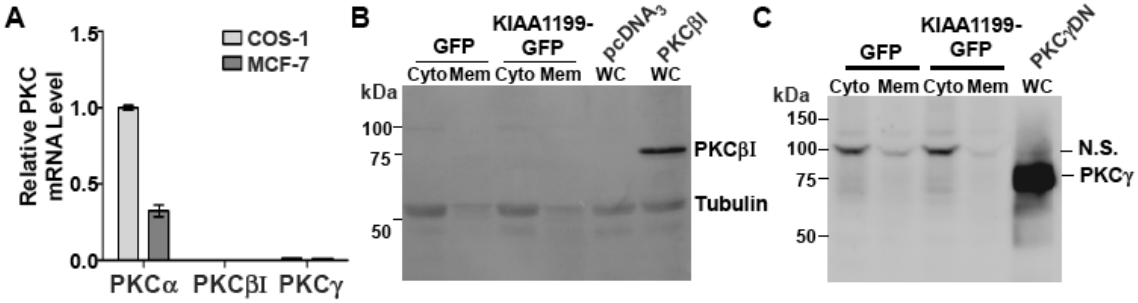

Figure 20 Neither the βI nor the γ isoform of PKC is involved in KIAA1199-mediated migration: (A) Total RNAs extracted from MCF-7 and COS-1 cells were analyzed by real-time RT-PCR using primers specific for PKCα, βI and γ isoforms. Expression levels were normalized using housekeeping gene HPRT-1. Error bar represents the mean ± SD. (B, C) Fractionated cell lysates from MCF-7 stable cells were examined via Western blotting using anti-pan PKCβI (B) or anti-pan PKC γ (C) Abs. Whole cell lysate from COS-1 cells transfected with PKCβI cDNA or PKCγ^{K380R} cDNA was used as positive controls for detection of PKCβI or PKCγ, respectively. Tubulin (B) or non-specific bands (C) were used as loading controls.

Increased PKCα membrane localization was also recapitulated in KIAA1199-stably expressing COS-1 cells (Fig. 21A). Incubation of these cells with BAPTA-AM substantially diminished membrane-associated PKCα (Fig. 21A), which was also observed in MCF-7 stable cells (data not shown). These data demonstrate a functional link between increased cytosolic Ca^{2+} and PKCα activation. To examine whether PKCα is required for KIAA1199-mediated migration, PCKα was silenced in COS-1 cells using a shRNA approach. Decreased PKCα mRNA and protein expression were verified in cells infected with PKCα shRNA (Fig. 21B-a & b). Silencing of PKCα diminished KIAA1199-enhanced cell migration (Fig. 21B-c), confirming the cascade of KIAA1199-BiP-ER calcium leakage-PKCα in KIAA1199-mediated cell migration.

Figure 21

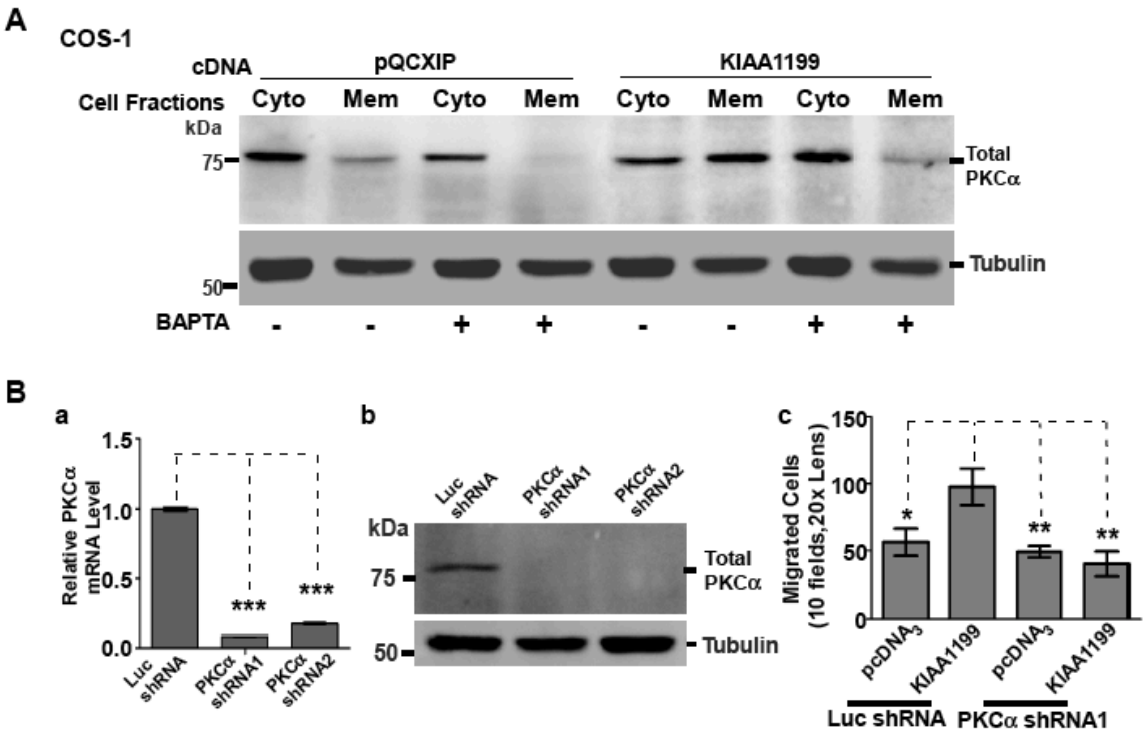

Figure 21 KIAA1199-mediated cell migration involves a signaling cascade of KIAA1199-BIP-ER calcium release-PKCα: (A) Western blotting analysis of fractionated cell lysates of COS-1 stable cells treated with DMSO or BATPA-AM using anti-pan PKCα Ab. Tubulin was used as a loading control. (B) Real-Time RT-PCR (a) and Western blotting analyses (b) of PKCα in COS-1 cells expressing shRNAs against luciferase or PKCα. c. Effect of silencing PKCα in COS-1 cells transfected with KIAA1199 or vector control on cell migration was examined by a Transwell chamber migration assay. Error bar represents the mean ±SD.

Mechanism of Upregulated KIAA1199 in Cancer: Hypoxia Results in Upregulation of KIAA1199 in Cancer Cells

This discovery of KIAA1199's critical role in cancer cell migration provides new insight into the driving force behind the increased expression level of KIAA1199 observed in various cancer cell lines and cancer tissues and as well as the inverse correlation with patient survival. However, questions still remain regarding the mechanism of upregulation of this gene in cancer cells. It is well known that hypoxia, or low oxygen tension, within tumors creates a natural selection process wherein more

aggressive cancer cells survive better. Since hypoxia is one of the most common stressors experienced by cells within solid tumors [106], and a correlation between KIAA1199 expression and hypoxic conditions was observed via microarray [133], we sought to determine whether hypoxia could cause induction of KIAA1199. To this end, a hypoxic model was established using a hypoxic chamber (1% O_2) and verified by measuring three intrinsic markers of hypoxia– VEGF secretion (by ELISA) and hypoxia-inducible factor-1α and -2α (HIF-1α and -2α) accumulation (by Western blot) (Fig. 22A-C). HeLa cells, a human epithelial cervical cancer cell line, were used as they are known to respond to hypoxic stress by induction of both HIF isoforms.

Figure 22

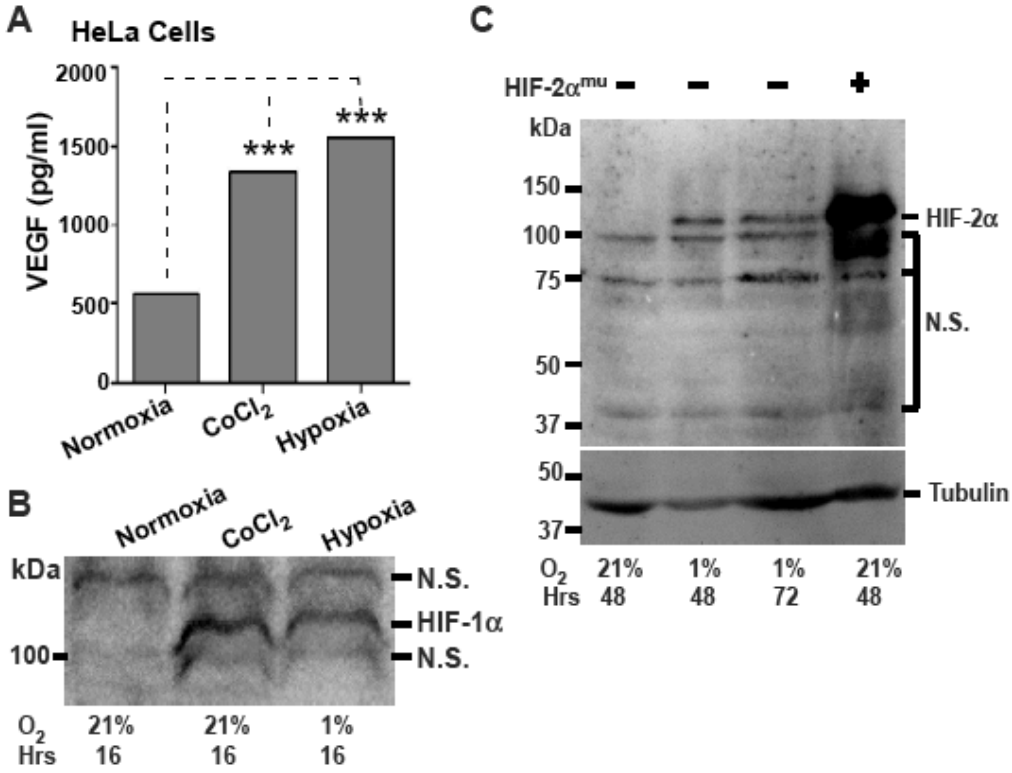

Figure 22 Verification of hypoxic conditions (1% O_2): HeLa cells were cultured under normoxic and hypoxic conditions for indicated times. The CM and cell lysates were examined by ELISA for VEGF secretion (A) and Western blotting for HIF-1α (B) and -2α (C), respectively. $CoCl_2$ treatment was used as a positive control. Constitutively active HIF-2α mutant (HIF-$2\alpha^{mu}$) cDNA was used for a HIF-2α control in Panel C. Either non-specific (N.S.) bands or tubulin was used as a loading control.

To begin to answer this question MCF-7 cells, which have a low mRNA level of KIAA1199 (Fig. 10A), were cultured under hypoxic or normoxic conditions for 4 days. RNA was analyzed using real-time RT-PCR with KIAA1199-specific primers. Hypoxia significantly enhanced KIAA1199 expression compared to cells cultured under normoxic conditions (Fig. 23A). This observation was also seen in HeLa cells after 48 hrs of hypoxia (Fig. 23B). Since both HIF-1α and -2α were stabilized under hypoxia (Fig. 22), two constitutively active HIF mutants, HIF-1α $^{P402A/P564A}$ (HIF-1α ^{mu}) and HIF-2α $^{P405A/P531A}$ (HIF-2α ^{mu}), which are resistant to hydroxylation under normoxic conditions [134, 135], were used to pinpoint which isoform is specifically required for hypoxia-induced KIAA1199 expression. MCF-7 cells transfected with HIF-2α ^{mu}, but not HIF-1α ^{mu} or vector control cDNA, displayed significantly elevated KIAA1199 expression as measured by real-time RT-PCR (Fig. 23C). Similar results were observed upon overexpression of HIF-2α ^{mu} in HeLa cells (Fig. 23D). These results suggest that HIF-2α is primarily responsible for upregulated KIAA1199 under hypoxic conditions. To determine whether the upregulation of KIAA1199 mRNA was due to enhanced KIAA1199 promoter activity, a pGL3-based luciferase reporter construct containing the characterized 1.4 kb KIAA1199 promoter [27] was utilized. Co-transfection of COS-1 cells with the KIAA1199-reporter construct and the HIF-2α ^{mu} cDNA resulted in an increase in KIAA1199 promoter activity (Fig. 23E). No significant induction of promoter activity was observed in cells expressing either vector or HIF-1α ^{mu} even at the highest amount of cDNA tested.

Figure 23

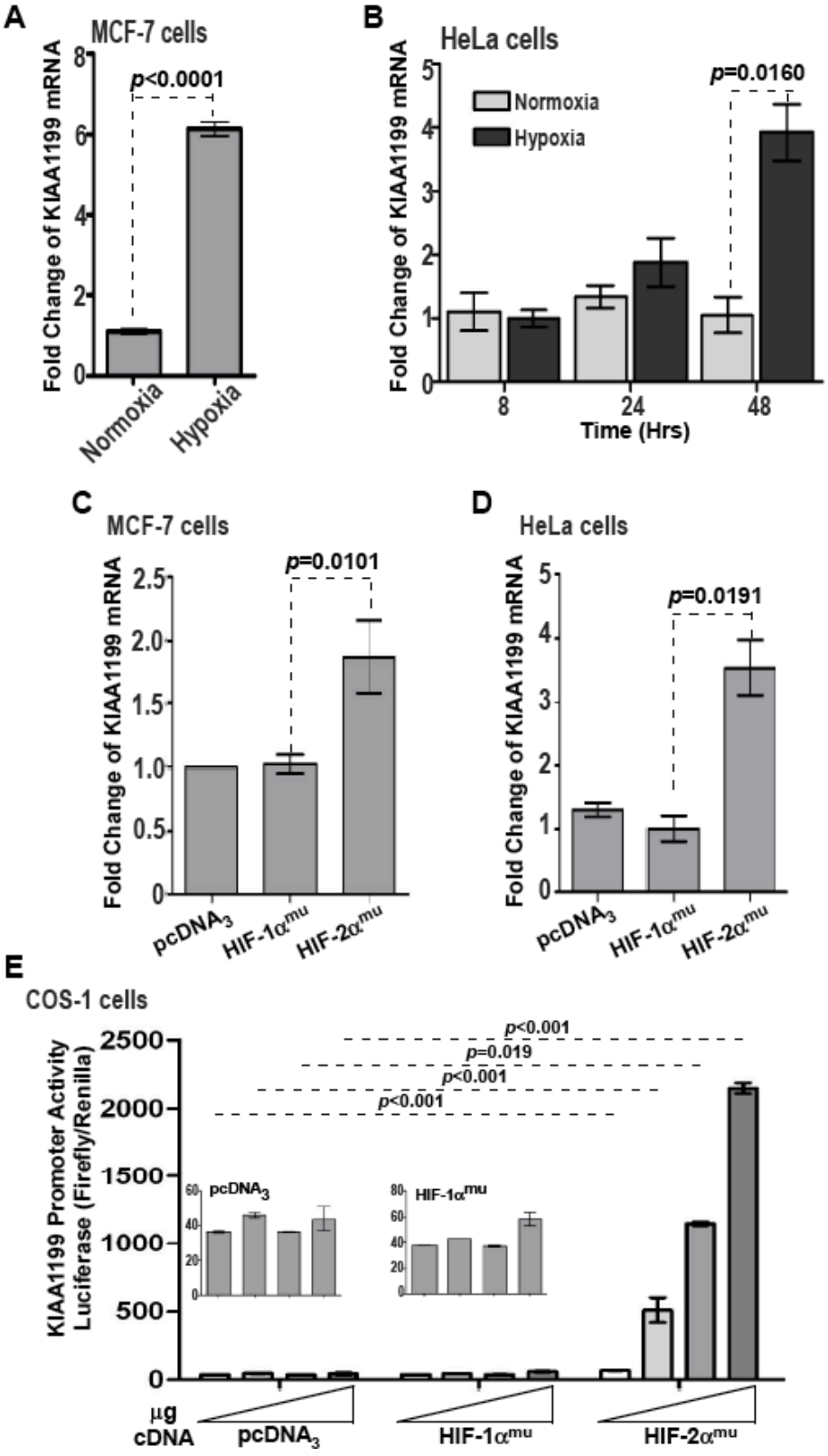
A
MCF-7 cells
p<0.0001
Fold Change of KIAA1199 mRNA
Normoxia
Hypoxia
B
HeLa cells
p=0.0160
Normoxia
Hypoxia
Fold Change of KIAA1199 mRNA
Time (Hrs)
C
MCF-7 cells
p=0.0101
Fold Change of KIAA1199 mRNA
pcDNA3
HIF-1αmu
HIF-2αmu
D
HeLa cells
p=0.0191
Fold Change of KIAA1199 mRNA
E
COS-1 cells
p<0.001
p=0.019
p<0.001
p<0.001
KIAA1199 Promoter Activity
Luciferase (Firefly/Renilla)
pcDNA3
HIF-1αmu
µg cDNA
pcDNA3
HIF-1αmu
HIF-2αmu

Figure 23 Hypoxia results in upregulation of KIAA1199 in cancer cell lines: (A -D) Real Time RT-PCR analysis of KIAA1199 mRNA expression in MCF-7 and HeLa cells cultured under normoxic or hypoxic (A & B) or transfected with HIF-α mutant cDNAs (C & D). (E) Dual luciferase reporter assay using lysates from COS-1 cells transfected with a consistent amount of KIAA1199 promoter-luciferase reporter cDNA along with increasing amounts of vector control or HIF mutants cDNAs as indicated. Error bar represents the mean ±SD.

Based on the increased promoter activity of KIAA1199 and the presence of a putative hypoxic response element (HRE) spanning -125 bp to -120 bp (GCGTG) in the sense orientation of the promoter, as predicted by bioinformatics analysis, it was hypothesized that HIF-2α is playing a direct role in the upregulation of KIAA1199 under hypoxia. To address this, a KIAA1199/pGL3 reporter construct was generated via site direct mutagenesis such that the predicted HRE was deleted (ΔHRE). HeLa cells were transfected with either the control pGL3, wild-type or the ΔHRE KIAA1199 reporter cDNA and cultured under hypoxic conditions for 48 hours followed by a luciferase reporter assay. Exposure to hypoxic stress significantly increased the basal promoter activity of KIAA1199 (Fig. 24A), further supporting the results shown in Fig. 23. However, hypoxia failed to induce the activity of the ΔHRE KIAA1199 promoter to the same level observed in cells expressing the wild-type promoter (Fig. 24A). A recent study in our laboratory indicates that transcription factors AP-1 and NF-κB also contribute to KIAA1199 promoter activity [27], which may explain why a complete inhibition of luciferase activity was not seen upon HRE site deletion.

To further investigate whether HIF-2α binds directly to the KIAA1199 promoter, a chromatin immunoprecipitation (ChIP) assay coupled with quantitative PCR was used. Overexpression of HIF-2α ^{mu} in HeLa cells caused a significant increase in HRE occupancy at the proximal KIAA1199 promoter compared to $pcDNA_3$ vector control (Fig. 24B). This observation was confirmed in HeLa cells cultured under hypoxia (Fig. 24B). Collectively, these data provide a potential molecular mechanism for hypoxia-upregulated KIAA1199 expression in solid tumors.

To determine whether hypoxia-induced KIAA1199 expression results in enhanced cell migration, KIAA1199 shRNA-2-silenced HeLa cells transiently transfected with HIF-2α ^{mu} or vector control were examined in a wound-healing migration assay.

Expression of HIF-2α^{mu} in control cells (Luc shRNA) significantly induced cell migration as evidenced by increased closure of the wounded area (Fig. 24C). In contrast, knockdown of KIAA1199 in HeLa cells significantly attenuated the expected HIF-2α-induced increase in cell migration. Together, these data suggest a role for KIAA1199-mediated migration as a way for cancer cells to escape hypoxic conditions therefore increasing survival of these more aggressive cells.

Figure 24

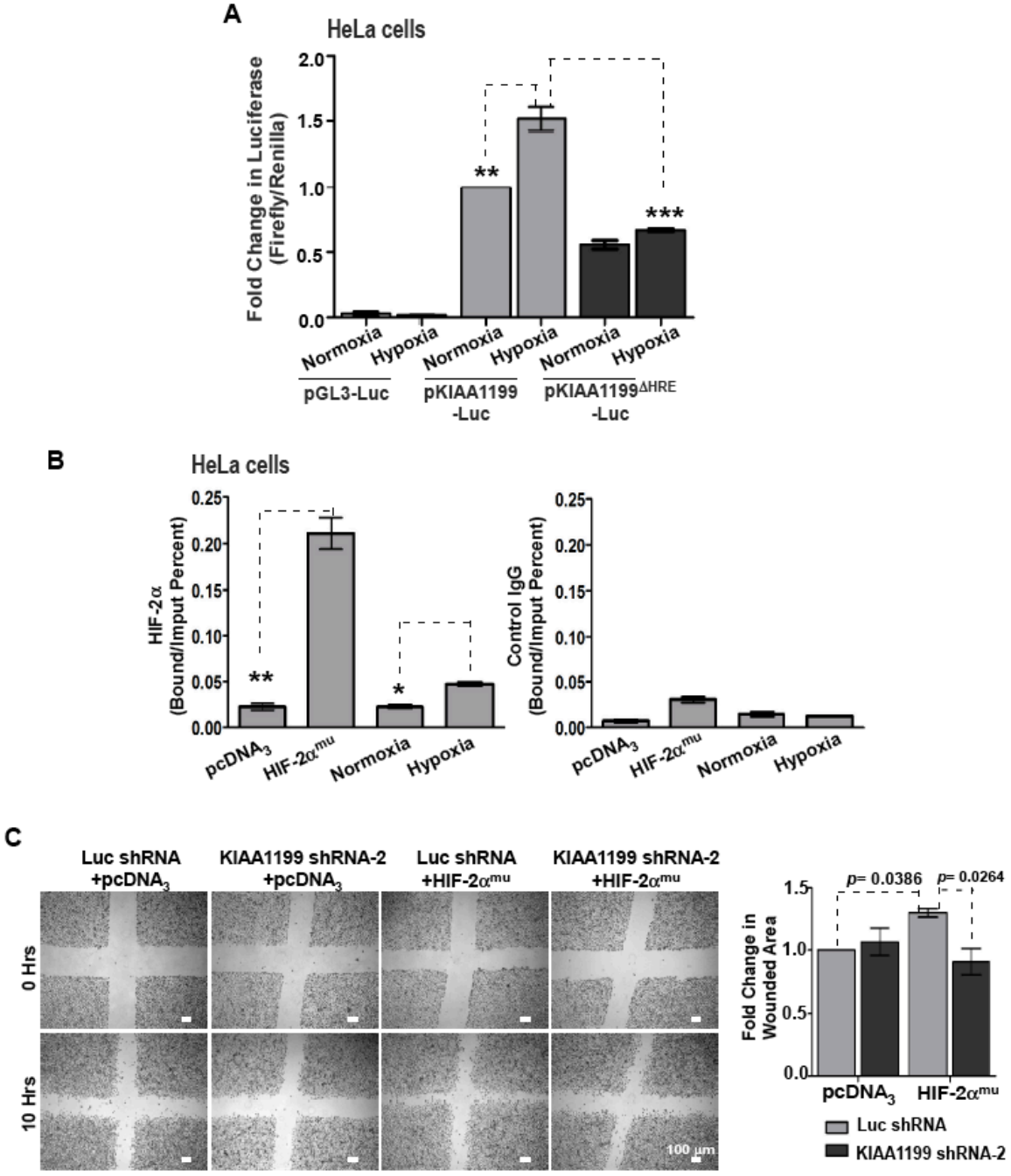

Figure 24 KIAA1199 plays a role in migration downstream of HIF-2α: (A) Dual luciferase reporter assay using lysates from HeLa cells transfected with pGL3 basic (control), wild-type KIAA1199, or ΔHRE KIAA1199 promoter-luciferase reporter cDNAs cultured under normoxia or hypoxia for 48 hrs. (B) ChIP assay using HeLa cells either transfected with indicated cDNAs or cultured under normoxia or hypoxia for 48

hrs. A HIF-2α-specific Ab or an IgG control was used for chromatin immunoprecipitation. Primers spanning the HRE within the KIAA1199 promoter region were used for real-time RT-PCR. (C) Scratch wound healing assay performed in HeLa cells expressing control or KIAA1199 shRNA transfected with either vector control or HIF-2α^{mu} cDNA. Images were taken at 0 hr and 18 hrs under 4x magnification (Left panel). Quantification of fold change in wounded area was performed using NIS Elements software (Right panel).

1.4 Discussion

Hitherto this publication, the only studies on KIAA1199 were in regards to its upregulation in various forms of cancer. However, the pathological consequences of this upregulation were unknown. The key significant findings reported here are the unraveling of the pathological role of KIAA1199 in cancer cell migration, the elucidation of the signaling pathway downstream of KIAA1199-mediated cell migration, and the unveiling of the mechanism of induction of KIAA1199 in response to hypoxic stress, depicted in figure 25. We show that elevated levels of KIAA1199 are exhibited in both invasive human cancer cell lines and breast cancer tissues and provide evidence to suggest that hypoxia, and more specifically HIF-2α, may play a primary role in the induction of KIAA1199. Our studies link KIAA1199 expression to cell migration based on the reversal of EMT upon silencing of endogenous KIAA1199 in invasive cancer cells. Not surprisingly, silencing of KIAA1199 also results in abrogation of cell invasion, which requires cell migration. Subsequent studies show that increased expression of KIAA1199 causes an increased migratory capacity of non-aggressive cancer cells and a loss of epithelial-like traits. Furthermore, we demonstrate that KIAA1199 induces cancer cell migration via a BiP-Ca^{2+}-PKCα cascade. Hence, this study establishes KIAA1199 as both a potential biomarker for cancer diagnosis and target for cancer therapy aimed at preventing cancer progression.

Our study demonstrates that ER localization of KIAA1199 is a prerequisite for enhanced cell migration because loss of ER retention results in abrogation of cell migration. KIAA1199 has been shown to be localized primarily in the cytoplasm of cells [23, 24, 26], although nuclear localization of KIAA1199 has been reported in colon adenocarcinomas [25]. Nevertheless, detailed cellular distribution has not been

previously reported. Here we have demonstrated for the first time that both endogenous and exogenous KIAA1199 are localized in the ER, and this ER localization requires a special motif (the B-domain) rather than the conventional ER retention signals. Additional data suggest that cooperation of this motif with other KIAA1199 domains is required for cell migration.

Further characterization reveals that KIAA1199 interacts with BiP via the B-domain to retain KIAA1199 in the ER. We provide evidence to suggest a functional interaction between KIAA1199 and BiP: 1) deletion of the B-domain results in loss of interaction with BiP, ER retention, and cell migratory abilities; and 2) silencing of BiP results in reduced KIAA1199-mediated cell migration. Collectively, our data indicate that the KIAA1199-BiP interaction is a specific, stable cellular event required for ER retention and subsequent KIAA1199-mediated cell migration. Although the exact role of this binding in KIAA1199-mediated cancer cell migration will require further study, BiP expression has been shown to negatively correlate with patient survival, and silencing of BiP has been shown to abrogate gastric cancer and head and neck cancer cell invasion [67, 73].

The mechanism underlying KIAA1199-mediated cell migration relies on ER Ca^{2+} leakage followed by PKCα activation. Calcium is a vital second messenger that is strictly maintained in the cell due to its involvement in numerous cellular processes, including development, apoptosis, transcriptional regulation, and cell motility [136], with the ER serving as the major storage site [82]. A rise in intracellular Ca^{2+} has been shown to lead to activation of a variety of signaling cascades, including MAPK, PKC, and integrin signaling, all of which are known to play roles in cell movement [99]. Our study demonstrates a requirement for KIAA1199-induced cytosolic Ca^{2+} accumulation in cell migration. Although the exact mechanism of KIAA1199-induced Ca^{2+} release needs further elucidation, recent studies have reported proteins that were found to cause changes in steady-state levels of Ca^{2+} via various mechanisms, including Bcl-2 and Presenilin [137, 138]. Of particular interest is another KIAA protein, known as Fam38A or KIAA0233 that is also localized to the ER. Fam38A has been shown to mediate cell adhesion via a pathway that requires increased release of calcium resulting in

downstream signaling that ultimately leads to integrin activation [139]. Furthermore, elevated levels of cytoplasmic Ca^{2+} have been correlated with increased migration, which has been found to be dependent on PKC activation [99]. These findings support the involvement of PKCα activation downstream of Ca^{2+} signaling in KIAA1199-mediated migration. Additionally, PKCα has been shown to be specifically involved in cancer cell motility and invasion, and it correlates with aggressiveness [102].

Cancer cells within solid tumors experience a wide range of stressors and signals that cause the induction or repression of specific gene targets that collectively can lead to more aggressive cells [140]. Hypoxic stress has been shown to play a vital role in cancer cell transcriptional reprogramming leading to various phenotypic changes, including increased tumor aggressiveness [106]. Our data support KIAA1199 as a novel gene product that is induced upon exposure of cancer cells to hypoxic conditions as part of the reprogramming associated with increased migratory capacity. Since HIF-1α and -2α are closely related and share a consensus binding sequence on target genes [141], questions remain as to how HIF-2α, but not HIF-1α, regulates KIAA1199 gene transcription. In a genome-wide ChIP analysis, approximately 45% and 65% of the sequences bound by HIF-1α and HIF-2α, respectively, contained the HRE consensus motif [111]. Furthermore, both *Hif*-1α and *Hif*-2α knockout mice exhibit embryonic lethality [142, 143], indicating non-redundant roles during development and possibly in different types of cancer. On the other hand, many of the target genes were reported to bind both isoforms [111]. These conflicting data further demonstrate the complexity of the transcriptional reprogramming that occurs in response to hypoxic stress. Our results showing that only constitutively active HIF-2α bound to and activated the KIAA1199 promoter suggest that cooperation between HIF-2α and other transcription factors bound at the native KIAA1199 promoter may promote selective recruitment of HIF-2α to this site. A better understanding of these processes might elucidate the basic biology of how specific responses to hypoxia are coordinated, and how specific pharmacological manipulation of hypoxia pathways might be developed to interfere with KIAA1199 expression in human cancer.

It seems likely that there is not a unique route through which tumor cells gain the capacity to invade. It is clear that tumor cells are able to shift among a variety of pathways if a particular mobility-fostering cascade becomes blocked. Nonetheless, the current study widens our understanding of cancer cell migration and provides a novel target for preventing cancer invasion and metastasis. Our data demonstrate that alterations in KIAA1199's expression contribute to the loss of epithelial cell architecture and reduced cellular aggressiveness, making KIAA1199 a strong candidate for a bona fide human invasion-promoting gene.

Figure 25

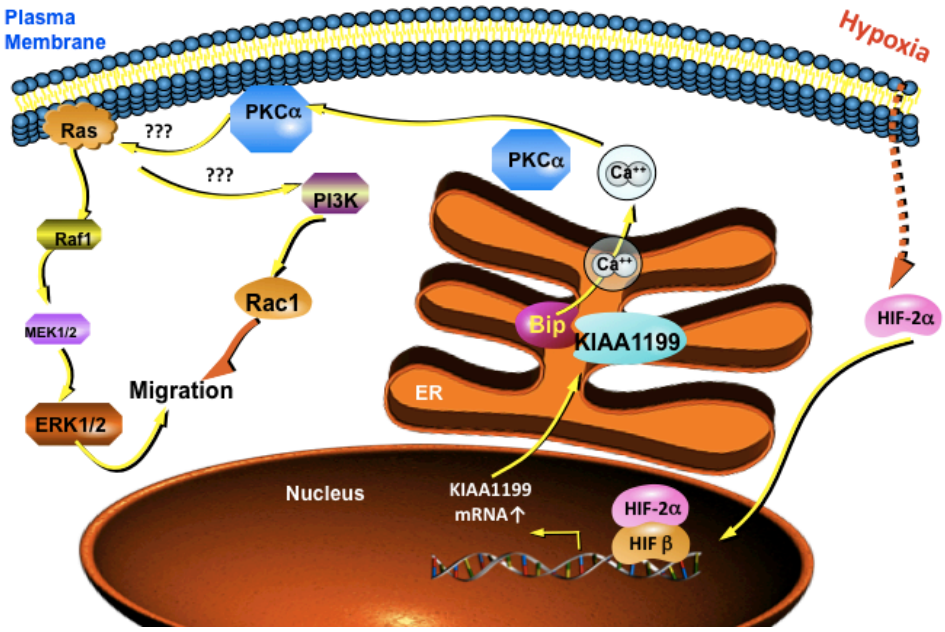

Fig. 25 Hypothetical model of KIAA1199-mediated cell migration: KIAA1199 expression is upregulated in cancer cells upon exposure to hypoxic conditions via direct binding of HIF-2α to the KIAA1199 promoter. KIAA1199 protein within the ER interacts with BiP and causes Ca^{2+} leakage from the ER resulting in accumulation of cytosolic Ca^{2+} levels. Increased cytosolic Ca^{2+} leads to PKCα translocation and activation that results in activation of downstream signaling pathways involved in enhancing cancer cell migration.

1.5 Materials and Methods

Materials: Oligo primers were synthesized by Operon. RNAi-Ready pSIREN Retro-Q vector for specific gene silencing and pQCXIP retroviral vector for generation of stable cells were purchased from Clontech. D1ER expression plasmid was kindly provided by Dr. Roger Tsien (UCSD) [130]. Anti-Myc antibody (Ab) was purchased from Roche. The $pcDNA_{3.1}$-myc expression vector, anti-PKCγ pT674 Ab, and Organelle Lights reagents were purchased from Invitrogen. Anti-KIAA1199 Ab was produced by PrimmBiotech using the C-terminus of the KIAA1199 protein between Gly1108-Thr1340 as an antigen. Anti-PDI Ab was purchased from AssayDesign. Anti-BiP, -α/β-tubulin, -β-actin, and -Twist-1 Abs were purchased from Cell Signaling Technology. Anti-XBP-1, -pan-PKCγ, and anti-Cytokeratin 8/18 Abs were purchased from Santa Cruz Biotechnology. Anti-PKCα and anti-PKCβI Abs were purchased from Enzo Life Sciences. Anti-N-cadherin and HIF-1α Abs was purchased from BD Transduction Laboratories. HIF-2α Ab was purchased from Novus Biologicals. Anti-Vimentin Ab, ConA and Phalloidin were purchased from Sigma. SNAP-Capture beads and anti-SNAP Ab were purchased from New England Biolabs. PKCγK380R cDNA (Addgene plasmid 21239), PKCβI cDNA (Addgene plasmid 16378) [144], HIF-1α P402A/P564A (Addgene plasmid 18955), and HIF-2α P405A/P531A (Addgene plasmid 18956) [134] were purchased from Addgene. The human breast cancer tissue microarray samples (BR804, BC08013a, and BR10010a) were purchased from US Biomax Inc.

Cell Lines, Treatment of Cells, and Transfection: monkey COS-1, human fibrosarcoma HT-1080, human colon cancer SW480 and HCT116, human breast epithelial cancer MCF-7 and MDA-MB 231, and human cancer MDA-MB 435 cell lines were purchased from ATCC. The GP2-293 cell line used for retrovirus production was purchased from Clontech. All cells were maintained in DMEM-high glucose (Invitrogen) containing 10% FBS and 1% Pen/Strep. For transient transfection of cells, polyethyleneimine (MW: 250 K, Polysciences) was incubated with plasmid DNA for 30 min at room temperature before adding to cells. Medium was replaced after 16 hrs. Assays were performed after 48 hrs. For hypoxic conditions cells were incubated using a BioSpherix ProOx C21 CO_2 and O_2 controller set to 1% O_2 and 5% CO_2.

DNA Constructions: To clone full-length KIAA1199 cDNA, a sequential cDNA library screening approach was used. Since under physiological conditions KIAA1199 was found to be mainly expressed in the spinal cord (data not shown), human spinal cord 5´-Stretch Plus cDNA library assembled in lgt10 vector (Invitrogen) was used. After 4 rounds of cDNA library screenings, a final 6.7 kb cDNA that contained a 4.083 kb open-reading frame (ORF) and non-coding sequences at both the 3' and 5' ends was obtained. Using the PCR approach, the N-terminus and C-terminus of KIAA1199 spanning the ORF were sequentially cloned into $pcDNA_{3.1}$/myc-His(A) vector at Xho I-EcoRI-KpnI sites along with a Myc tag in frame at the C-terminus (KIAA1199-Myc/$pcDNA_{3.1}$). To generate stable cells expressing KIAA1199, the N-terminus and C-terminus spanning of the KIAA1199 ORF including the Myc tag were sequentially cloned into pQCXIP retroviral vector. Pooled stable cells were selected using puromycin treatment.

To facilitate visualization of KIAA1199, GFP cDNA from pEGFPC1 (Clontech) was amplified by PCR and cloned into the KIAA1199-Myc/$pcDNA_{3.1}$ plasmid at the KpnI site to generate KIAA1199-GFP/$pcDNA_{3.1}$. To clone KIAA1199 cDNA into pSNAP vector, the XhoI and KpnI sites of KIAA1199 were first converted into EcoRV sites. The resultant EcoRV fragment was then inserted into pSNAP-tag vector (NEB) to generate the KIAA1199-SNAP construct. Site-directed mutagenesis and two-step PCR approaches [145] were used to generate deletion mutants of KIAA1199 cDNAs. Primers used are listed in Table 2.

The construction of the 1.4 kb KIAA1199 promoter luciferase reporter construct was previously described [27]. Deletion of the HRE binding site within the KIAA1199 promoter was carried out using a site-directed mutagenesis kit (Agilent Technologies) with the 1.4 kb KIAA1199 promoter serving as the template. To examine the promoter activity, Cells were transiently transfected with the promoter constructs along with Renilla luciferase reporter gene using polyethyleneimine. After 48 hrs of transfection, firefly and Renilla luciferase activities were measured using the Dual-Glo Luciferase assay system (Promega).

Small interfering oligonucleotides specific for human KIAA1199 and control luciferase were designed using Block-iT RNAi Designer (Invitrogen) for mammalian RNA

interference. Based on practical guidelines for selecting highly effective siRNA sequences for mammalian RNA [146], two specific shRNAs for KIAA1199 mRNA were selected and synthesized: shRNA1: CCTCTCCATCCATCATACATT, spanning positions 1997–2017 and shRNA2: CCATCTGGCTCATCAACTT, spanning positions 3457–3475. A sequence of GCTTCCTGTCAC derived from miR-23 [146] was used as a shRNA loop. Oligos were annealed and cloned into the RNAi-Ready pSIREN-Retro Q vector (Clontech) at BamHI and EcoRI sites. Luciferase, PKCα, and BiP shRNAs were generated in a similar way. Oligoes used for these shRNA constructs were listed in Table 2.

All constructs were confirmed by DNA sequencing.

Quantitative Real-Time PCR: RNA from cultured cells was isolated using Qiagen RNeasy Kit according to the manufacturer's instructions. Reverse transcriptase (BioRad iScript cDNA Synthesis Kit) was used to generate cDNA. Quantitative real-time PCR was performed using BioRad iQ SYBR-Green Super Mix on a BioRad iQ5 Real Time PCR machine. Relative expression was calculated using the DDCt method. HPRT-1 was used as an internal control.

Breast Cancer Datasets: All datasets were obtained through the NCBI/GEO database with the following accession numbers: Stockholm Cohort: GSE 1456; Rotterdam Cohort: GSE 2034; and Uppsala cohort: GSE 3494. Patients were dichotomized using the mean value of KIAA1199 for each cohort and a Kaplan-Meier survival curve was produced for each cohort using the clinical information of the samples. Log Rank (Mantel Cox) was used to determine statistical significance.

Laser capture microdissection (LCM): Cancer and normal epithelial cells in FFPE tissue sections were isolated by LCM technique using a Leica Laser Microscope. UV-energy was set to 82 and UV-Focus was set to 76 for the collection of cells. Total RNA was extracted from the isolated cells by using nano-RNA isolation kit (Epicentre) according to the manufacturer's instruction and amplified using Genisphere's SenseAmp Plus for Low Molecular Weight followed by real-time RT-PCR.

Immunohistochemistry: FFPE tissue sections (5 μm) of human adult breast containing either benign or breast carcinoma tissues, as well as sections from the human breast tissue

array from US Biomax Inc., were examined using a standard immunohistochemistry method. Antigen retrieval was achieved by boiling tissue sections for 30 minutes in 0.01M sodium citrate, pH 4. Sections were blocked for one hour in 1% BSA at room temperature and incubated in rabbit anti-KIAA1199 antibodies, at 1:25 dilution at 4°C overnight. After washing, samples were treated with 3% H_2O_2 followed by incubation with HRP-conjugated anti-rabbit IgG at 1:50 dilution, and then by Biotin-XX-Tyramide amplification (Invitrogen, Carlsbad, CA), performed according to manufacturer's instructions, and streptavidin-HRP at 1:100 dilution. All antibodies and streptavidin-HRP were diluted in 1% BSA, and sections were washed 4 times in TBS between staining steps. Stained sections were visualized using 3,3'-diaminebenzidine tetrahydrochloride (DAB) and counterstained with hematoxylin.

Western Blotting: Cell lysate and trichloroacetic acid (10% TCA, final concentration)-precipitated proteins derived from the conditioned medium of transfected cells were resolved by 10% polyacrylamide gel electrophoresis. The proteins were then transferred to nitrocellulose membranes and probed with corresponding primary antibodies. After extensive washing with TBS-T (20mM Tris–HCl, pH 7.6, 137mM NaCl, 0.1% Tween), the membranes were incubated with horseradish peroxidase (HRP)-conjugated secondary antibody followed by detection with SuperSignal West Femto Maximum Sensitivity Substrate (Pierce).

Cycloheximide (CHX) Half-Life Assay: COS-1 cells transiently transfected with cDNAs as indicated were cultivated in the presence or absence of 10 μg/ml CHX in serum-free medium for indicated time points. The conditioned medium was collected. TCA precipitation was performed, and cells were lysed using phospho lysis buffer containing both phosphatase and protease inhibitors. Proteins derived from the conditioned medium and cell lysates were then examined by Western blotting.

SNAP Pull-Down Assay and Proteomic Analysis: COS-1 cells transiently transfected with a control plasmid containing a SNAP tag or KIAA1199-SNAP plasmids were lysed followed by incubation with SNAP beads (NEB). For proteomic analysis, bound proteins were released by trypsin digestion. Resulting peptides were analyzed on a Thermo LTQ Orbitrap XL mass spectrometer and the resulting mass spectra were analyzed by Inspect

search. For the BiP pull-down assay, bound proteins were eluted using SDS-sample buffer under reducing conditions followed by Western blotting using anti-BiP antibody. Kinex™ Antibody Microarray: Proteins from MCF-7 cells stably transfected with vector or KIAA1199 cDNAs were lysed, and protein extracts were subjected to an antibody microarray screen at the Kinexus Bioinformatics Corporation. The screen uses antibodies to track the expression levels and phosphorylation states of 700 cell signaling proteins in duplicate (utilizing over 300 phospho site-specific and 500 pan-specific antibodies). Details of the strategies and protocols can be found on the Kinex web site (www.Kinexus.ca).

Cytosolic Calcium Measurement: Cytosolic Ca^{2+} was monitored using Calcium Green-1/AM (Invitrogen) [49]. Cells were collected, washed with 2% FBS/PBS, and loaded with 1 μM Calcium Green-1/AM in 2% FBS/PBS for 30 min at room temperature to minimize compartmentalization. Cells were then washed in PBS to remove excess dye and analyzed by flow cytometry using Ex/Em of 506/531 in the presence of PI. Cytosolic calcium was also monitored using FURA-2AM (Invitrogen). Stable cells were loaded with 5 μM FURA-2AM in FBS-free medium for 30 min at room temperature, washed with FBS-free medium, and loaded into a 96-well black, clear-bottom plate. Excitation was measured at 340 and 380nm and emission at 520nm; the 340/380 ratio reflects bound/unbound Ca^{2+}.

ER Calcium Measurement: ER Ca^{2+} was measured using the ER-cameleon D1ER [130]. COS-1 and MCF-7 cells stably expressing empty vector or KIAA1199 cDNA were transfected with D1ER cDNA, and live imaging was conducted using a Zeiss LSM 510 Meta NLO two-photon laser scanning confocal microscope system with 5% CO_2 and 37°C. D1ER was excited at 458 nm and emission filters of 522-704 (YFP, FRET channel) and 458-490 (CFP) were used. Baseline images were taken for 20-30 cells per sample excluding highly fluorescent or dim cells. Cells were treated with 3 mM EGTA + 2 μM ionomycin and images taken to determine R_{max} and R_{min} respectively [147]. A region of interest (ROI) was formed for each image and the YFP/CFP, proportional to the level of ER calcium, was calculated.

Cellular Fractionation: Cells were fractionated for PKC experiments using a standard approach described previously [99] followed by Western blotting using antibodies against different PKC isoforms. Cellular fractionation for detection of KIAA1199 was performed using Qproteome Cell Compartment Kit from Qiagen.

Scratch Wound Healing Assay: Cells were grown to form a monolayer. A T-shaped wound was scratched into the monolayer using a sterile 10 μl pipet tip. The cells were washed with PBS to remove lifted cells, and complete medium was added. The cells were photographed using a 4x objective under light microscopy (Nikon) at times 0 hr and 18 hrs. The area of the wound was measured using NIS Elements BR software and fold change in percentage of wound closer was calculated.

Transwell Chamber Migration Assay: Polycarbonate membranes with 8 μm pore size (Neuro Probe) were inserted into Blind-Well chemotactic chambers (Neuro Probe). Prior to seeding into the transwell inserts, Cells were released from plates with trypsin-EDTA followed by the addition of DMEM medium with 10% FBS. The lower chemotactic chamber was filled with DMEM containing 10% FBS (200 μl). Cells were counted using an automated cell counter (Cellometer Auto T4, Nexcelom). The upper chamber was filled with 25,000 cells suspended in DMEM plus 1% FCS to a final volume of 200 μl. Chambers were incubated for 18 hrs at 37°C and 5% CO_2 in a humidified tissue culture incubator. Cells on the upper surface were then removed from the filter with a cotton swab and washed 3 times with PBS. Cells remaining on the lower surface were fixed in 4% paraformaldehyde (PFA)/PBS and stained with 0.1% crystal violet. The number of cells in 10 random fields of the filters was counted (20x objective) to obtain the total number of migrated cells.

Dot-Based Cell Migration Assay: A mixture of cell and collagen type I (1.5 mg/ml final concentration) was dotted onto a 96-well plate. After solidification, the cell-matrix was covered with complete medium containing 10% FBS. Cells that had migrated away from cell-matrix dots were microscopically determined after 18 hr incubation.

Phagokinetic Cell Migration Assay: The basic procedure was described previously [148]. Briefly, coverslips treated with L-lysine (50 μg/ml) were coated with 0.5% BSA followed by air drying. The coverslips, placed in 12-well plates, were incubated with

freshly made colloidal gold particles for 1 hr followed by washing with PBS. Cells (1 x 10^4/well) were plated onto colloidal gold particle-coated coverslips and incubated at 37°C for 18 hrs followed by fixation with 4% PFA/PBS. Migrated cells were observed and photographed under light microscopy (Nikon). Images were processed and measured using NIH image software (ImageJ).

Three-Dimensional Invasion Assay: Explained in Chapter 2.5 Materials and Methods section.

Chromatin Immunoprecipitation (ChIP): The ChIP assay was performed based on the Abcam X-ChIP (cross-linked) protocol using anti-HIF-2α Ab. Briefly, cellular proteins were cross-linked with chromosomal DNA by 0.75% formaldehyde followed by sonication. Lysates containing 25 μg DNA were immunoprecipitated by HIF-2α Ab or normal rabbit IgG as a control (Millipore) at 4°C overnight in the presence of protein-A agarose beads. Any DNA fragment bound to immunoprecipitated HIF-2α was amplified by quantitative real-time PCR using a pair of primers (listed in Table 2) spanning the HRE site within the KIAA1199 promoter. Immunoprecipitated DNA was calculated according to the bound (immunoprecipitated chromatin)/input ratio.

Statistics: Student's unpaired two sided *t*-test was used to assess differences with *p* values ≤ 0.05 specifically stated in figures and *$p < 0.001$ denoted as* ***. Pooled data were presented as either mean ±SD for all real-time RT-PCR analyses or mean ±SEM for other analyses of three independent experiments. A Chi-square test was used to analyze difference in intensity staining grade among breast cancer tissue samples in different stages. Patients' survival curve was estimated based on the Kaplan-Meier method and compared using a log-rank test. All experiments were repeated at least three times.

Table 2: Primers

Primer in Application	Strand	Primer Sequence
KIAA1199	For	5’ ATGGTACCCAAAGAAGGGCTGAGAATCC
promoter	Rev	5’ ATAGATCTGCCCTCTTACCTCTGGGTCT
ChIP Assay	For	5’ GCGTGGAGGGAAGTTTCAT
	Rev	5’ AGGCCGCTTTTATAGCCACT
KIAA1199	For	5’ GCTCTTGAGTTGCATGGACA
qPCR	Rev	5’ ACCGCGTTCAAATACTGGAC
KIAA1199 ORF	For	5’ AACTCGAGCACAACCATGGGAGCTGCTGGGAGGCA
	Rev	5’ GGGGTACCTCACAACTTCTTCTTCTTCACCAC
KIAA1199 ΔA	For	5’ ATCAAGCTTTTGTTCCAGACAGAGCATGGCGAA
	Rev	5’ GGGGTACCTCACAACTTCTTCTTCTTCACCAC
KIAA1199 ΔB	For	5’ TAATACGACTCACTATAGGG
	Rev	5’ GCGGAATTCCAGAGCCTCGATGTCCATGATA
KIAA1199 ΔC	For	5’ TAATACGACTCACTATAGGG
	Rev	5’ GCGGAATTCGTACATTATCCTCCAAGTTCAG
KIAA1199 ΔD	For	5’ TAATACGACTCACTATAGGG
	Rev	5’ GCGGAATTCTGACGCAGCGAGAGAATGTATG
KIAA1199 ΔE	For	5’ TAATACGACTCACTATAGGG
	Rev	5’ GCGGAATTCGCTTGTCCTTGGCAGAGGC
PKCα shRNA-1	sense	5’ GATCCGAACAACAAGGAATGACTTGCTTCCTGT CACAAGTCATTCCTTGTTGTTCTTTTTTG
	anti-sense	5’ AATTCAAAAAAGAACAACAAGGAATGACTTGTG ACAGGAAGCAAGTCATTCCTTGTTGTTCG
PKCα shRNA-2	sense	5’ GATCCGCGTCCTGTTGTATGAAATGCGCTTCC TGTCACGCATTTCATACAACAGGACGCTTTTTTG
	anti-sense	5’ AATTCAAAAAAGCGTCCTGTTGTATGAAATGC GTGACAGGAAGCGCATTTCATACAACAGGACGCG
PKCα qPCR	For	5’ GACGAGGAAGGAAACATGGA
	Rev	5’ TCCCAACACCATGAGGAAAT
PKCβI qPCR	For	5’ CTCCACTCCTGCTTCCAGAC
	Rev	5’ GAACAGACCGATGGCAATTT
PKCγ qPCR	For	5’ CTACATAGCCCCGGAGATCA
	Rev	5’ GAAAGCGACTTGGGGTAGGT
BiP shRNA-1	sense	5’GATCCGCCTAAATGTTATGAGGATCAGCTTCCTGTCACTG ATCCTCATAACATTTAGGCTTTTTTG
	anti-sense	5’AATTCAAAAAAGCCTAAATGTTATGAGGATCAGTGACAG GAAGCTGATCCTCATAACATTTAGGCG
BiP shRNA-2	sense	5’GATCCGCGCATTGATACTAGAAATGAGCTTCCTGTCACTC ATTTCTAGTATCAATGCGCTTTTTTG
	anti-sense	5’AATTCAAAAAAGCGCATTGATACTAGAAATGAGTGACAG GAAGCTCATTTCTAGTATCAATGCGCG
BiP qPCR	For	5’ GCTCGACTCGAATTCCAAAG
	Rev	5’ TGACACCTCCCACAGTTTCA

1.6 Current and Future Directions

Overall, our observations have reinforced the connections between KIAA1199, BiP, ER Ca^{2+} leakage, and PKCα activation. However, our understanding of the downstream pathways potentially involved in KIAA1199-enhanced cell migration is far from complete. Further work will certainly be required to understand the complete mechanistic basis of the effects that we have observed. For instance, the identification of effector molecules that lie downstream of PKCα in the KIAA1199-mediated pathway would provide a more complete understanding of the entire mechanism and could be helpful in determining a way to target KIAA1199. Numerous pathways, including integrins and MAPK have been shown to be activated by PKCs. Preliminary data suggests that ERK is not involved in the KIAA1199 pathway, but various other pathways have yet to be explored in relation to KIAA1199.

The interaction of KIAA1199 and BiP also warrants further investigation. Given the long half-life of KIAA1199 and its constant association with BiP, upregulated KIAA1199 in the ER may also function as part of an undiscovered BiP chaperoning complex. We are currently investigating this possibility. Furthermore, additional deletion/mutation analyses are being undertaken to pinpoint the specific residues within the B-domain that promote BiP binding and associated signaling. Once this region is identified and further characterized studies can be performed to determine the consequences of inhibiting this interaction and the precise role of BiP in these cellular changes via KIAA1199 can be elucidated. Preliminary data also demonstrates that expression of KIAA1199 induces BiP protein expression and promoter activity (Fig. 26A & B). Due to BiP's role in cellular adaptation to stress, we are looking into the possibility of a role for KIAA1199 in cell survival in response to stress, including hypoxia.

Other important questions that remain unanswered are concerned with the calcium changes induced by KIAA1199. How does KIAA1199 cause ER calcium leakage and an increase in cytosolic calcium? Do the KIAA1199-mediated calcium changes affect any other cellular process including EMT-MET or play different roles in different cell types? New preliminary studies further support our conclusion that the rise in cytosolic calcium is due to calcium leakage from an intracellular source since this change is still observed

in the absence of extracellular calcium (Fig. 26C). Further evidence is provided by data demonstrating that by inhibiting calcium release from IP_3R via Xec, KIAA1199 expression no longer results in an increase in cytosolic calcium levels (Fig. 26D), suggesting the IP_3R is required for ER calcium leak induced by KIAA1199. However these studies need to be repeated. If the IP_3R is found to be involved, expression levels and possible interaction with KIAA1199 will be assessed. It would also be of interest to determine the precise role for the BiP interaction in these calcium alterations. Overall, the studies presented herein open the door to a variety of new hypotheses regarding both KIAA1199 specifically and the general role of calcium dynamics in cancer.

Figure 26

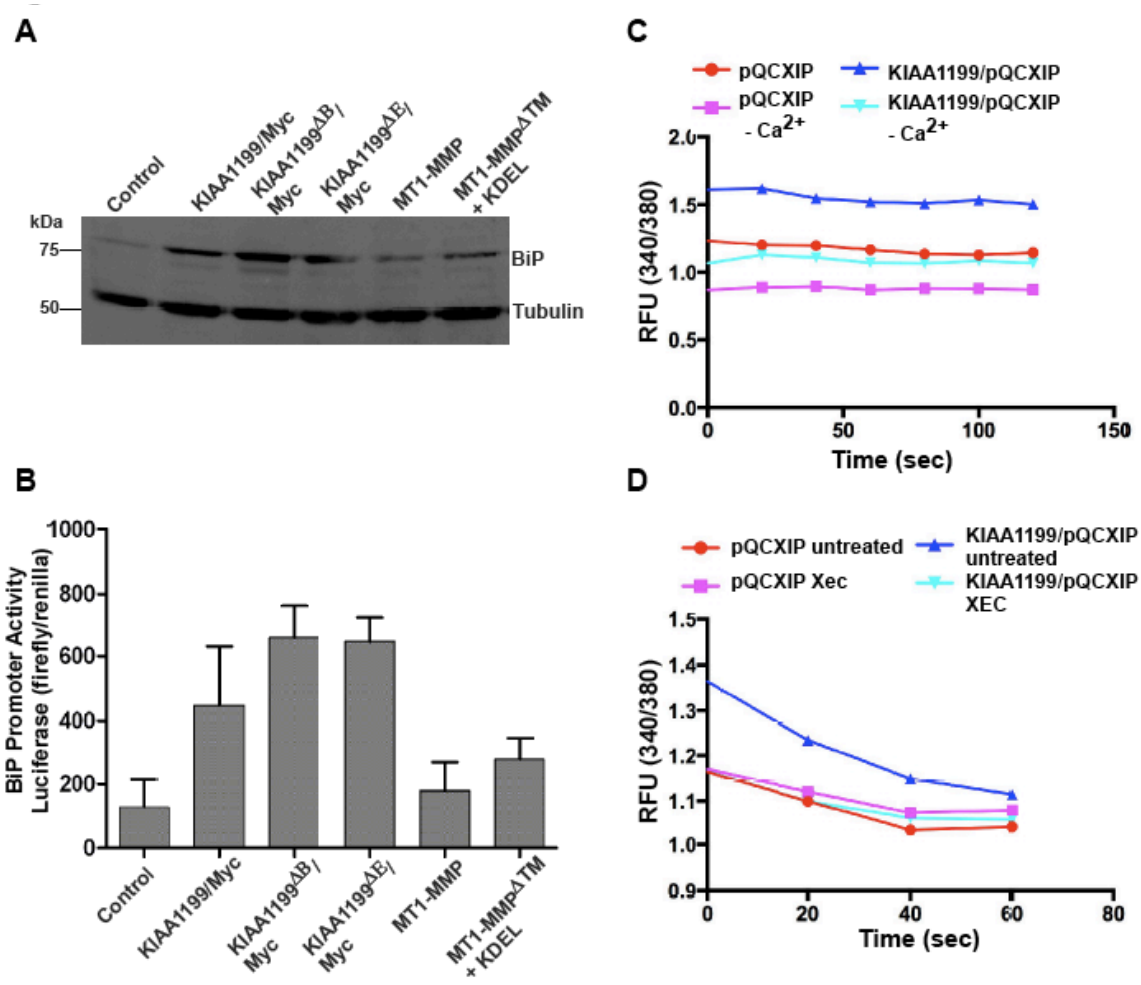

Figure 26 Future Directions: (A) Cell lysates from COS-1 cells transfected with indicated cDNAs were analyzed by Western blotting. (B) Dual luciferase reporter assay using lysates from COS-1 cells co-transfected with BiP promoter-luciferase reporter and

indicated cDNAs. (C & D) Spectrofluorometry of cytosolic Ca^{2+} in FURA-2AM-loaded MCF-7 cells stably expressing KIAA1199 or vector control cDNA. (C) Cells were washed and resuspended in buffer without or with (- Ca2+) 0.5 mM EGTA to chelate any calcium present following cell loading. (D) Cells were untreated or treated with 1 μM Xestospongin C (XeC), an IP_3R inhibitor, during and after cell loading.

Chapter 2: Development of a Novel Three-Dimensional (3D) Invasion Assay for Anti-cancer Drug Discovery

2.1 Summary

The lack of high-throughput screening assays designed to identify anti-invasive drugs is a major hurdle in the war against cancer. Presented is the development of a novel 3D invasion assay with high-throughput (HT) potential that involves surrounding cell-collagen hemispheres/dots within a cover layer of collagen to create a 3D environment through which the cancer cells can invade. Sensitivity was demonstrated by the ability to distinguish varying levels of invasiveness of prostate cancer cell lines. A dose-dependent inhibition of MDA-MB-231 invasion by anti-β1-integrin antibody demonstrates the efficacy. A Z-factor of 0.65 was obtained by comparing the effects of DMSO and anti-β1-integrin antibody on the invasion of DU145 cells. Standardization was accomplished by designing a pitted 96-well plate to create a designated location for the cell-collagen droplet and by using dialdehyde dextran to inhibit collagen contraction in order to maintain size and shape. Automated readout is possible by utilizing a motorized stage on an inverted microscope and counting Hoechst stained cells within an invasive zone created using imaging software. As proof of principle, the NCI Diversity Compound Library was screened against MDA-MB-231 cells. Nine compounds exhibiting high potency and low toxicity were identified, including DX-52-1, a compound reported to inhibit migration. The results indicate this innovative drug-screening platform is a simple, precise, and easy to replicate 3D invasion assay for anti-cancer drug discovery.

2.2 Background

2.2A Treating Metastasis – Drug Screening Approaches

Although it well known that cancer metastasis accounts for the majority of treatment failures in cancer patients, there still remains a lack of treatment strategies targeting this multistage process [149]. For this reason, it is well recognized that discovering novel drugs that can target cancer cell invasion, a critical and early step of metastasis, is imperative in winning the war against cancer. Due to the necessity for both migratory and proteolytic activity in cancer cell invasion, drugs that can inhibit either one or both of these can potentially be used to prevent cancer dissemination [150]. Despite all the progress that has been made in understanding cancer cell invasion and the molecular players involved, current drug discovery programs have failed in identifying effective drug candidates. Therefore, it has become increasingly clear that new HT technologies for anti-cancer drug discovery are required.

In designing a novel HT drug-screening assay there are two different approaches to consider: target-specific and phenotypic based screens. For the past few decades, drug discovery programs have primarily focused on target-based screening, which has resulted in a handful of successful drugs, including tamoxifen and trastuzumab. The harsh reality, though, is that most drugs designed against one specific target fail in preclinical studies [151]. Target based drug discovery is based on identifying compounds that can affect one specific molecular target found to play a role in a particular disease. Once a "druggable" target is chosen and validated based on prevalence and role of the target in the disease, compounds can be tested and optimized for their ability to affect this specific molecule. However, these steps are extremely limiting due to the fact that candidates are tested against one specific target from a known, small pool of molecular players. Furthermore, all the effort, time, and monetary expenses expended for biochemical target identification, validation, screening, and lead optimization before even determining the safety and biological effect of the compound in a cell-based, disease relevant system and could therefore prove to be fruitless. These characteristics are outlined by Frank Sams-Dodd [152].

A shift is now being made to utilize cell-based systems that directly test cellular response, such as cell invasion, upon drug treatment to circumvent the limitations of strictly target-based studies. Phenotypic screening allows for the simultaneous examination of the efficacy, safety and biological effect of candidate compounds on cancer cells, ultimately saving time and money. In direct contrast to target based screens, the compounds that do not show the desired cellular effect in a phenotypic screen would immediately be eliminated and no additional time or cost would be spent on optimization. Additionally, phenotypic screens can directly test solubility and cell permeability of potential drugs since the screens utilize cell-based methods. By testing for an observable trait, there are also no limitations as to the target molecules. These advantages of cell-based phenotypic screens are summarized by Eugene C. Butcher [153]. An obvious caveat that exists with phenotypic screens is the lack of information on the drug target and mechanism of action, which limits the ability to predict of off-target effects. However, new technologies are being developed to alleviate this issue [154] and the FDA is approving an increasing number of drugs prior to target identification.

2.2B 2D VS 3D Cell Culture Systems

In recent years it has become clear that utilizing 3D cell based assays that more closely mimic *in vivo* conditions would offer a higher predictive value and better optimization for future clinical efficacy of potential drugs. A 3D cell-based screening assay is an ideal model for drug discovery based on the facts that similar gene expression profiles are observed in 3D cultured cancer cells and *in vivo* tumors, and the behavior of cancer cells cultured in 3D more truthfully mimic behavior of cells *in vivo* [155]. It has also been shown that the phenotypic responses of cancer cells to various drugs, such as inhibition of migratory ability, are significantly altered when cultured in a 3D environment as compared to a 2D environment [156]. Cancer cell invasion is a process that occurs in a 3D environment wherein other cells as well as extracellular matrix components surround and affect the cancer cells. For this reason, considerable efforts have been focused on developing practical 3D cell based high-throughput screening (HTS) assays for cancer drug discovery. However, current 3D culture systems, including

muticellular spheroids, cellular multilayer, matrix-embedded cultures, hollow-fiber bioreactors, and *ex vivo* cultures, are more commonly utilized for basic and applied tumor biology and have not yet been incorporated into mainstream drug development programs due to the lack of simple, reproducible techniques and protocols for rapid and standardized data acquisition [157]. Thus, the major hurdle that exists in developing novel 3D HTS aimed at inhibiting invasion is the lack of a cost effective, rapid, and standardized assay for quantitatively testing invasive ability. By incorporating a 3D culturing system into a standardized, phenotypic assay the likelihood of identifying compounds that will truly inhibit invasion *in vivo* will increase substantially.

Herein, we provide a novel, qualitative, HT 3D cell-based assay for screening drugs with anti-invasion capabilities. By utilizing a novel pitted plate design, along with dialdehyde dextran collagen matrix to prevent contraction, we have developed an invasion assay that is standardized and easily and automatically quantified. We provide evidence that our 3D Invasion assay is reproducible, effective, easy and rapid to perform, and sensitive enough to identify positive compounds that inhibit cancer cell invasion. The potential for these positive hits to have a high impact on patients with cancer by preventing dissemination supports the use of this assay in the current drug discovery program.

2.3 Results

Establishment of a Quantitative 3D invasion Assay for Evaluating Cancer Cell Invasion

Recognizing the need for a 3D HT assay that tests invasive ability of cells, we have developed a 3D collagen based invasion assay that is technically easy and rapid to set up. The initial step involves the formation of cell-collagen invasion dots by combining a specified amount of cancer cells with type I collagen (3 mg/ml) at a 1:1 volumetric ratio resulting in a 1.5 mg/ml final concentration of collagen and 4e7 cells/mL. The resulting cell-collagen mixtures are then dotted into a 96-well plate (1 μL/well) and allowed to solidify for 10 minutes, forming a hemisphere with a distinct boundary and shape. Following solidification, the cell-collagen dots are embedded within a cover-layer of type I collagen (1.5 mg/ml) and allowed to solidify for an additional 3 minutes. Media with or without drug is then added to each well and the cells are allowed to invade into the surrounding matrix for a specified amount of time. The total number of invaded cells can then be quantified. The steps for our novel 3D HT invasion assay are depicted in Fig. 27A.

In order for an assay to be utilized as a screening tool for invasive ability it needs to be sensitive enough to detect small differences in invasive capacity of various cell types. Our assay was tested in this capacity by utilizing human androgen independent (DU145 and PC3) and dependent (LNCaP) prostate cancer cell lines, as well as LNCaP cells expressing membrane type 1 matrix metalloproteinase (MT1-MMP/MMP-14), which differ in their level of aggressiveness. MT1-MMP has been shown to be involved in cancer cell dissemination and its expression alone can induce invasion of non-aggressive cell types [6]. The indicated cells were prepared as outlined in Fig. 27A. Media was added and the cells were allowed to invade for 18 hrs. As shown in Fig. 27Ba, c, & d, wild-type LNCaP cells failed to invade into the surrounding collagen, while the metastatic DU145 and PC3 cells show increased numbers of invasive cells, clearly demonstrating the range of aggressiveness of these cancer cell lines. Furthermore, the effect of MT1-MMP expression on cell invasion was easily determined by an increase in

the number of invaded cells in MT1-MMP expressing LNCaP cells as compared to wild-type cells (Fig. 27Ba & b). Together, these data highlight the sensitivity of our assay to distinguish varying degrees of invasiveness and the capability to test the effects of individual genes on cancer cell invasion.

To determine the efficacy of our assay, a dose response test was performed using MDA-MB-231, an invasive breast cancer cell line, and an anti-βI integrin Ab, which is known to inhibit cell invasion. The MDA-MB-231 cells were prepared as described in Fig. 27A. Following the addition of the cover layer of collagen, media with or without the indicated concentrations of anti-βI integrin Ab was added to the wells and the cells were allowed to invade for 18 hrs. A dose-dependent inhibition of MDA-MB-231 cell invasion upon treatment with the anti-βI integrin Ab was easily observed and quantified (Fig. 27C). Together, these data demonstrate the capability of our 3D invasion assay to be used as an anti-invasive drug-screening tool.

In order for an assay to be considered useful as a HTS tool, it must be robust enough to detect differences between the controls and the positive hits. There needs to exist a clear separation between the values given by the negative control and those given by the positive control, while at the same time having little deviation within each group. The robustness of an assay is defined by its Z factor, described by Zhang as Z factor=1-3xSSD/R (SSD: Sum of Standard Deviations; R: absolute value of the difference between positive and negative controls) [158]. A Z factor between 0.5 and 1 indicates that there is enough separation between the distributions of the individual groups, which results in a low probability of obtaining false positives. To determine the Z factor of our 3D invasion assay, the effects of DMSO and the anti-βI integrin Ab treatment on invasion of DU145 cells or LNCaP cells expressing MT1-MMP-GFP chimeric cDNA were tested. Data collected on 5 different days were analyzed using the Z factor equation (data not shown). A Z-factor of 0.65 and 0.72 from DU145 cells and MT1-MMP-GFP-expressing LNCaP cells, respectively, was calculated indicating that our 3D HT invasion assay meets the criteria of an excellent assay for HT screening.

Figure 27

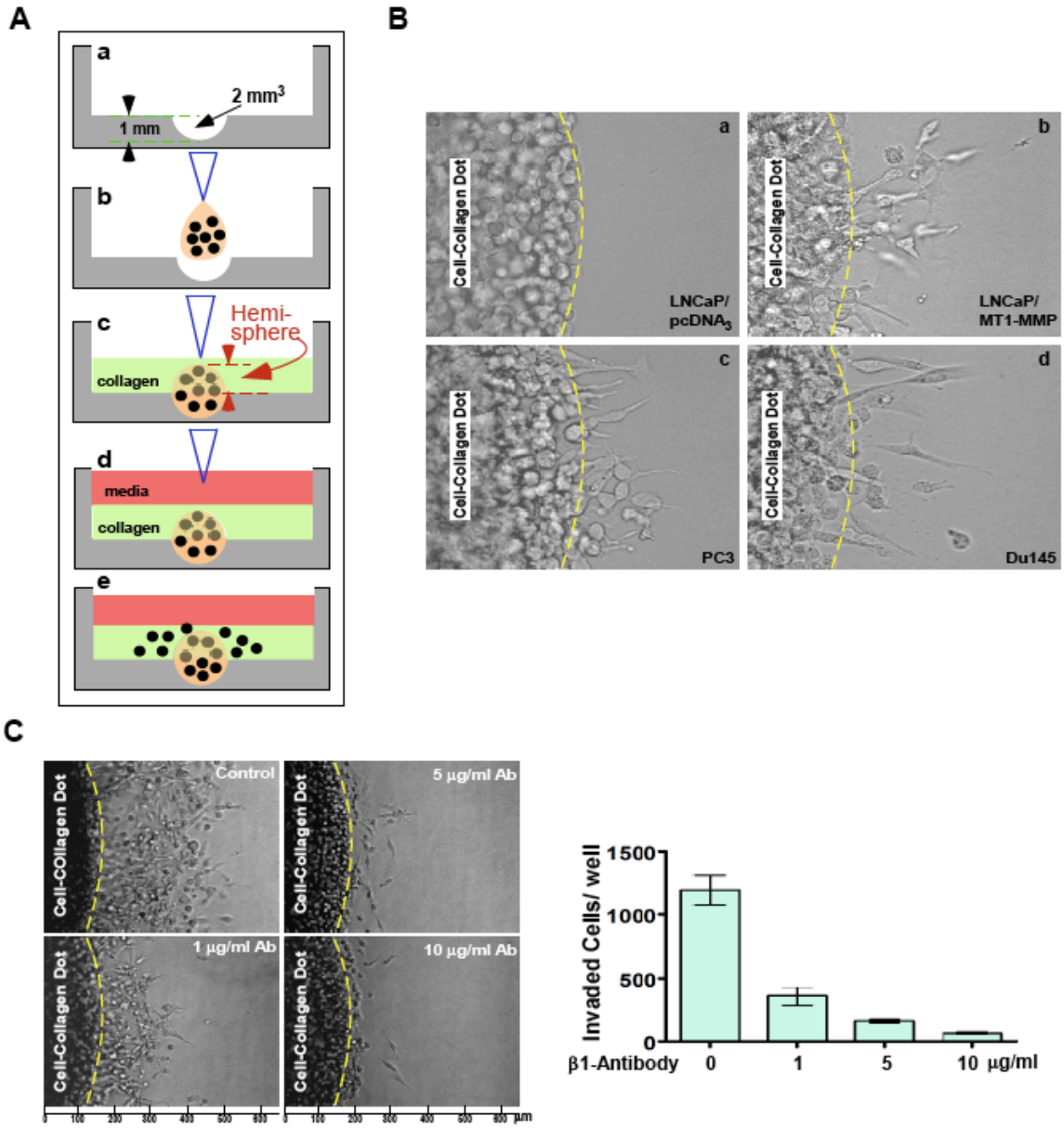

Figure 27 Establishment and Assessment of a Quantitative 3D invasion Assay for Evaluating Cancer Cell Invasion: (A) A schematic diagram of 3D invasion assay (a) A tooled 96-well plate with a hemispheric pit of defined size at the center of each well; (b) cell-collagen mixture is dotted into the pits and allowed to solidify at 37°C to create cell-collagen spheres; (c) the protruding cell-collagen hemisphere of each sphere is covered with a layer of collagen and allowed to solidify; (d) medium containing compounds is added, and plate is incubated for 18-24 hrs; and (e) invaded cells are counted. Black dots represent cells. Diagram not to scale. (B & C) Evaluation of the assay was assessed using: (B) non-invasive human prostate cancer LNCaP cells (a), LNCaP stably transfected with MT1-MMP cDNA (b), human prostate cancer PC3 cells (c) and DU145

(d) cells prepared as described in A. Bar: 50 μm. (C) MDA-MB-231 cells the presence of IgG control or anti-β1-integrin Ab at indicated concentrations. After an 18 hour incubation at 37°C, invasive ability was microscopically determined. *The experiments presented in A & B were performed by Dr. Jian Cao.

Standardization of the Developed Invasion Assay

However, the most common obstacles that hinder efforts in developing 3D HTS are standardization and automated readout. Although our 3D invasion assay is simple and fast, size homogeneity and placement of the cell-matrix invasion dots create a hurdle for these criteria. In order to standardize and allow for automated readout using imaging software, we have designed a pitted 96-well plate with a 2 mm^3 pit in the center of each well, shown in Fig. 28A. The pit is of uniform size and location within each well allowing for automatic movement of a motorized stage and therefore automated imaging and quantification of cell invasion. To demonstrate the advantage of the pit, we imaged the invasion of HT1080 GFP cells, a human fibrosarcoma cell line, following 18hrs incubation. The original boundary of the cell-collagen dot is easily detected based on the edge of the pit (Fig. 28B).

In order to quantitatively analyze the number of invaded cells the NIS-Elements imaging software was utilized. After invading for 18hrs, HT1080 cells were stained with Hoechst dye for 30 minutes and washed for 30 minutes in PBS followed by image acquisition. Both phase contrast and nuclear-stained images of HT1080 cells were taken for each well; a representative image is shown in Fig. 28C. To automate the quantification, a threshold from the phase contrast image was adjusted to create a binary zone between the pit area and the invasion area and this defined binary zone was applied to the Hoechst image. The number of invaded cells within the invasion area was then automatically counted (step outlined in Fig 28Da-e). Using the 10x objective lens and a motorized stage (Prior Scientific, Inc.) installed on a Nikon TE2000s inverted microscope, we determined that scanning an entire 96 well plate, with 4 images per well, could be completed within 6 minutes (data not shown). These images highlight the major advantage of our standardized, pitted plate as compared to other 3D assays currently used. The ability to rapidly acquire and analyze data allows for screening of a large number of compounds in a short time frame, which is necessary for HTS and is what has

hindered the use of phenotypic based assays in a HT manner. The other 3D culture techniques do not allow for standardization due to heterogeneity in size and location and thus could not be utilized in large scale screening protocols.

Optimizing the 3D invasion Assay

The pit controls the initial size, shape, and location of the cell-collagen dot, but it is also important to ensure that the size does not change over time. A common limitation of collagen is contraction due to remodeling of collagen fibrils by various cell types [159-161], which can change the overall size. Other invasion assays that utilize collagen as the ECM component would be limited by this characteristic of collagen as well. To demonstrate this, HT1080 cells were used as previously outlined and imaged at time 0 and after invading for 18 hours. After 18 hours, the cell-collagen dots contracted, significantly decreasing the diameter and therefore preventing an accurate quantification of cell invasion beyond the parameter of the pit, (Fig. 28E, top panel). As the size changes, the initial border of the dot and surrounding matrix is no longer the same and the invaded cells are not distinguishable from the those left behind after contraction. Thus, without inhibiting this contraction, the quantification of invaded cells becomes impossible.

To prevent collagen contraction, the addition of dialdehyde dextran was assessed. Dialdehyde dextran is formed by oxidizing dextran, which creates free aldehyde groups that are available to react with the amino groups of lysine residues of the collagen. This cross-linking has been shown to harden various forms of hydrogels increasing their stability [162, 163]. Additionally, dialdehyde dextran has been tested for use with various drug delivery systems [164, 165]. A 2.5% dialdehyde dextran solution was mixed with the HT1080 cell-collagen mixture to get a final solution of 0.25% dextran and 1.5 mg/ml collagen before dropping into each well. As shown in Fig. 28E (bottom panel), the addition of dialdehyde dextran significantly inhibited collagen contraction. The use of dialdehyde dextran maintained the original size of the cell-collagen dot throughout the time course and had no inhibitory effect on cancer cell invasion. The addition of the

dialdehyde dextran allows the assay to remain standardized regardless of the cell type used, which is a vital aspect of any assay that is going to be used for drug development.

Figure 28

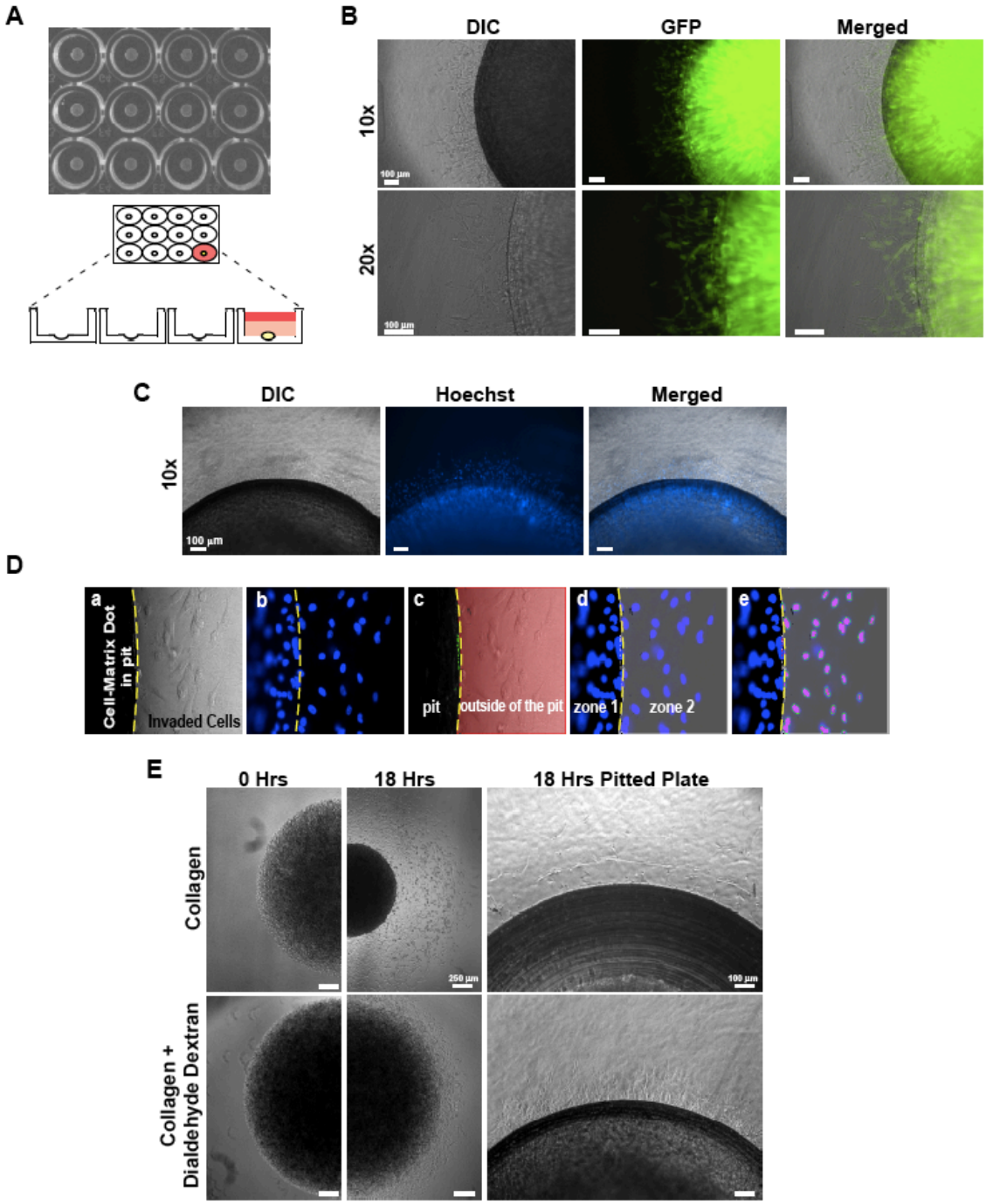

Figure 28 Standardization and Automation of the 3D Invasion Assay: (A) Image of pitted 96-well plate. (B) Phase contrast and fluorescent images of HT1080 cells expressing GFP

after assembly and 18 hrs incubation in the pitted plate. Invaded cells are seen extending beyond the original pit boundary. (C) Phase contrast and fluorescent images of invaded HT1080 cells stained with Hoechst dye. (D) After assembly and 18 hrs incubation, HT1080 cells were stained with Hoechst and the plate was placed on a motorized stage. Both phase contrast and fluorescent images (a & b) were acquired using a Nikon TE-2000s controlled by the NIS Elements imaging software. After obtaining all images, a threshold of the phase contrast image (a) of the first well was adjusted to create two binary zones (c) between the pit area and outside of the pit area. The defined binary was applied to Hoechst image (b) to create two zones (zone 1 & zone 2) (d). Invaded cells in zone 2 (d) were then automatically counted (e). Based on the given threshold, the invaded cells in the remaining wells were determined. (E) HT1080 cells were mixed with collagen as described in Figure 27A with or without the addition of 0.25% dialdehyde dextran before overlaying with collagen. Phage contrast images were taken at time 0 (initially after setting up the assay) and 18 hrs after invasion to demonstrate collagen contraction.

Since the purpose of our assay is to identify compounds that specifically inhibit cancer cell invasion as opposed to promoting cell death, being able to distinguish these two effects in the initial screen would eliminate the need for a secondary cytotoxicity assay. Propidium iodide (PI) is a common intercalating fluorescent molecule that can only enter dead cells and therefore can be used to indirectly test cell viability. By co-staining the cell-collagen dots with Hoechst and PI, the total cell count and the dead cell count can be simultaneously determined. To assess this approach using our invasion assay, HT1080 GFP cells were treated with DMSO, staurosporine (STS), a kinase inhibitor known to induce apoptosis [166, 167], Paclitaxel (taxol), a chemotherapeutic drug that stabilizes microtubules which inhibits cell division and invasion and eventually leads to cell death [168, 169], or anti-βI-integrin Ab as a control for drug treatment that decreases cell invasion without causing cell death. After an 18 hour incubation, the DMSO treated HT1080 GFP cells showed invasion into the surrounding collagen matrix with very little PI staining (Fig. 29A). In contrast, cells treated with anti-βI-integrin Ab had decreased invasive ability but a similar level of PI staining (Fig. 29B). Treatment with STS caused a significant increase in cell death, as evidenced by increased PI staining, and therefore the cells displayed abrogated cell invasion (Fig. 29C). Taxol, a slower acting drug, caused a significant reduction in cell invasion with a slight increase in cell death (Fig. 29D). These data demonstrate the ability of this assay to distinguish

between drugs that specifically inhibit invasive ability and fast acting cytotoxic drugs that appear to inhibit cell invasion but in fact cause cancer cell death.

Figure 29

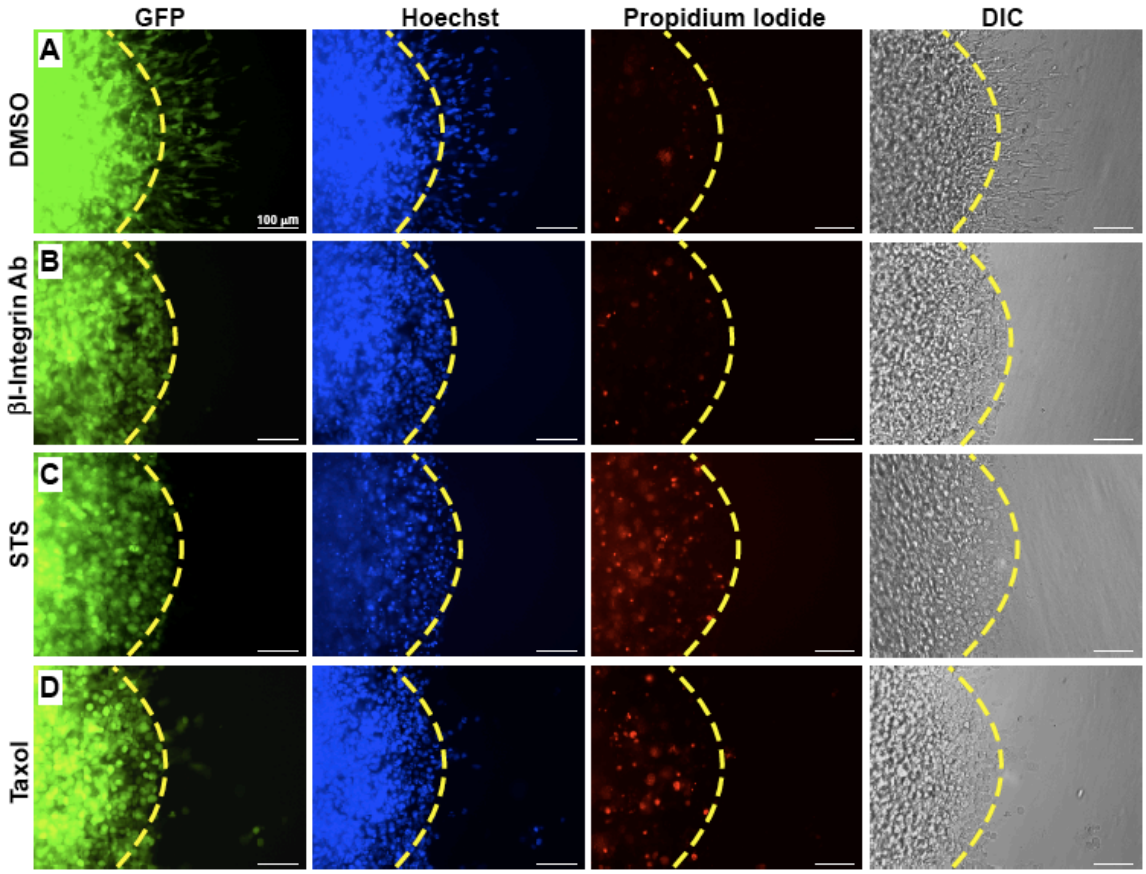

Figure 29 Simultaneous determination of invading and dead cells: HT1080 cells expressing GFP were assembled in the 3D invasion assay in the presence of (a) DMSO, (b) 500 nM STS, (c) 1 mM paclitaxel (Taxol), or (d) 5 mg/ml of the β1-integrin Ab for 18 hrs. The cells were then stained with Hoechst and PI for 30 mins and washed for 30 mins followed by microscopic examination.

Current Assays for Monitoring Cancer Cell Invasion

To demonstrate the timing and standardization limitations of other cell scattering assays, LNCaP cells stably expressing MT1-MMP and SK-3rd breast cancer stem-like cells were used as models in the single cell and multicell spheroid approaches [157, 170]. A single cell suspension of either MT1-MMP-GFP (MT1-GFP) or GFP control LNCaP cells was mixed with type I collagen and their cell scattering ability was examined daily. The LNCaP GFP cells failed to invade through the collagen, while in contrast, expression

of MT1-GFP increased the invasive capacity (Fig. 30Aa). However, these results were observed only after 6 days. In Fig. 30Ab the multicellular spheroid method was employed using SK-3rd cells cultured under hypoxic conditions, which is known to increase the trafficking of MT1-MMP to the cell surface [171]. First, the cells were cultured for 12 days in ultra-low attachment dishes to allow for mammosphere formation. The cell spheroids were then manually transferred and embedded in type I collagen and cultured under hypoxic conditions (1% O_2). Invading cells could be seen moving away from the initial cell aggregate only after 3 days (Fig. 30Ab). In an effort to reduce run time and increase size homogeneity, a technique was previously developed that utilizes microcarrier beads as a scaffold for aggregate formation [172]. LNCaP MT1-MMP expressing cells were cultured in ultra-low attachment dishes in the presence of beads for 24 hours. Following the transfer and embedment in collagen, cell invasion away from the bead was imaged after a 3 day incubation period (Fig. 30Ac).

In order to directly compare our novel 3D invasion assay to currently used 3D cell scattering assay, we tested the inhibitory effect of either tissue inhibitor of metalloproteinase-2 (TIMP-2, an endogenous inhibitor of MT1-MMP) [173] or the anti-PEX Ab (directed against the MT1-MMP hemopexin domain) [174] on MT1-MMP induced LNCaP cell invasion. The cells were set up as described in Fig.27A with the addition of either TIMP-2 or the anti-PEX Ab to the cell culture medium. By directly counting the number of invaded cells, TIMP-2 and the anti-PEX Ab were shown to inhibit MT1-MMP induced invasion by approximately 80% and 90%, respectively (Fig. 30B). For the commonly used 3D cell scattering assay [126, 175, 176], LNCaP MT1-GFP expressing cells mixed with type I collagen and plated in a 6 well dish were cultured for 6 days in the presence or absence of TIMP-2 or anti-PEX Ab (Fig. 30C). MT1-GFP expressing LNCaP cells clearly demonstrate an invasive phenotype based on the cell dispersion through the collagen following proliferation over time. Treatment with either TIMP-2 or the anti-PEX Ab decreased the scattering ability of MT1-GFP expressing LNCaP cells as compared to untreated or IgG treated cells as evidence by formation of cell aggregates. However, the ability to quantify the invaded cells, which enables the use of a percent inhibition threshold when determining positive hits from screens,

distinguishes our assay from scattering assays. Additionally, our assay requires minimal set up time, which allows for rapid screening capabilities. Overall, these images provide clear, qualitative data demonstrating cancer cell invasion but are not conducive to HTS approaches required for drug discovery programs. Table 3 briefly outlines 5 of the most commonly used 3D invasion assays, including the three depicted in Fig. 30, with respect to 4 essential qualities of any method designed for HTS: rapid completion time, quantification, standardization, and automated data acquisition. This table highlights the major advantages of our novel 3D invasion assay over the current approaches used to study cell invasion.

Figure 30

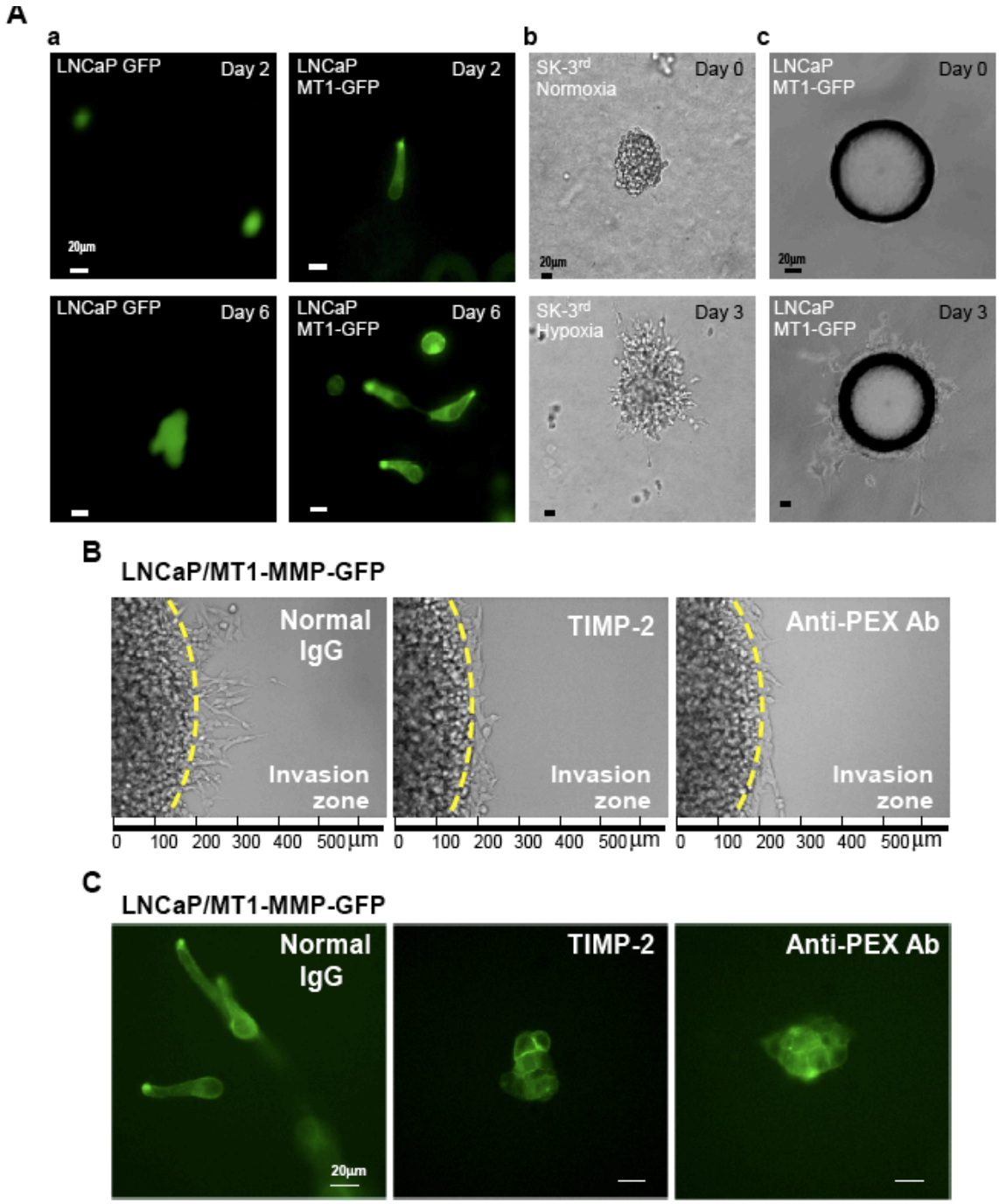

Figure 30 Existing 3D assays that monitor cell invasive capability: (A) a. Single-cell scattering assay: Single, isolated LNCaP stable cells were mixed with type I collagen (1.5 mg/ml) and examined daily under the fluorescence microscope. GFP control cells gradually form aggregates, whereas MT1-MMP-GFP cells showed a scattered growth pattern by day 6. b. Aggregate scattering assay: SK-3rd cells were cultured on ultra-low attachment dishes for 12 days to form mammospheres. The spheres were transferred and

embedded in type I collagen and cultured under normoxic or hypoxic conditions. A scattered pattern was seen after 3 days under hypoxia. c. Microcarrier bead scattering assay: MMP-14 expressing LNCaP cells were cultured onto microcarrier beads for 24 hrs, then the cell-coated beads were transferred into type I collagen. Invaded cells were seen as a scattered pattern at day 3. (B & C) The effect of normal Ig G control (Rabbit, 10mg/ml), TIMP-2 (10 nM), or anti-MT1-MMP-hemopexin domain Ab (10 mg/ml) on MT1-MMP-induced LNCaP cell invasion was evaluated via the 3D invasion assay and 3D cell scattering assay. For 3D cell scattering the cells were cultured for 6 days and the culture media containing fresh TIMP-2 or Abs were replaced every other day. Cell morphologic change was examined using fluorescent microscopy and photographed on day 6. Bar: 20 μm. *The experiments presented in this figure were performed by Dr. Jian Li.

Table 3 Comparisons of 3D Invasion Assays

3D Invasion Assays	Brief Description of Method	Assembly Time	Quantifi-cation	Standard-ization	Automated Readout	Ref.
Cell Scattering	Mixed cells in collagen matrix and check for cell scattering	1 hrs	No	No	No	[175, 176]
Cell Aggregates	various ways to form aggregates which are then embedded in matrices	4-6 days	Yes	No	No	[157, 170]
Microfluidic Assay	microchannels filled w/ matri-ces & allowed to gel; cell droplets added	6 hrs	Yes	No	No	[177]
Nested Collagen Matrices	Contracted polymerized cell-matrix mixture placed on top of collagen, then covered w/ collagen	24 hrs	Yes	No	No	[178]
Microcarrier Beads	Cells coated onto beads; the coated beads mixed w/ matrices.	1 day	Yes	No	No	[172]
3D HTS Invasion	Cell-collagen mixture placed into invasion plate and covered with collagen	30 mins	Yes	Yes	Yes	No

Validation of the HT Capacity of the 3D Invasion Assay

As a proof of principle that our assay can positively identify drugs with anti-invasive capabilities, we screened the National Cancer Institute's (NCI) Diversity Set 2 Compound Library using MDA-MB-231 cells, an aggressive, triple negative, human breast cancer cell line. The cancer cells were mixed with collagen and dotted into each well of a 96 well plate followed by the addition of the cover layer of collagen. The compounds from the NCI library were added to the wells at a final concentration of 10 μM. DMSO, which is the vehicle for the compounds, and anti-βI integrin Ab were used as the negative and positive controls, respectively. Positive hits were determined based on a threshold of >70% inhibition of invasion. Based on this threshold, 24 positive hits

were found for MDA-MB-231 cells, 9 of which were confirmed to be <25% cytotoxic based on a MTT assay (Fig. 31A). One of these hits was a known anti-migratory compound, DX-52-1 [179], providing further proof that our assay can successfully identify compounds capable of inhibiting cancer cell invasion (Fig. 31B).

Due to the fact that target identification is helpful for predicting side effects and optimizing lead candidates, it is important to have downstream assays that can help elucidate the possible mechanisms of action of the positive hits. Since invasion requires both migratory and proteolytic activity, a vital first step is to distinguish between these two cellular properties. Utilizing DX-52-1 as an example, the conventional Transwell chamber migration assay and a non-specific protease assay (Sigma) were employed to distinguish between inhibition of proteolytic and migratory ability. As shown by Fig. 31C & D, DX-52-1 significantly abrogated MDA-MB-231 cell migration but had no significant effect on proteolytic activity. These data indicate that the inhibition of the invasive behavior of the MDA-MB-231 cells by DX-52-1 was due to an effect on migratory ability, which is supported by published reports [179]. Narrowing down the potential cellular processes affected by the compounds will focus future studies aimed at ascertaining the target(s) of the drug.

Figure 31

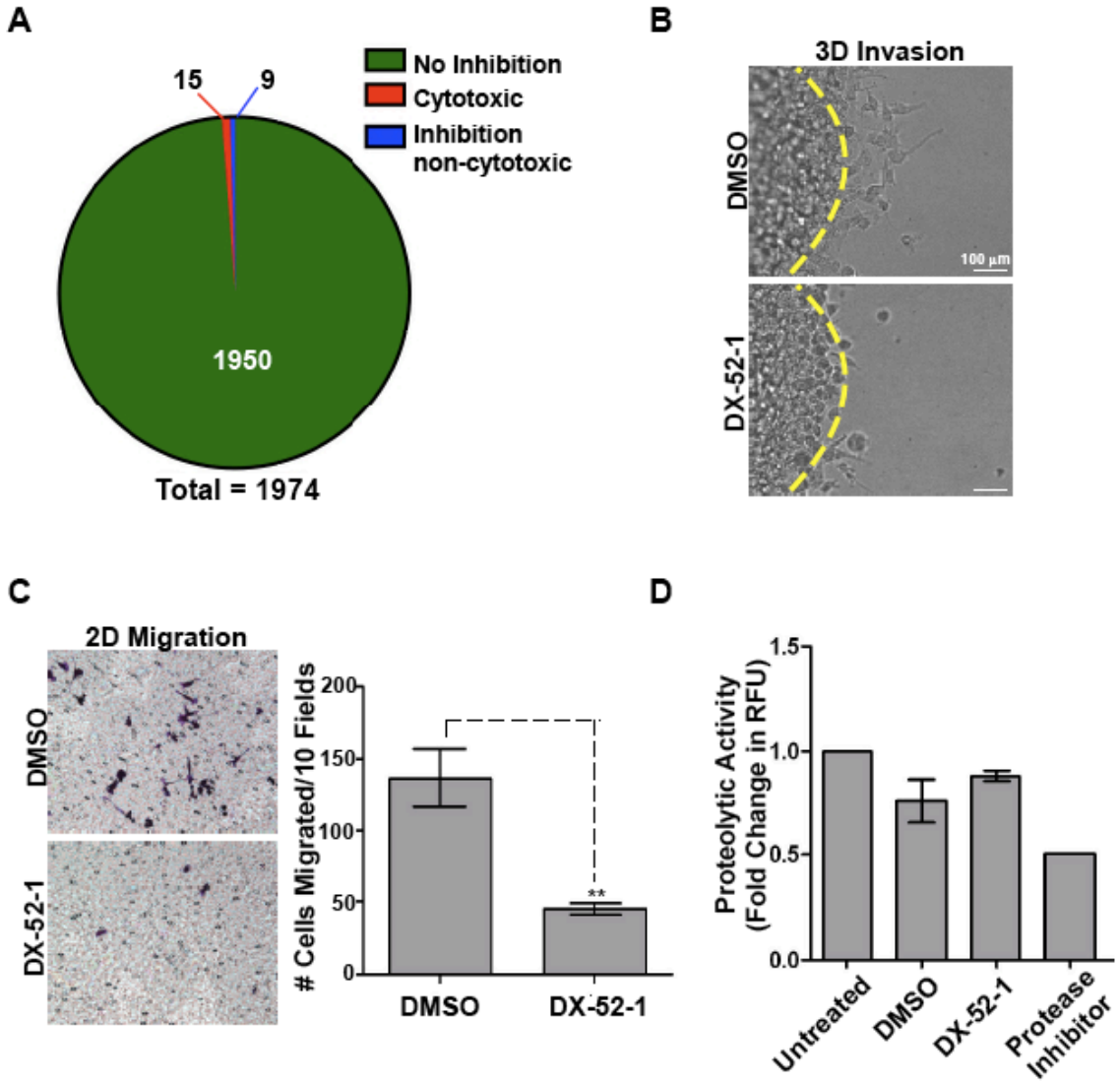

Figure 31 Proof of Principle: (A) The NCI Diversity Set II Compound Library was screened using the 3D invasion assay and MDA-MB-231 cells, resulting in 24 positive hits, 9 of which were inhibitory but not cytotoxic (MTT assay). (B) DX-52-1 was positively identified as an anti-invasive compound through the screen. Representative images shown for DMSO control and DX-52-1 (10 µM) after 18 hrs incubation. (C) Transwell chamber migration performed with MDA-MB-231 cells treated with DMSO or DX-52-1 for 18 hrs. Representative images of membrane shown in left panel. Quantification of cell migration shown in right panel. (D) Fluorescent Protease Detection assay (Sigma) performed with cell lysates from MDA-MB-231 cells treated with DMSO or DX-52-1 for 18 hrs.

2.4 Discussion

Although there are numerous assays available for studying cancer cell invasion, none of them are currently suitable for HTS. Drug screening programs rely on the ability to test and analyze thousands of compounds in a rapid and reproducible manner, which requires an assay that is standardized and generates quantifiable data. As demonstrated in Fig. 30, previously established cell scattering assays require an extended period of time to generate results, which is not conducive to HTS. In addition, while the data is qualitatively observable, the results are not quantitative. Furthermore, the multicellular spheroid based methods are also technically challenging due to the requirement for transferring the aggregates and they do not allow for easy standardization of size and placement, which hinders automated readout potential.

These limitations lower the potential for HTS capabilities and highlight the urgency of the development of a 3D invasion assay that is both quick and easy to perform and allows for quantitative data as opposed to only qualitative images. Herein we have designed a method that requires minimal time and labor to set up and run. The use of our pitted plate along with the combination of collagen and dialdehyde dextran creates a tool for standardization and permits automated readout, which are two aspects lacking in current protocols. Additionally, based on the results shown in Fig. 27B, our assay also has the potential to be utilized as a combined phenotypic and target based approach due to the ability of our assay to detect changes in invasive capabilities due to one gene. With the advent of our novel 3D invasion assay into the mainstream anti-cancer drug discovery program, numerous advancements will be made in not only our general understanding of cancer cell invasion but also in our ability to better treat cancer dissemination, ultimately making cancer a manageable disease as opposed to a life-threatening one.

2.5 Materials and Methods

Materials: Type I collagen (acetic acid-extracted native from rat tail tendon) and Propidium iodide (1 μg/mL) were purchased from BD Bioscience Discovery Labware. Recombinant TIMP-2 and anti-MT1-MMP hemopexin domain Ab was purchased from CHEMICON Interantional, Inc. RNAi-Ready pSIREN Retro-Q vector for specific gene silencing and pQCXIP retroviral vector for generation of stable cells were purchased from Clontech. Hoechst nuclear stain was purchased from Invitrogen. The anti-βI integrin Ab was purchased from GE Healthcare. Staurosporine, Paclitaxel, and dextran (Mw=500,000) were purchased from Sigma.

Cell Lines, Treatment of Cells, and Transfection: human fibrosarcoma HT-1080, human prostate cancer LNCaP, DU145, and PC3, human breast epithelial cancer MDA-MB-231 cell lines were purchased from ATCC. The GP2-293 cell line used for retrovirus production was purchased from Clontech. The LNCaP cells expressing MT1-MMP-GFP or GFP alone were previously described [126]. The cells were maintained in DMEM-high glucose or RPMI 1640 medium (Invitrogen) containing 10% FBS and 1% Pen/Strep. The SK-3rd cells and mammosphere formation were previously described. Briefly, these cells were cultured in ultra-low attachment dishes (Corning) in suspension with DMEM-F12 (Cellgro) medium supplemented with B27 (1:50, Invitrogen), EGF (20ng/mL BD Biosciences), 0.4% bovine serum albumin (Sigma), and 4 μg/mL insulin (Sigma) [171]. For hypoxic conditions cells were incubated using a BioSpherix ProOx C21 CO_2 and O_2 controller set to 1% O_2 and 5% CO_2.

3D Invasion Assay: Make cell dotting collagen A (3 mg/ml) and cover collagen B (1.5 mg/ml) as the recipe states (*All components should be kept on ice throughout the experiment):

Collagen A (0.5 ml): 0.25 ml of Collagen Solution Type I (6 mg/ml)
+ 0.1 ml of 5X DMEM;

Collagen B (2.0 ml): 0.9 ml of Collagen Solution Type I (3.34 mg/ml)
+ 0.4 ml of 5X DMEM

Spin down the desired total number of cells to be used (every droplet needs 4e4 cells) and resuspend in complete media equivalent to half the desired total volume (1 μl/well is needed). Adjust the pH of Collagen A to approximately 7.4 using 2N NaOH and bring the final volume to 0.5 ml using H_2O. Mix the cells with collagen A 1:1 (v/v) then add dialdehyde dextran to get a final percentage of 0.25%. Gently drop 1 μl of the cell-collagen mixture in the pit. A multi-channel pipette can be used. Ultimately, automated liquid handling system may be used. After finishing half the plate, incubate the plate @ 37°C for 10 min to allow the dot to solidify but not dry. If the dot appears completely white, the pellet may have dried. While the cell-collagen dot solidifies, adjust the pH of Collagen B to ~7.4 using 2N NaOH and bring the final volume to 2 ml using H_2O. Using 80 μl of collagen B, cover the first dot to check if it solidified. If not, put the plate @ 37°C for a longer period of time, but be cautious not to let the dots dry. Once solidified, cover all dots. Put the plate @ 37°C for 3 min and let the cover collagen solidify. Treat cells with vehicle, candidate drugs or positive control in 80 μl of complete media. Incubate the plate for 18-24 hrs. Manually or automatically count invaded cells outside of pit by microscopy.

Staining of invaded cells: For automated cell count, stain cells using Hoechst 33342 nuclear stain (25 μg/ml) with PI (2.5 μg/ml) for 30 minutes in PBS followed by washing for 30 mins with PBS. Create two binary zones by adjusting the threshold of the phase image and apply the threshold to the Hoechst image to separate invaded cells from initial dot to allow for automated counting.

Oxidation of dextran to form dialdehyde dextran: 2.5 g dextran was dissolved into 100 mL diH_2O. Sodium periodate ($NaIO_4$) (1.65 g) was added into the dextran solution under agitation so as to oxidize the dextran into dextran dialdehyde. The mixture was stirred overnight at room temperature protected from light. After completion of the overnight reaction, 1 mL ethylene glycol was added to quench the reaction and the solution was stirred for another hour. The solution was then dialyzed against 1L of diH_2O for 3 days with the water being changed every day. The solution was lyophilized forming a white sponge and then reconstituted with diH_2O to get a final concentration of 2.5% dialdehyde dextran. *Special thanks to Dr. Xiaojun Yu for his help with this procedure.

Protease Assay: Protease Fluorescent Detection Kit from Sigma was used according to manufacturers instructions. Briefly, cell lysates were incubated overnight at @ 37°C with FITC-labeled casein substrate. Lysates were TCA precipitated and spun down. The supernatants containing the fragmented FITC-casein was then combined with assay buffer and fluorescence intensity was measured with excitation at 485 nm and emission at 535 nm using a SpectraMax Gemini Em (Molecular Devices) fluorescent plate reader.

2.6 Current and Future Directions

The introduction of our novel HT 3D invasion assay into the current drug discovery program will now allow for the rapid testing of many compounds that can specifically inhibit cell invasion. We believe that the drugs identified utilizing our screen can potentially have profound effects on the way we treat cancer. The screening of the NCI compound library not only served as a proof of concept but also provided a list of potential drug candidates. The next step in this project will be to further analyze these hits for their potential use as anti-cancer drugs. As done for DX-52-1, the hits will each be tested in conventional migration assays as well as the non-specific protease assay. Additionally, to acquire more information about the molecular effects of these compounds, antibody arrays to compare vehicle or compound treated cell lysates will be performed. The data resulting from these few studies will provide clues to potential mechanisms of action. To test the *in vivo* efficacy and other possible effects, including effects on angiogenesis, we will employ the chick chorioallantoic membrane (CAM) assay. This method has been used to study invasion and metastasis of human tumor cells in addition to angiogenesis [180]. Together, these studies will provide evidence as to whether or not these positive hits are worth pursing through more in depth more *in vivo* studies.

References

1. Hanahan, D. and R.A. Weinberg, *The hallmarks of cancer.* Cell, 2000. **100**(1): p. 57-70.
2. Hanahan, D. and R.A. Weinberg, *Hallmarks of cancer: the next generation.* Cell, 2011. **144**(5): p. 646-74.
3. Gupta, G.P. and J. Massague, *Cancer metastasis: building a framework.* Cell, 2006. **127**(4): p. 679-95.
4. Bacac, M. and I. Stamenkovic, *Metastatic cancer cell.* Annual Review of Pathology-Mechanisms of Disease, 2008. **3**: p. 221-247.
5. Kassis, J., et al., *Tumor invasion as dysregulated cell motility.* Seminars in Cancer Biology, 2001. **11**(2): p. 105-117.
6. Cao, J., et al., *Membrane type 1-matrix metalloproteinase promotes human prostate cancer invasion and metastasis.* Thromb Haemost, 2005. **93**(4): p. 770-8.
7. Chang, C. and Z. Werb, *The many faces of metalloproteases: cell growth, invasion, angiogenesis and metastasis.* Trends Cell Biol, 2001. **11**(11): p. S37-43.
8. Friedl, P. and K. Wolf, *Plasticity of cell migration: a multiscale tuning model.* J Cell Biol, 2010. **188**(1): p. 11-9.
9. Jiang, P., A. Enomoto, and M. Takahashi, *Cell biology of the movement of breast cancer cells: intracellular signalling and the actin cytoskeleton.* Cancer Lett, 2009. **284**(2): p. 122-30.
10. Friedl, P. and K. Wolf, *Tumour-cell invasion and migration: diversity and escape mechanisms.* Nat Rev Cancer, 2003. **3**(5): p. 362-74.
11. Huang, C., K. Jacobson, and M.D. Schaller, *MAP kinases and cell migration.* Journal of Cell Science, 2004. **117**(20): p. 4619-4628.
12. Dillon, R.L. and W.J. Muller, *Distinct Biological Roles for the Akt Family in Mammary Tumor Progression.* Cancer Research, 2010. **70**(11): p. 4260-4264.
13. Kalluri, R. and R.A. Weinberg, *The basics of epithelial-mesenchymal transition.* Journal of Clinical Investigation, 2009. **119**(6): p. 1420-1428.
14. Polyak, K. and R.A. Weinberg, *Transitions between epithelial and mesenchymal states: acquisition of malignant and stem cell traits.* Nat Rev Cancer, 2009. **9**(4): p. 265-73.
15. Schmidt, C., *When Tumor Cells Travel*, in *collaborations results magazine*. 2007.
16. Reed, J.C., et al., *Proto-oncogene expression in cloned T lymphocytes: mitogens and growth factors induce different patterns of expression.* Oncogene, 1987. **1**(2): p. 223-8.
17. Zucker, S., et al., *Rapid trafficking of membrane type 1-matrix metalloproteinase to the cell surface regulates progelatinase a activation.* Lab Invest, 2002. **82**(12): p. 1673-1684.
18. Yu, M., et al., *Complex Regulation of Membrane-Type Matrix Metalloproteinase Expression and Matrix Metalloproteinase-2 Activation by Concanavalin a in*

Mda-Mb-231 Human Breast-Cancer Cells. Cancer Research, 1995. **55**(15): p. 3272-3277.
19. Diatchenko, L., et al., *Suppression subtractive hybridization: A method for generating differentially regulated or tissue-specific cDNA probes and libraries.* Proceedings of the National Academy of Sciences of the United States of America, 1996. **93**(12): p. 6025-6030.
20. Guo, J., et al., *GG: a domain involved in phage LTF apparatus and implicated in human MEB and non-syndromic hearing loss diseases.* FEBS Lett, 2006. **580**(2): p. 581-4.
21. He, Q.Y., et al., *G8: a novel domain associated with polycystic kidney disease and non-syndromic hearing loss.* Bioinformatics, 2006. **22**(18): p. 2189-91.
22. Michishita, E., et al., *Upregulation of the KIAA1199 gene is associated with cellular mortality.* Cancer Lett, 2006. **239**(1): p. 71-7.
23. Abe, S., S. Usami, and Y. Nakamura, *Mutations in the gene encoding KIAA1199 protein, an inner-ear protein expressed in Deiters' cells and the fibrocytes, as the cause of nonsyndromic hearing loss.* J Hum Genet, 2003. **48**(11): p. 564-70.
24. Sabates-Bellver, J., et al., *Transcriptome profile of human colorectal adenomas.* Mol Cancer Res, 2007. **5**(12): p. 1263-75.
25. Birkenkamp-Demtroder, K., et al., *Repression of KIAA1199 attenuates Wnt-signalling and decreases the proliferation of colon cancer cells.* Br J Cancer, 2011. **105**(4): p. 552-61.
26. Matsuzaki, S., et al., *Clinicopathologic significance of KIAA1199 overexpression in human gastric cancer.* Ann Surg Oncol, 2009. **16**(7): p. 2042-51.
27. Kuscu, C., et al., *Transcriptional and Epigenetic Regulation of KIAA1199 Gene Expression in Human Breast Cancer.* Plos One, 2012. **7**(9).
28. Katz, M., I. Amit, and Y. Yarden, *Regulation of MAPKs by growth factors and receptor tyrosine kinases.* Biochim Biophys Acta, 2007. **1773**(8): p. 1161-76.
29. Lester, R.D., et al., *Erythropoietin promotes MCF-7 breast cancer cell migration by an ERK/mitogen-activated protein kinase-dependent pathway and is primarily responsible for the increase in migration observed in hypoxia.* J Biol Chem, 2005. **280**(47): p. 39273-7.
30. Hauck, C.R., et al., *Inhibition of focal adhesion kinase expression or activity disrupts epidermal growth factor-stimulated signaling promoting the migration of invasive human carcinoma cells.* Cancer Res, 2001. **61**(19): p. 7079-90.
31. Klemke, R.L., et al., *Regulation of cell motility by mitogen-activated protein kinase.* J Cell Biol, 1997. **137**(2): p. 481-92.
32. Pullikuth, A.K. and A.D. Catling, *Scaffold mediated regulation of MAPK signaling and cytoskeletal dynamics: a perspective.* Cell Signal, 2007. **19**(8): p. 1621-32.
33. Tan, M., et al., *Upregulation and activation of PKC alpha by ErbB2 through Src promotes breast cancer cell invasion that can be blocked by combined treatment with PKCa and Src inhibitors.* Oncogene, 2006. **25**(23): p. 3286-3295.

34. Hugo, H., et al., *Epithelial-mesenchymal and mesenchymal - Epithelial transitions in carcinoma progression.* Journal of Cellular Physiology, 2007. **213**(2): p. 374-383.
35. Thompson, E.W. and D.F. Newgreen, *Carcinoma invasion and metastasis: A role for epithelial-mesenchymal transition?* Cancer Research, 2005. **65**(14): p. 5991-5995.
36. Thiery, J.P. and J.P. Sleeman, *Complex networks orchestrate epithelial-mesenchymal transitions.* Nature Reviews Molecular Cell Biology, 2006. **7**(2): p. 131-142.
37. Yang, J., et al., *Twist, a master regulator of morphogenesis, plays an essential role in tumor metastasis.* Cell, 2004. **117**(7): p. 927-39.
38. Li, J.L. and B.H.P. Zhou, *Activation of beta-catenin and Akt pathways by Twist are critical for the maintenance of EMT associated cancer stem cell-like characters.* BMC Cancer, 2011. **11**.
39. Lombaerts, M., et al., *E-cadherin transcriptional downregulation by promoter methylation but not mutation is related to epithelial-to-mesenchymal transition in breast cancer cell lines.* British Journal of Cancer, 2006. **94**(5): p. 661-671.
40. Blick, T., et al., *Epithelial mesenchymal transition traits in human breast cancer cell lines.* Clinical & Experimental Metastasis, 2008. **25**(6): p. 629-642.
41. Hazan, R.B., et al., *Cadherin switch in tumor progression.* Gastroenteropancreatic Neuroendocrine Tumor Disease: Molecular and Cell Biological Aspects, 2004. **1014**: p. 155-163.
42. Onder, T.T., et al., *Loss of E-cadherin promotes metastasis via multiple downstream transcriptional pathways.* Cancer Res., 2008. **68**(10): p. 3645-3654.
43. Hollestelle, A., et al., *Loss of E-cadherin is not a necessity for epithelial to mesenchymal transition in human breast cancer.* Breast Cancer Res Treat, 2013.
44. Tanaka, H., et al., *Monoclonal antibody targeting of N-cadherin inhibits prostate cancer growth, metastasis and castration resistance.* Nature Medicine, 2010. **16**(12): p. 1414-U96.
45. Vuoriluoto, K., et al., *Vimentin regulates EMT induction by Slug and oncogenic H-Ras and migration by governing Axl expression in breast cancer.* Oncogene, 2011. **30**(12): p. 1436-1448.
46. Mendez, M.G., S.I. Kojima, and R.D. Goldman, *Vimentin induces changes in cell shape, motility, and adhesion during the epithelial to mesenchymal transition.* Faseb Journal, 2010. **24**(6): p. 1838-1851.
47. Hebert, D.N. and M. Molinari, *In and out of the ER: Protein folding, quality control, degradation, and related human diseases.* Physiological Reviews, 2007. **87**(4): p. 1377-1408.
48. Hosoi, T. and K. Ozawa, *Endoplasmic reticulum stress in disease: mechanisms and therapeutic opportunities.* Clinical Science, 2010. **118**(1-2): p. 19-29.

49. Thomas, C.G. and G. Spyrou, *ERdj5 Sensitizes Neuroblastoma Cells to Endoplasmic Reticulum Stress-induced Apoptosis.* Journal of Biological Chemistry, 2009. **284**(10): p. 6282-6290.
50. Lu, P.D., H.P. Harding, and D. Ron, *Translation reinitiation at alternative open reading frames regulates gene expression in an integrated stress response.* Journal of Cell Biology, 2004. **167**(1): p. 27-33.
51. Lee, A.H., N.N. Iwakoshi, and L.H. Glimcher, *XBP-1 regulates a subset of endoplasmic reticulum resident chaperone genes in the unfolded protein response.* Molecular and Cellular Biology, 2003. **23**(21): p. 7448-7459.
52. Kokame, K., H. Kato, and T. Miyata, *Identification of ERSE-II, a new cis-actin element responsible for the ATF6-dependent mammalian unfolded protein response.* Journal of Biological Chemistry, 2001. **276**(12): p. 9199-9205.
53. Lee, K., et al., *IREI-mediated unconventional mRNA splicing and S2P-mediated ATF6 cleavage merge to regulate XBP1 in signaling the unfolded protein response.* Genes & Development, 2002. **16**(4): p. 452-466.
54. Rutkowski, D.T. and R.J. Kaufman, *A trip to the ER: coping with stress.* Trends Cell Biol, 2004. **14**(1): p. 20-8.
55. Schroder, M., *Endoplasmic reticulum stress responses.* Cellular and Molecular Life Sciences, 2008. **65**(6): p. 862-894.
56. Hendershot, L., et al., *Inhibition of immunoglobulin folding and secretion by dominant negative BiP ATPase mutants.* Proceedings of the National Academy of Sciences of the United States of America, 1996. **93**(11): p. 5269-5274.
57. Haas, I.G., *Bip (Grp78), an Essential Hsp70 Resident Protein in the Endoplasmic-Reticulum.* Experientia, 1994. **50**(11-12): p. 1012-1020.
58. Ma, K., K.M. Vattem, and R.C. Wek, *Dimerization and release of molecular chaperone inhibition facilitate activation of eukaryotic initiation factor-2 kinase in response to endoplasmic reticulum stress.* Journal of Biological Chemistry, 2002. **277**(21): p. 18728-18735.
59. Liu, C.Y., Z.H. Xu, and R.J. Kaufman, *Structure and intermolecular interactions of the luminal dimerization domain of human IRE1 alpha.* Journal of Biological Chemistry, 2003. **278**(20): p. 17680-17687.
60. Bertolotti, A., et al., *Dynamic interaction of BiP and ER stress transducers in the unfolded-protein response.* Nature Cell Biology, 2000. **2**(6): p. 326-332.
61. Shen, J.S., et al., *ER stress regulation of ATF6 localization by dissociation of BiP/GRP78 binding and unmasking of golgi localization signals.* Developmental Cell, 2002. **3**(1): p. 99-111.
62. Kabani, M., et al., *Dependence of endoplasmic reticulum-associated degradation on the peptide binding domain and concentration of BiP.* Molecular Biology of the Cell, 2003. **14**(8): p. 3437-3448.
63. Hegde, N.R., et al., *The role of BiP in endoplasmic reticulum-associated degradation of major histocompatibility complex class I heavy chain induced by cytomegalovirus proteins.* Journal of Biological Chemistry, 2006. **281**(30): p. 20910-20919.

64. Healy, S.J.M., et al., *Targeting the endoplasmic reticulum-stress response as an anticancer strategy.* European Journal of Pharmacology, 2009. **625**(1-3): p. 234-246.
65. Martinon, F., *Targeting endoplasmic reticulum signaling pathways in cancer.* Acta Oncologica, 2012. **51**(7): p. 822-830.
66. Lee, A.S., *GRP78 induction in cancer: therapeutic and prognostic implications.* Cancer Res, 2007. **67**(8): p. 3496-9.
67. Zhang, J., et al., *Association of elevated GRP78 expression with increased lymph node metastasis and poor prognosis in patients with gastric cancer.* Clin Exp Metastasis, 2006. **23**(7-8): p. 401-10.
68. Fu, Y., J. Li, and A.S. Lee, *GRP78/BiP inhibits endoplasmic reticulum BIK and protects human breast cancer cells against estrogen starvation-induced apoptosis.* Cancer Res, 2007. **67**(8): p. 3734-40.
69. Dong, D.Z., et al., *Critical role of the stress chaperone GRP78/BiP in tumor proliferation, survival, and tumor anglogenesis in transgene-induced mammary tumor development.* Cancer Research, 2008. **68**(2): p. 498-505.
70. Reddy, R.K., et al., *Endoplasmic reticulum chaperone protein GRP78 protects cells from apoptosis induced by topoisomerase inhibitors - Role of ATP binding site in suppression of caspase-7 activation.* Journal of Biological Chemistry, 2003. **278**(23): p. 20915-20924.
71. Ranganathan, A.C., et al., *Functional coupling of p38-induced up-regulation of BiP and activation of RNA-dependent protein kinasel-like endoplasmic reticulum kinase to drug resistance of dormant carcinoma cells (vol 66, pg 1702, 2006).* Cancer Research, 2006. **66**(6): p. 3345-3345.
72. Su, R., et al., *Grp78 promotes the invasion of hepatocellular carcinoma.* BMC Cancer, 2010. **10**: p. 20.
73. Chiu, C.C., et al., *Glucose-regulated protein 78 regulates multiple malignant phenotypes in head and neck cancer and may serve as a molecular target of therapeutic intervention.* Molecular Cancer Therapeutics, 2008. **7**(9): p. 2788-2797.
74. Dudek, J., et al., *Functions and pathologies of BiP and its interaction partners.* Cellular and Molecular Life Sciences, 2009. **66**(9): p. 1556-69.
75. Berridge, M.J., M.D. Bootman, and H.L. Roderick, *Calcium signalling: dynamics, homeostasis and remodelling.* Nat Rev Mol Cell Biol, 2003. **4**(7): p. 517-29.
76. Berridge, M.J., P. Lipp, and M.D. Bootman, *The versatility and universality of calcium signalling.* Nature Reviews Molecular Cell Biology, 2000. **1**(1): p. 11-21.
77. Clapham, D.E., *Calcium signaling.* Cell, 2007. **131**(6): p. 1047-1058.
78. Cole, K. and E. Kohn, *Calcium-mediated signal transduction: biology, biochemistry, and therapy.* Cancer Metastasis Rev, 1994. **13**(1): p. 31-44.
79. Monteith, G.R., et al., *Calcium and cancer: targeting Ca2+ transport.* Nat Rev Cancer, 2007. **7**(7): p. 519-30.
80. Parkash, J. and K. Asotra, *Calcium wave signaling in cancer cells.* Life Sci, 2010. **87**(19-22): p. 587-95.

81. Camello, C., et al., *Calcium leak from intracellular stores--the enigma of calcium signalling.* Cell Calcium, 2002. **32**(5-6): p. 355-61.
82. Park, M.K., O.H. Petersen, and A.V. Tepikin, *The endoplasmic reticulum as one continuous Ca(2+) pool: visualization of rapid Ca(2+) movements and equilibration.* EMBO J, 2000. **19**(21): p. 5729-39.
83. Coe, H. and M. Michalak, *Calcium binding chaperones of the endoplasmic reticulum.* General Physiology and Biophysics, 2009. **28**: p. F96-F103.
84. Haigh, N.G. and A.E. Johnson, *A new role for BiP: closing the aqueous translocon pore during protein integration into the ER membrane.* Journal of Cell Biology, 2002. **156**(2): p. 261-270.
85. Alder, N.N., et al., *The molecular mechanisms underlying BiP-mediated gating of the Sec61 translocon of the endoplasmic reticulum.* Journal of Cell Biology, 2005. **168**(3): p. 389-399.
86. Huang, J.B., et al., *Identification of channels promoting calcium spikes and waves in HT1080 tumor cells: their apparent roles in cell motility and invasion.* Cancer Res, 2004. **64**(7): p. 2482-9.
87. Giannone, G., et al., *Calcium rises locally trigger focal adhesion disassembly and enhance residency of focal adhesion kinase at focal adhesions.* J Biol Chem, 2004. **279**(27): p. 28715-23.
88. Amuthan, G., et al., *Mitochondrial stress-induced calcium signaling, phenotypic changes and invasive behavior in human lung carcinoma A549 cells.* Oncogene, 2002. **21**(51): p. 7839-49.
89. Amuthan, G., et al., *Mitochondria-to-nucleus stress signaling induces phenotypic changes, tumor progression and cell invasion.* EMBO J, 2001. **20**(8): p. 1910-20.
90. Tauzin, S., et al., *The Naturally Processed CD95L Elicits a c-Yes/Calcium/PI3K-Driven Cell Migration Pathway.* Plos Biology, 2011. **9**(6).
91. Newton, A.C., *Protein kinase C: poised to signal.* American Journal of Physiology-Endocrinology and Metabolism, 2010. **298**(3): p. E395-E402.
92. Cazaubon, S., F. Bornancin, and P.J. Parker, *Threonine-497 Is a Critical Site for Permissive Activation of Protein-Kinase C-Alpha.* Biochemical Journal, 1994. **301**: p. 443-448.
93. Newton, A.C., *Protein kinase C: Structural and spatial regulation by phosphorylation, cofactors, and macromolecular interactions.* Chemical Reviews, 2001. **101**(8): p. 2353-2364.
94. Webb, B.L., S.J. Hirst, and M.A. Giembycz, *Protein kinase C isoenzymes: a review of their structure, regulation and role in regulating airways smooth muscle tone and mitogenesis.* Br J Pharmacol, 2000. **130**(7): p. 1433-52.
95. Parekh, D.B., W. Ziegler, and P.J. Parker, *Multiple pathways control protein kinase C phosphorylation.* EMBO J, 2000. **19**(4): p. 496-503.
96. Bartlett, P.J., et al., *Single cell analysis and temporal profiling of agonist-mediated inositol 1,4,5-trisphosphate, Ca2+, diacylglycerol, and protein kinase C signaling using fluorescent biosensors.* Journal of Biological Chemistry, 2005. **280**(23): p. 21837-21846.

97. Spitaler, M. and D.A. Cantrell, *Protein kinase C and beyond.* Nat Immunol, 2004. **5**(8): p. 785-90.
98. Oancea, E. and T. Meyer, *Protein kinase C as a molecular machine for decoding calcium and diacylglycerol signals.* Cell, 1998. **95**(3): p. 307-18.
99. Rucci, N., et al., *A novel protein kinase C alpha-dependent signal to ERK1/2 activated by alphaVbeta3 integrin in osteoclasts and in Chinese hamster ovary (CHO) cells.* J Cell Sci, 2005. **118**(Pt 15): p. 3263-75.
100. Bordeleau, F., et al., *Keratin 8/18 modulation of protein kinase C-mediated integrin-dependent adhesion and migration of liver epithelial cells.* Mol Biol Cell, 2010. **21**(10): p. 1698-713.
101. Lahn, M., et al., *Protein kinase C alpha expression in breast and ovarian cancer.* Oncology, 2004. **67**(1): p. 1-10.
102. Lonne, G.K., et al., *PKC alpha expression is a marker for breast cancer aggressiveness.* Molecular Cancer, 2010. **9**.
103. Ng, T., et al., *Ezrin is a downstream effector of trafficking PKC-integrin complexes involved in the control of cell motility.* Embo Journal, 2001. **20**(11): p. 2723-2741.
104. Brahimi-Horn, M.C., J. Chiche, and J. Pouyssegur, *Hypoxia and cancer.* J Mol Med, 2007. **85**(12): p. 1301-7.
105. Ruan, K., G. Song, and G. Ouyang, *Role of hypoxia in the hallmarks of human cancer.* J Cell Biochem, 2009. **107**(6): p. 1053-62.
106. Harris, A.L., *Hypoxia--a key regulatory factor in tumour growth.* Nat Rev Cancer, 2002. **2**(1): p. 38-47.
107. Wang, G.L., et al., *Hypoxia-inducible factor 1 is a basic-helix-loop-helix-PAS heterodimer regulated by cellular O2 tension.* Proc Natl Acad Sci U S A, 1995. **92**(12): p. 5510-4.
108. Jiang, B.H., et al., *Hypoxia-inducible factor 1 levels vary exponentially over a physiologically relevant range of O2 tension.* Am J Physiol, 1996. **271**(4 Pt 1): p. C1172-80.
109. Lee, J.W., et al., *Hypoxia-inducible factor (HIF-1)alpha: its protein stability and biological functions.* Exp Mol Med, 2004. **36**(1): p. 1-12.
110. Dachs, G.U., et al., *Targeting gene expression to hypoxic tumor cells.* Nat Med, 1997. **3**(5): p. 515-20.
111. Mole, D.R., et al., *Genome-wide association of hypoxia-inducible factor (HIF)-1alpha and HIF-2alpha DNA binding with expression profiling of hypoxia-inducible transcripts.* J Biol Chem, 2009. **284**(25): p. 16767-75.
112. Chan, D.A. and A.J. Giaccia, *Hypoxia, gene expression, and metastasis.* Cancer Metastasis Rev, 2007. **26**(2): p. 333-9.
113. Subarsky, P. and R.P. Hill, *The hypoxic tumour microenvironment and metastatic progression.* Clin Exp Metastasis, 2003. **20**(3): p. 237-50.
114. Peinado, H. and A. Cano, *A hypoxic twist in metastasis.* Nat Cell Biol, 2008. **10**(3): p. 253-4.

115. O'Toole, E.A., et al., *Hypoxia induces epidermal keratinocyte matrix metalloproteinase-9 secretion via the protein kinase C pathway.* J Cell Physiol, 2008. **214**(1): p. 47-55.
116. Yang, M.H., et al., *Direct regulation of TWIST by HIF-1alpha promotes metastasis.* Nat Cell Biol, 2008. **10**(3): p. 295-305.
117. Cummins, E.P., et al., *Prolyl hydroxylase-1 negatively regulates IkappaB kinase-beta, giving insight into hypoxia-induced NFkappaB activity.* Proc Natl Acad Sci U S A, 2006. **103**(48): p. 18154-9.
118. Osorio-Fuentealba, C., et al., *Hypoxia stimulates via separate pathways ERK phosphorylation and NF-kappaB activation in skeletal muscle cells in primary culture.* J Appl Physiol, 2009. **106**(4): p. 1301-10.
119. Huber, M.A., et al., *NF-kappaB is essential for epithelial-mesenchymal transition and metastasis in a model of breast cancer progression.* J Clin Invest, 2004. **114**(4): p. 569-81.
120. Naugler, W.E. and M. Karin, *NF-kappaB and cancer-identifying targets and mechanisms.* Curr Opin Genet Dev, 2008. **18**(1): p. 19-26.
121. Espina, V., et al., *Laser-capture microdissection.* Nat Protoc, 2006. **1**(2): p. 586-603.
122. Pawitan, Y., et al., *Gene expression profiling spares early breast cancer patients from adjuvant therapy: derived and validated in two population-based cohorts.* Breast Cancer Res, 2005. **7**(6): p. R953-64.
123. Wang, Y., et al., *Gene-expression profiles to predict distant metastasis of lymph-node-negative primary breast cancer.* Lancet, 2005. **365**(9460): p. 671-9.
124. Miller, L.D., et al., *An expression signature for p53 status in human breast cancer predicts mutation status, transcriptional effects, and patient survival.* Proc Natl Acad Sci U S A, 2005. **102**(38): p. 13550-5.
125. Harms, J.F. and D.R. Welch, *MDA-MB-435 human breast carcinoma metastasis to bone.* Clin Exp Metastasis, 2003. **20**(4): p. 327-34.
126. Cao, J., et al., *Membrane type 1 matrix metalloproteinase induces epithelial-to-mesenchymal transition in prostate cancer.* J Biol Chem, 2008. **283**(10): p. 6232-40.
127. Cao, J., et al., *The C-terminal region of membrane type matrix metalloproteinase is a functional transmembrane domain required for pro-gelatinase A activation.* J Biol Chem, 1995. **270**(2): p. 801-5.
128. Dong, D., et al., *A critical role for GRP78/BiP in the tumor microenvironment for neovascularization during tumor growth and metastasis.* Cancer Res, 2011. **71**(8): p. 2848-57.
129. Chen, J.P., et al., *TRPM7 regulates the migration of human nasopharyngeal carcinoma cell by mediating Ca(2+) influx.* Cell Calcium, 2010. **47**(5): p. 425-32.
130. Palmer, A.E., et al., *Bcl-2-mediated alterations in endoplasmic reticulum Ca2+ analyzed with an improved genetically encoded fluorescent sensor.* Proc Natl Acad Sci U S A, 2004. **101**(50): p. 17404-9.

131. Farrar, W.L. and W.B. Anderson, *Interleukin-2 stimulates association of protein kinase C with plasma membrane.* Nature, 1985. **315**(6016): p. 233-5.
132. Blobe, G.C., et al., *Selective regulation of expression of protein kinase C (PKC) isoenzymes in multidrug-resistant MCF-7 cells. Functional significance of enhanced expression of PKC alpha.* J Biol Chem, 1993. **268**(1): p. 658-64.
133. Elvidge, G.P., et al., *Concordant regulation of gene expression by hypoxia and 2-oxoglutarate-dependent dioxygenase inhibition: the role of HIF-1alpha, HIF-2alpha, and other pathways.* J Biol Chem, 2006. **281**(22): p. 15215-26.
134. Yan, Q., et al., *The hypoxia-inducible factor 2alpha N-terminal and C-terminal transactivation domains cooperate to promote renal tumorigenesis in vivo.* Mol Cell Biol, 2007. **27**(6): p. 2092-102.
135. van de Sluis, B., et al., *COMMD1 Promotes pVHL and O2-Independent Proteolysis of HIF-1alpha via HSP90/70.* PLoS One, 2009. **4**(10): p. e7332.
136. Chakraborty, A., et al., *Casein kinase-2 mediates cell survival through phosphorylation and degradation of inositol hexakisphosphate kinase-2.* Proc Natl Acad Sci U S A, 2011. **108**(6): p. 2205-9.
137. Foyouzi-Youssefi, R., et al., *Bcl-2 decreases the free Ca2+ concentration within the endoplasmic reticulum.* Proc Natl Acad Sci U S A, 2000. **97**(11): p. 5723-8.
138. Brunello, L., et al., *Presenilin-2 dampens intracellular Ca2+ stores by increasing Ca2+ leakage and reducing Ca2+ uptake.* J Cell Mol Med, 2009. **13**(9B): p. 3358-69.
139. McHugh, B.J., et al., *Integrin activation by Fam38A uses a novel mechanism of R-Ras targeting to the endoplasmic reticulum.* J Cell Sci, 2010. **123**(Pt 1): p. 51-61.
140. Mahadevan, N.R. and M. Zanetti, *Tumor stress inside out: cell-extrinsic effects of the unfolded protein response in tumor cells modulate the immunological landscape of the tumor microenvironment.* J Immunol, 2011. **187**(9): p. 4403-9.
141. Tian, H., S.L. McKnight, and D.W. Russell, *Endothelial PAS domain protein 1 (EPAS1), a transcription factor selectively expressed in endothelial cells.* Genes Dev, 1997. **11**(1): p. 72-82.
142. Tian, H., et al., *The hypoxia-responsive transcription factor EPAS1 is essential for catecholamine homeostasis and protection against heart failure during embryonic development.* Genes Dev, 1998. **12**(21): p. 3320-4.
143. Iyer, N.V., et al., *Cellular and developmental control of O2 homeostasis by hypoxia-inducible factor 1 alpha.* Genes Dev, 1998. **12**(2): p. 149-62.
144. Soh, J.W. and I.B. Weinstein, *Roles of specific isoforms of protein kinase C in the transcriptional control of cyclin D1 and related genes.* J Biol Chem, 2003. **278**(36): p. 34709-16.
145. Cao, J., et al., *The propeptide domain of membrane type 1 matrix metalloproteinase is required for binding of tissue inhibitor of metalloproteinases and for activation of pro-gelatinase A.* J.Biol.Chem., 1998. **273**(52): p. 34745-34752.

146. Ui-Tei, K., et al., *Guidelines for the selection of highly effective siRNA sequences for mammalian and chick RNA interference.* Nucleic Acids Res, 2004. **32**(3): p. 936-48.
147. McCombs, J.E., E.A. Gibson, and A.E. Palmer, *Using a genetically targeted sensor to investigate the role of presenilin-1 in ER Ca2+ levels and dynamics.* Mol Biosyst, 2010. **6**(9): p. 1640-9.
148. Dufour, A., et al., *Role of the hemopexin domain of matrix metalloproteinases in cell migration.* J.Cell Physiol, 2008. **217**(3): p. 643-651.
149. Perret, G.Y. and M. Crepin, *New pharmacological strategies against metastatic spread.* Fundam Clin Pharmacol, 2008. **22**(5): p. 465-92.
150. Sahai, E., *Illuminating the metastatic process.* Nat Rev Cancer, 2007. **7**(10): p. 737-49.
151. Nicola Normanno, A.M., Antonella De Luca, Maria Carmela Piccirillo, Marianna Gallo, Monica R Maiello, and Francesco Perrone, *Target-based therapies in breast cancer: current status and future perspective.* Endocrine-Related Cancer, 2009. **16**(3): p. 675-702.
152. Sams-Dodd, F., *Target-based drug discovery: is something wrong?* Drug Discov Today, 2005. **10**(2): p. 139-47.
153. Butcher, E.C., *Can cell systems biology rescue drug discovery?* Nat.Rev.Drug Discov., 2005. **4**(6): p. 461-467.
154. Hart, C.P., *Finding the target after screening the phenotype.* Drug Discov.Today, 2005. **10**(7): p. 513-519.
155. Griffith, L.G. and M.A. Swartz, *Capturing complex 3D tissue physiology in vitro.* Nat.Rev.Mol.Cell Biol., 2006. **7**(3): p. 211-224.
156. Millerot-Serrurot, E., et al., *3D collagen type I matrix inhibits the antimigratory effect of doxorubicin.* Cancer Cell Int, 2010. **10**: p. 26.
157. Kunz-Schughart, L.A., et al., *The use of 3-D cultures for high-throughput screening: the multicellular spheroid model.* J.Biomol.Screen., 2004. **9**(4): p. 273-285.
158. Zhang, J.H., T.D. Chung, and K.R. Oldenburg, *A Simple Statistical Parameter for Use in Evaluation and Validation of High Throughput Screening Assays.* J.Biomol.Screen., 1999. **4**(2): p. 67-73.
159. Nien, Y.D., et al., *Fibrinogen inhibits fibroblast-mediated contraction of collagen.* Wound Repair and Regeneration, 2003. **11**(5): p. 380-385.
160. Kraning-Rush, C.M., et al., *The role of the cytoskeleton in cellular force generation in 2D and 3D environments.* Physical Biology, 2011. **8**(1).
161. Zhu, Y.K., et al., *Contraction of fibroblast-containing collagen gels: Initial collagen concentration regulates the degree of contraction and cell survival.* In Vitro Cellular & Developmental Biology-Animal, 2001. **37**(1): p. 10-16.
162. Swarna Vinodh Kanth, A.R., Jonnalagadda Raghava Rao, Balachandran Unni Nair, *Stabilization of type I collagen using dialdehyde cellulose.* process biochemistry, 2009. **44**: p. 869-874.

163. Etienne Schacht, B.B., An Van Den Bulcke, Nadine De Rooze, *Hydrogels prepared by crosslinking of gelatin with dextran dialdehyde.* Reactive and Functional Polymers, 1997. **33**: p. 109-116.
164. Draye, J.P., et al., *In vitro release characteristics of bioactive molecules from dextran dialdehyde cross-linked gelatin hydrogel films.* Biomaterials, 1998. **19**(1-3): p. 99-107.
165. Cortesi, R., et al., *Dextran cross-linked gelatin microspheres as a drug delivery system.* Eur J Pharm Biopharm, 1999. **47**(2): p. 153-60.
166. Xue, L.Y., S.M. Chiu, and N.L. Oleinick, *Staurosporine-induced death of MCF-7 human breast cancer cells: a distinction between caspase-3-dependent steps of apoptosis and the critical lethal lesions.* Experimental Cell Research, 2003. **283**(2): p. 135-145.
167. Zhang, X.D., S.K. Gillespie, and P. Hersey, *Staurosporine induces apoptosis of melanoma by both caspase-dependent and -independent apoptotic pathways.* Molecular Cancer Therapeutics, 2004. **3**(2): p. 187-197.
168. Yvon, A.M.C., P. Wadsworth, and M.A. Jordan, *Taxol suppresses dynamics of individual microtubules in living human tumor cells.* Molecular Biology of the Cell, 1999. **10**(4): p. 947-959.
169. Terzis, A.J., et al., *Proliferation, migration and invasion of human glioma cells exposed to paclitaxel (Taxol) in vitro.* British Journal of Cancer, 1997. **75**(12): p. 1744-1752.
170. Yu, F., et al., *let-7 regulates self renewal and tumorigenicity of breast cancer cells.* Cell, 2007. **131**(6): p. 1109-23.
171. Li, J., et al., *Conversion of Stationary to Invasive Tumor Initiating Cells (TICs): Role of Hypoxia in Membrane Type 1-Matrix Metalloproteinase (MT1-MMP) Trafficking.* Plos One, 2012. **7**(6).
172. Ghajar, C.M., et al., *A novel three-dimensional model to quantify metastatic melanoma invasion.* Molecular Cancer Therapeutics, 2007. **6**(2): p. 552-61.
173. Cao, J., et al., *Distinct roles for the catalytic and hemopexin domains of membrane type 1-matrix metalloproteinase in substrate degradation and cell migration.* J.Biol.Chem., 2004. **279**(14): p. 14129-14139.
174. Wang, P., J. Nie, and D. Pei, *The hemopexin domain of membrane-type matrix metalloproteinase-1 (MT1-MMP) Is not required for its activation of proMMP2 on cell surface but is essential for MT1-MMP-mediated invasion in three-dimensional type I collagen.* J Biol Chem, 2004. **279**(49): p. 51148-55.
175. Loerke, D., et al., *Quantitative imaging of epithelial cell scattering identifies specific inhibitors of cell motility and cell-cell dissociation.* Sci Signal, 2012. **5**(231): p. rs5.
176. Shintani, Y., M.J. Wheelock, and K.R. Johnson, *Phosphoinositide-3 kinase-Rac1-c-Jun NH2-terminal kinase signaling mediates collagen I-induced cell scattering and up-regulation of N-cadherin expression in mouse mammary epithelial cells.* Mol Biol Cell, 2006. **17**(7): p. 2963-75.
177. Echeverria, V., et al., *An automated high-content assay for tumor cell migration through 3-dimensional matrices.* J Biomol Screen, 2010. **15**(9): p. 1144-51.

178. Grinnell, F., et al., *Nested collagen matrices: a new model to study migration of human fibroblast populations in three dimensions.* Experimental Cell Research, 2006. **312**(1): p. 86-94.
179. Kahsai, A.W., et al., *Quinocarmycin analog DX-52-1 inhibits cell migration and targets radixin, disrupting interactions of radixin with actin and CD44.* Chemistry & Biology, 2006. **13**(9): p. 973-983.
180. Deryugina, E.I. and J.P. Quigley, *Chick embryo chorioallantoic membrane model systems to study and visualize human tumor cell metastasis.* Histochem Cell Biol, 2008. **130**(6): p. 1119-30.